สัญญาเลขที่ R2558B050

รายงานวิจัยฉบับสมบูรณ์

การดัดแปรพื้นผิวอนุภาคนาโนแมกนีไทท์ด้วยพอลิเมอร์ร่วมระหว่างพอลิเอทธิลีนไกลคอล เมทิล เมทาอะไครเลท และพอลิอะคริลิกแอซิด

Surface modification of magnetite nanoparticles with poly(ethylene glycol)methyl methacrylate-poly(acrylic acid)

คณะผู้วิจัย	สังกัด
1. รองศาสตราจารย์ ดร.เมธา รัตนากรพิทักษ์	มหาวิทยาลัยนเรศวร
2. ผู้ช่วยศาสตราจารย์ ดร.บุญจิรา รัตนากรพิทักษ์	มหาวิทยาลัยนเรศวร
3. นางสาวพัชรินทร์ กัณหาเขียว	มหาวิทยาลัยนเรศวร

สนับสนุนโดยงบประมาณแผ่นดิน ประจำปี 2558 มหาวิทยาลัยนเรศวร

Acknowledgement

The authors acknowledge The National Research Council of Thailand (NRCT) (R2558B050) for financial support of this work. Miss Patcharin Kanhakeaw especially thanks the Center of Excellence for Innovation in Chemistry (PERCH-CIC), Office of the Higher Education Commission, Ministry of Education for the scholarship.

Abstract

This work presented the surface modification of magnetite nanoparticle (MNP) with poly(acrylic acid)(PAA) homopolymer or PAA-poly(ethylene glycol) methyl ether methacrylate (PEGMA) copolymer to obtain water dispersible MNP with pH sensitive surfaces. The particles were prepared by a thermal decomposition reaction of iron (III) acetylacetonate ($Fe(acac)_3$), an iron precursor, in benzyl alcohol to obtain MNP with a narrow-size distribution. They were then surface modified with poly(*tert*-butyl acrylate)(P(*t*-BA)) homopolymer or P(*t*-BA)-PEGMA copolymer *via* atom transfer radical polymerization (ATRP) using a "grafting from" strategy, followed by the *t*-BA group deprotection. The loading molar ratio of *t*-BA to PEGMA was systematically varied (100:0, 75:25, 50:50 and 25:75, respectively) such that the grafting density of the carboxyl groups on the MNP surface after the deprotection can be fine tuned.

The kinetic studies indicated that PEGMA showed a higher reactivity in ATRP than that of P(*t*-BA) in the copolymerization. Moreover, the accelerated rate of monomer conversion was also observed in P(*t*-BA) as increasing PEGMA composition in the copolymer. The reaction progress in each step of the synthesis was monitored *via* fourier transform infrared spectroscopy (FTIR). Transmission electron microscopy (TEM) revealed that the particles were spherical with a narrow size distribution and well dispersible in water after the deprotection. Gel permeation chromatography (GPC) showed the molecular weight of the copolymer increased with the increase of the monomer conversion. The percentages of the polymeric composition in the complexes in each step of the reaction were determined *via* thermogravimetric analysis (TGA). The (co)polymer-coated MNP exhibited pH-responsive properties; the particles became more negatively charged surface and showed a decrease in hydrodynamic size as increasing pH of the dispersion. This novel copolymer-MNP complex with pH sensitive surface and magnetically guidable properties might be advantageous for the further conjugations either *via* covalently or ionically with bioentities.

บทคัดย่อ

งานวิจัยนี้ศึกษาการดัดแปรพื้นผิวอนุภาคนาโนแมกนีไทท์ด้วยโฮโมพอลิเมอร์ชนิดพอลิอะไครลิกแอซิด (PAA) หรือ พอลิเมอร์ร่วมระหว่างพอลิอะไครลิกแอซิดและพอลิเอทิลีนไกลคอลเมธาไครเลท (PAA-PEGMA) เพื่อให้ได้อนุภาคนาโนแมกนีไทท์ที่กระจายได้ดีในน้ำและสามารถตอบสนองต่อการเปลี่ยนแปลงพีเอชได้ อนุภาคนาโนแมกนีไทท์นี้เตรียมได้จากปฏิกิริยาการแตกสลายของไอรอนอะซิติลอะซิโตเนทในเบนซิลแอลกอฮอล์ ทำให้ได้อนุภาคนาโนแมกนีไทท์ที่มีขนาดใกล้เคียงกัน จากนั้นทำการดัดแปรพื้นผิวอนุภาคนาโนแมกนีไทท์ด้วยโฮโมพอลิเมอร์ชนิดพอลิทีบิวทิลอะไครเลทหรือพอลิเมอร์ร่วมระหว่างพอลิทีบิวทิลอะไครเลทและพอลิเอทิลีนไกลคอลเมธาไครเลท ด้วยปฏิกิริยาอนุมูลอิสระแบบเอทีอาร์พี ตามด้วยปฏิกิริยาการตัดหมู่ทีบิวทิลเพื่อเกิดเป็นพอลิอะไครลิกแอซิด โดยในการทดลองได้ใช้อัตราส่วนโดยโมลระหว่างทีบิวทิลอะไครเลทต่อพอลิเอทิลีนไกลคอลเมธาไครเลท เป็น 100:0, 75:25, 50:50 and 25:75 ตามลำดับ เพื่อให้ได้อนุภาคนาโนแมกนีไทท์ที่มีปริมาณหมู่กรดคาร์บอกซิลิกที่แตกต่างกัน

จากผลการศึกษาจลนศาสตร์ของปฏิกิริยาพบว่า พอลิเอทิลีนไกลคอลเมธาไครเลท มีอัตราการเกิดปฏิกิริยาอนุมูลอิสระแบบเอทีอาร์พีได้เร็วกว่าพอลิทีบิวทิลอะไครเลท และเมื่อเพิ่มปริมาณของพอลิเอทิลีนไกลคอลเมธาไครเลทในปฏิกิริยาพบว่าอัตราการเกิดปฏิกิริยาของพอลิทีบิวทิลอะไครเลทจะมีค่าเพิ่มเร็วมากขึ้น ในการทดลองได้ติดตามการดำเนินไปของปฏิกิริยาด้วยเทคนิคเอฟทีไออาร์ นอกจากนี้จากเทคนิคทีอีเอ็มพบว่าอนุภาคนาโนแมกนีไทท์มีรูปร่างกลมและมีขนาดใกล้เคียงกัน สามารถกระจายตัวได้ดีในน้ำเมื่อมีการกำจัดหมู่ทีบิวทิลออกแล้ว ผลการทดลองจากเทคนิคจีพีซี พบว่า น้ำหนักโมเลกุลของพอลิเมอร์มีค่าเพิ่มมากขึ้นเมื่อคอนเวอร์ชันของปฏิกิริยาเพิ่มมากขึ้น ผลการทดลองจากเทคนิคทีจีเอสามารถใช้หาค่าเปอร์เซ็นต์พอลิเมอร์ในแต่ละขั้นตอนของปฏิกิริยาได้ อนุภาคนาโนแมกนีไทท์ที่เคลือบด้วยพอลิเมอร์นี้สามารถแสดงสมบัติการตอบสนองต่อการเปลี่ยนปลงพีเอชได้ โดยเมื่อพีเอชเพิ่มมากขึ้น (มีความเป็นเบสมากขึ้น) จะมีดีกรีของประจุลบมากขึ้นและมีค่าไฮโดรไดนามิกส์ลดลง ด้วยสมบัติที่ดีเหล่านี้จึงคาดว่าอนุภาคนาโนแมกนีไทท์นี้สามารถนำไปประยุกต์ในการตรึงสารชีวโมเลกุลอื่นๆด้วยพันธะโควาเลนต์หรือไอออนิกได้

LIST OF CONTENTS

LIST OF CONTENTS (CONT.)

LIST OF TABLES

LIST OF FIGURES

LIST OF FIGURES (CONT.)

Figures **Page**

LIST OF FIGURES (CONT.)

Figures **Page**

LIST OF FIGURES (CONT.)

Figures **Page**

LIST OF FIGURES (CONT.)

LIST OF FIGURES (CONT.)

Figures **Page**

ABBREVIATIONS

MNPs	=	Magnetite Nanoparticles
BTPAm	=	2-bromo-2-methyl-N-(3-(triethoxysilyl) propanamide
ATRP	=	Atom Transfer Radical Polymerization
PEGMA	=	Poly (ethylene glycol) methyl ether methacrylate
P(*t*-BA)	=	Poly(*tert*-butyl acrylate)
t-BA	=	*tert*-butyl acrylate
PAA	=	Poly(acrylic acid)
$Fe(acac)_3$	=	Iron (III) acetylacetonate
APS	=	3-aminopropyl triethoxysilane
TEA	=	Triethylamine
BIBB	=	2-bromoisobutyryl bromide
CuBr	=	Copper (I) bromide
PMDETA	=	N,N,N′,N′′,N′′-pentamethyldiethylenetriamine
$CDCl_3$	=	deuterated chlorotom
M_s	=	saturation magnetization
$\overline{M}_n$	=	number average molecular weight
MW	=	molecular weight distribution
nm	=	nanometer
M	=	molar
mol/L	=	mole/litter
NMR	=	Nuclear Manetic Resonance spectroscopy
FTIR	=	Fourier Transform Infrared Spectroscopy
TGA	=	Thermogravimetric Analysis
GPC	=	Gel Permeation Chromatography
VSM	=	Vibrating Sample Magnetometry
TEM	=	Transmission Electron Microscopy
Conv.	=	conversion

CHAPTER I

INTRODUCTION

Rationale for the study

Magnetite nanoparticle (MNP, Fe_3O_4) has been extensively studied over the past decade for use in various biomedical applications, including magnetic resonance imaging (MRI) contrast enhancement, targeted drug delivery, hyperthermia, catalysis, biological separation, biosensors, and diagnostic medical devices. However, because of their large surface area/volume ratio, the nanometer sized iron oxide cores tend to agglomerate into large clusters and lose the specific properties associated with their initial nanometer dimensions [1]. Therefore, their surfaces might be coated with organic polymers [2] or inorganic materials [3, 4] to obtain necessary stability to the particle for applications. Several methods have been developed to prepare polymer coating on a particle surface such as physical adsorption of polymer [5], emulsion polymerization in the presence of nanoparticles [6] and the so-called "grafting to" [7, 8] and "grafting from" [9, 10] methods. The "grafting to" method involves the reaction of reactive functional groups in the polymer with complementary active groups on the particle surface. In general, the grafting density of "grafted to" polymer chains is limited because of the steric hindrance effect. Conversely, the "grafting from" approach which utilizes active species on the surface to initiate polymerization, usually results in high grafting density [1].

The recent progress in polymerization methods gives rise to the molecular design and synthesis of well-defined polymers by controlled/living radical polymerizations (CRPs), including nitroxide-mediated radical polymerization (NMRP) [11], reversible addition fragmentation chain transfer (RAFT) polymerizations [12] and atom transfer radical polymerization (ATRP) [13, 14]. Of the CRP methods, atom transfer radical polymerization (ATRP) has become one of the most successful methods for the polymerization and block copolymerization of a wide range of monomer in a controlled manner. Therefore, the ATRP method was utilized to modify MNP with well-controlled polymer because of the facile functionalization

of MNP with ATRP initiating species (halides) for surface-initiated controlled polymerization.

In recent years, there has been increasing research about surface modification with polyelectrolytes, which are polymers containing ionizable groups [15]. In polar solvents such as water, these groups can dissociate, leaving charges on polymer chains and releasing counterions in solution. Examples of polyelectrolytes include polystyrene sulfonate, polyacrylic and polymethacrylic acids and their salts, DNA and other polyacids and polybases [15]. For example, well-defined polyacrylic acid (PAA) brushes can be prepared *via* ATRP of *tert*-butylacrylate, followed by hydrolysis of the *tert*-butyl ester protective groups [16] and sodium acrylate with subsequent hydrolysis [17]. In the cases of reversible binding of biomolecules in bioseparation application, the well-define PAA brushes are generally used as the negative charged polyelectrolytes, which can electrostatically bind positively charged enzymes, such as lysozyme [18] and pectinase [19]. PAA brushes have also been used for covalent coupling of both positively and negatively charged biomolecules [20].

In the current work, we focused on the surface modification of MNP with PAA homopolymer or PAA/ poly(ethylene glycol) methyl ether methacrylate (PEGMA) copolymer (75/25, 5050 and 25/75, respectively) *via* ATRP using a "grafting from" technique. Using controllable living ATRP, degree of negative charge due to carboxylate groups should be adjusted by varying the molar ratio of PAA to PEGMA on the particle surface. The tunable degrees of negative charge on MNP surface may be a great advantage in biomedical applications. For example, the well-defined PAA brushes can be used to separate specific proteins *via* ion exchange. Moreover, well-defined PAA brushes prepared *via* ATRP have been used to covalently bind a variety of biomolecules including bovine serum albumin (BSA) [17], avidin [17] and ribonuclease A (RNase A) [20].

To modify the particles surfaces, the initiator for ATRP was first covalently bonded onto the surface of the particles through the combination of ligand exchange reaction and condensation of triethoxysilane to obtain ATRP initiating sites on their surface. Then, the surface-initiated ATRP of poly(*tert*-butyl acrylate) (P(*t*-BA)) homopolymer and P(*t*-BA)/PEGMA copolymer mediated by a copper complex was carried out. Finally, the *t*-butyl groups on the particle surface were deprotected in

acidic dispersion to obtain the carboxylic group on its surface. Kinetic studies were studied to reveal the reaction reactivities of P(*t*-BA) and PEGMA in the (co)polymreization. GPC was also conducted to investigate the change of the molecular weight of the (co)polymers as a function of time. The particle size and size distribution of the (co)polymer-MNP complex were evidenced using TEM and their magnetic property was elucidated *via* VSM. The hydrodynamic diameter and zeta potential value of the complex was measured *via* PCS. In addition, quantitative analysis of the carboxylic groups presenting in the copolymer-MNP complex were also acquired from conductometric titration.

Purpose of the study

This work aims at the surface modification of MNP with PAA homopolymer and PAA-PEGMA statistical copolymer *via* atom transfer radical polymerization (ATRP) having various molar ratio of PAA to PEGMA for adjusting the degree of the negative charge on the particle surface.

Significance of the study

1. Synthesis of magnetite nanoparticle (MNP)

2. Surface modification of MNP with PAA homopolymer and PAA/PEGMA copolymer *via* ATRP and kinetic studies of the raction

3. Study on the properties of the polymer-coated MNP such as magnetic properties, polymer-MNP composition in the complexes, charges and hydrodynamic size, particle size and its distribution

CHAPTER II

LITERATURE REVIEW

This chapter focuses primarily on the fundamental and literature reviews on the topics relating to the current research. The objective of this work was to modify MNP surface with a covalently bonded copolymer of poly(acrylic acid) (PAA) and poly(ethylene glycol) methyl ether methacrylate (PEGMA) *via* ATRP reaction using a grafting-from technique. The molar ratios of these two polymers were adjusted in order to tune degree of negative charge due to the presence of PAA polyelectrolyte on the particle surfaces. Hence, this chapter includes the fundamentals of magnetic materials and magnetism, synthesis of MNP, polyelectrolyte, atom transfer radical polymerization (ATRP), surface modification of MNP with polymeric stabilizers and its applications.

Magnetism and magnetic material

Magnetism is a phenomenon by which materials assert an attractive or repulsive force on other materials. Magnetic forces are fundamental forces that arise due to the movement of electrically charged particles. Magnetic dipoles or magnetic moments can often result on the atomic scale due to the movements of electrons. Each electron has magnetic moments that originate from two sources. The first is the orbital motion of the electron around the nucleus. This motion can be considered as a current loop, resulting in a magnetic moment along its axis of rotation. The second source of electronic magnetic moment is due to a quantum mechanical property called spin.

In an atom, the orbital and spin magnetic moments of some electron pairs cancel each other. The overall magnetic moment of the atom is thus the sum of all of the magnetic moments of the individual electrons, accounting for moment cancellation between properly paired electrons. For the case of a completely filled electron shell or subshell, the magnetic moments completely cancel each other out. Thus only atoms with partially filled electron shells have a magnetic moment. The magnetic behavior

of materials can be classified into 5 categories based on their response to an external applied magnetic field: diamagnetism, paramagnetism, ferromagnetism, antiferromagnetism and ferrimagnetism [21].

Diamagnetic materials are composed of atoms that have no net magnetic moments. However, when exposed to a field, a weak negative magnetization is produced which causes repulsion instead of attraction. Diamagnetic materials have negative susceptibilty with magnitude of around -10 to -10^{-4} [22].

Paramagnetic materials such as liquid oxygen and aluminium show a weak magnetic attraction when placed near a magnet. Some atoms or ions in the material have a net magnetic moment due to unpaired electrons in partially filled orbitals (Figure 1A) [23]. In the presence of a field, there is a partial alignment of the atomic magnetic moments in the direction of the field resulting in a net positive magnetization and positive susceptibility.

Ferrimagnetic materials have two sets of magnetic dipole moments pointing in opposite directions. The magnetic moments do not cancel each other out because the dipole moment in one direction is smaller than the other (Figure 1D) [23].

The magnetic moments in a ferromagnet have the tendency to become aligned parallel to each other under the influence of a magnetic field (Figure 1B) [23]. However, unlike the moments in a paramagnet, these moments will then remain parallel when a magnetic field is not applied.

In antiferromagnetic materials (Figure 1C) [23], adjacent magnetic moments from the magnetic ions tend to align anti-parallel to each other without an applied field. Adjacent magnetic moments are equal in magnitude and opposite therefore there is no overall magnetization.

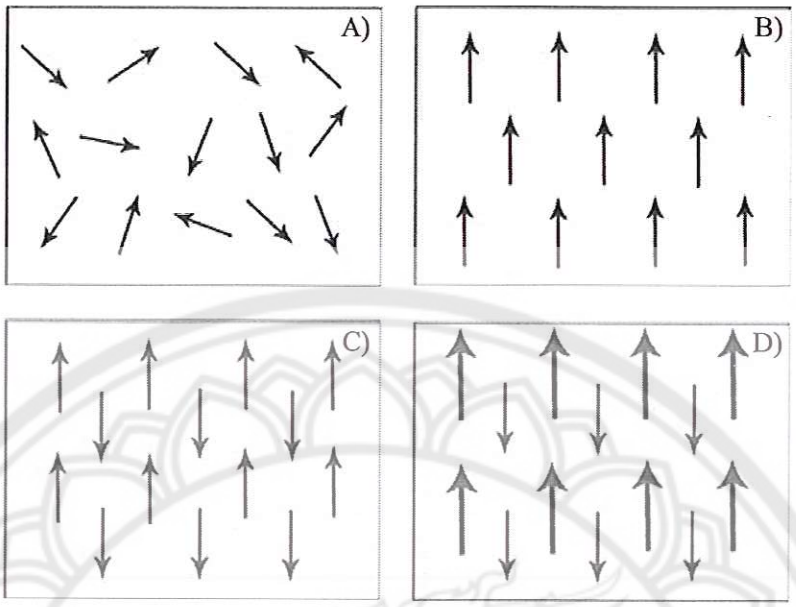

Figure 1 Schematic showing the magnetic dipole moments in, A) paramagnetic materials, B) ferromagnetic materials, C) antiferromagnetic materials and D) ferrimagnetism materials [23]

In the hysteresis loop or magnetization plot, the loop is generated by measuring the magnetic flux of a ferromagnetic material while the magnetizing force is changed [24].

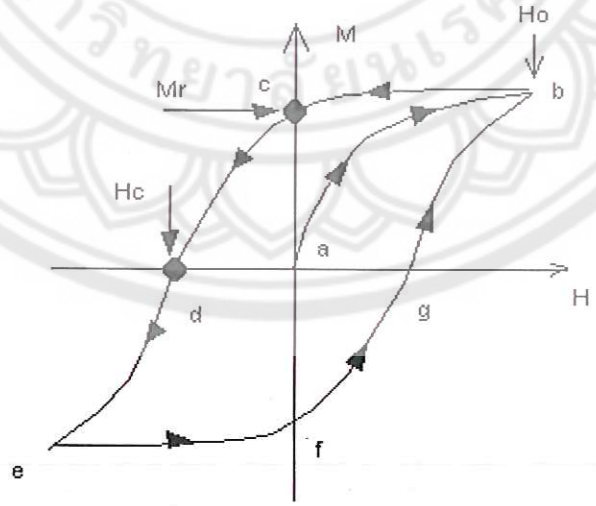

Figure 2 Hysteresis loop characteristic of typical magnetic materials [25]

As the external magnetic field (H) is increased, the induced magnetization (M) also increases [25]. The induced magnetization eventually saturates (point b). The curve between points "a" and "b" is called the magnetization curve. If the external field is reduced, the induced magnetization is also dropped, but it may not follow the original curve. If this is such a case, the material retains a certain permanent magnetization termed the remanence, M_r (point c). The remanence is the permanent magnetization that remains after the external field is removed. If the external field is further reduced, the remanence will be removed (point d). The external field for which the remanence goes to zero is termed the coercivity, H_c. The product of $M_r * H_c$ is the strength of the magnet. As the external field continues to reverse, permanent magnetization of the opposite sign is created in the magnet. A similar curve is traced for the negative direction with saturation (point e), remanence (point f) and coercivity (point g). The hysteresis curve then retraces point b-e if the field cycles.

Synthesis of magnetite nanoparticle (MNP)

Magnetite nanoparticle (Fe_3O_4, MNP) is a black, ferromagnetic mineral containing both Fe(II) and Fe(III) components. MNP possesses a cubic inverse spinel structure, with only Fe(II) atoms occupying the tetrahedral sites, whereas the octahedral sites are equally occupied be Fe(II) and Fe(III) atoms. The crystal structure of MNP is inverse spinel with a unit cell consisting of 32 oxygen atoms in a face-centered cubic (FCC) structure and a unit cell edge length of 0.839 nm [26, 27]

Synthesis of MNP in the nano range for various applications has been an active and challenging area of research during the last two decades [26]. During the reaction, several parameters have to be carefully controlled, including pH, concentration of the reactants, temperature, methods of mixing and rate of oxidation. The morphology of the MNP depends on the competition between several processes like nucleation, growth, aggregation and adsorption of impurities.

Recently, several synthesis methods of MNP have been established; chemical co-precipitation [28], organic colloids [29], hydrothermal [30] methods. The first two methods have been most prevalently attracted much attention and will be profoundly presented herein.

1. Co-precipitation

The chemical co-precipitation is most prevalent among other methods because of its direct, *in situ* coating step, wherein the particles are coated with various water-soluble biocompatible coating agents. However, the drawbacks of this method are that the particles with poor crystallinity, large aggregates (having many individual nanoparticles) and broad particle size distribution in the aqueous dispersion are obtained. For example, large aggregates of coated MNP have been synthesized *via* co-precipitation using dextran [31, 32], polyvinyl alcohol (PVA) [33], polyethylene oxide (PEO) [34] and poly(acrylic acid)(PAA) [35], either by *in situ* or post coating steps.

2. Thermal decomposition

The decomposition of organometallic precursors in organic solvents at high temperatures provides an efficient route to obtain highly crystalline and monodisperse particles with excellent magnetic properties. In particular, the so-called polyol method has demonstrated to be an effective and reproducible route to prepare oleic acid and oleylamine coated MNP [29], in which sample characteristics can be fine-tuned by simply modulating synthetic parameters such as reaction time, temperature, solvent and the reagent and/or solvent concentration [36].

Roca, et al. [37], have reported the synthesis of MNP with 2 different conditions *via* decomposition reaction. In the first condition, MNP was synthesized using iron acetylacetonate ($Fe(acac)_3$) as an iron precursor in phenyl ether and in the presence of oleic acid. The reaction mixture was heated to 200 °C and then refluxed at 250 °C. In the second condition, MNP was produced using iron pentacarbonyl ($Fe(CO)_5$) as an iron precursor in 1-octadecene. The mixture reaction was heated to 100 °C and then reflux at 320 °C. The 17 nm in diameter of MNP was observed in the second-condition synthesis (Figure 3), while that of the first method was 5 nm. The formation of larger particles in the second method was attributed to the use of high decomposition temperature of the iron precursor, resulting in a delay in the nucleation and therefore a smaller number of nuclei in the initial stages of the reaction were obtained.

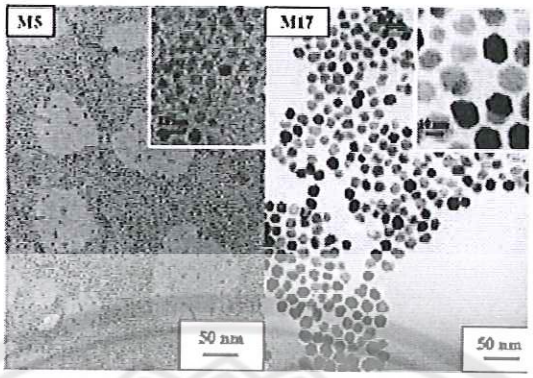

Figure 3 TEM images of MNPs prepared from $Fe(acac)_3$ having 5 nm (left) and from $Fe(CO)_5$ having 17 nm (right) in diameters [37]

Ravikumar, et al. [27], have reported the synthesis of PAA-coated super-paramagnetic MNP *via* two different methods; thermal decomposition of an organometallic iron precursor and co-precipitation of aqueous solutions of ferrous and ferric chloride salts. It was found that, PAA-coated MNP obtained in the thermal decomposition method were spherical, isolated and nearly monodispersed, having a mean size of 6±1 nm (Figure 4A). In the co-precipitation method, the particles aggregated with a mean size of 8±1 nm (Figure 4B).

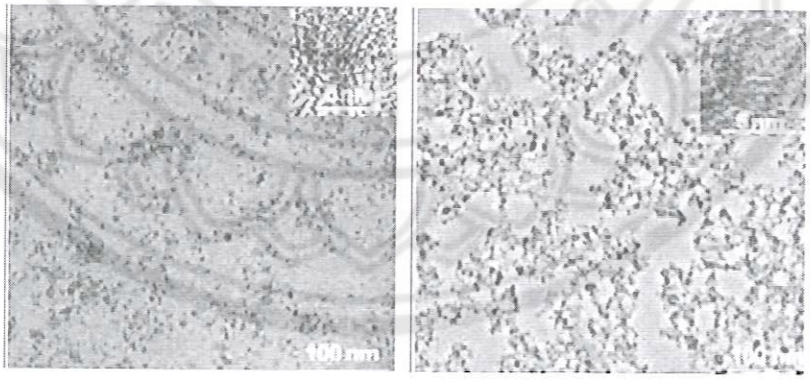

A) B)

Figure 4 TEM images of PAA-coated MNP prepared *via*, A) thermal decomposition and B) co-precipitation [27]

Surface modification of nanoparticle *via* atom transfer radical polymerization (ATRP)

Atom transfer radical polymerization (ATRP) is a recently developed "living" or "controlled" radical polymerization method (CRP), which does not require stringent experimental conditions. ATRP allows for the polymerization and block copolymerization of a wide range of functional monomers such as styrenes, (meth)acrylates, (meth)acrylamides, and (meth)acrylic acids in a controlled fashion, yielding polymers with narrowly dispersed molecular weights. Moreover, ATRP is tolerant of monomers with polar functionality. Thus, it allows the direct polymerization of functional monomers without involving the tedious protection and deprotection procedures [38]. In the polymerization, a transition metal complex is used for a catalyzed polymerization where the complex acts as a halogen transfer agent. The general mechanism is presented in Figure 5 [39].

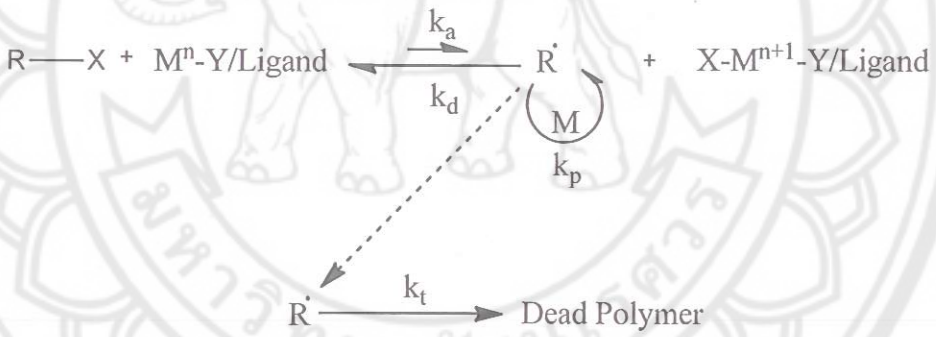

Figure 5 The mechanism of metal catalyzed ATRP [39]

Typically, the alkyl halogen (R-X) is homolytically cleaved by the transition metal complex in its lower oxidation state (M^n-Y/Ligand). This forms a radical ($R^{\bullet}$) and the transition metal complex in higher oxidation state (X-M^{n+1}-Y/Ligand) at a rate determined by the activation constant (k_a). The radical may then proceed to add to monomer units (M) to from a growing polymer. The growing polymer is subjected to normal propagation (k_p) and termination (k_t). To prevent premature termination, the radicals undergo a deactivation step (k_d) by reacting with the high oxidation state metal complex. The underlying advantage of ATRP is that the deactivation rate is

highly favored over the activation rate i.e. $k_d >> k_a$, and causes the equilibrium to lie to the left-hand side. This controls the production of radical species and creates polymers of defined molecular weight distributions (MWDs).

To date, there have been many metal-catalyzed ATRP polymerizations performed with many monomer and metal species summarized by Braunecker and Matyjaszewski [14]. These monomers include styrene, acrylates, acrylonitriles and acrylamides with the use of various transition metals in Group 4 and 6-11 in the periodic table.

By far the most commonly used transition metal complexes involve the use of Cu(I). This is called *direct* ATRP and uses the Cu(I)/alkyl halide method of initiators are generally derived from tertiary halides. Another common method is reverse ATRP and utilizes Cu(II) complexes coupled with azo-initiators, such as azobisisobutyronitrile (AIBN) and 2,2'-azobis (2-methylpropionamidine).2HCl (V50). The difference between direct and reverse ATRP is that the direct one uses a tertiary halide initiator coupled with a Cu(I) complex, while the reverse ATRP uses a Cu(II) complex which must first be reduced to Cu(I) (in solution) with the use of a conventional initiator. While the direct ATRP systems must have stringent controls over the presence of oxygen, it does not require the addition of other initiators to commence the reaction [39].

The ATRP method has been extensively utilized to modify surface with well-controlled polymers because of the facile functionalization of surface with ATRP initiating species (halides) for surface-initiated controlled polymerization (Figure 6) [40]. The general approach for a "grafting from" method involves the utilization of surface-initiated CRP methods, providing a brush-like morphology as seen in Figure 6. This method utilizes monodentate polymers with a single anchoring group at the end of polymer chain to stabilize the particle surface. ATRP has been performed from various surfaces, including planar surfaces, and surfaces of inorganic particles, colloids and polymer networks, and even from dendrimers

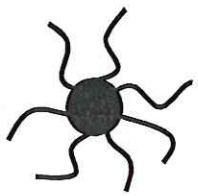

Figure 6 Morphology of composite magnetic polymer microsphere: brush-like morphology [40]

In the preparation of functional polymer brushes *via* surface-initiated ATRP, the presence of a uniform monolayer of initiators on the target substrate surfaces is indispensable [41] (Figure 7). Versatile immobilization methods of ATRP initiators have been developed for an extensive range of biomedical substrates, including inorganic surfaces of silicon, silica, titanium, gold and magnetite (Fe_3O_4), and surfaces of films such as polypropylene (PP), aromatic ring containing polymers, cellulose and nylon.

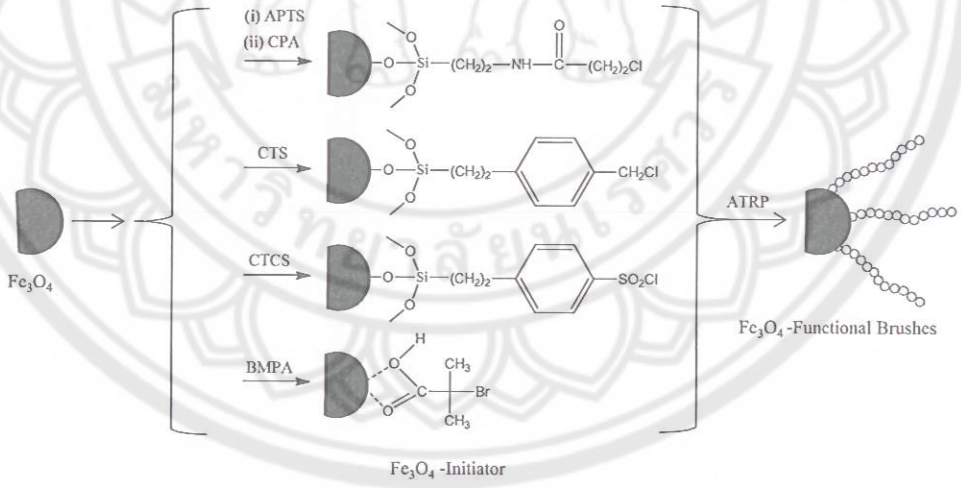

Figure 7 Methods for immobilizing ATRP initiators on substrate surfaces in the preparation of functional polymer brushes by surface-initiated ATRP (APTS: 3-aminopropyltriethoxysilane; CPA: 3-chloropropionic acid; CTS: 4-(chloromethyl)phenyl trichlorosilane; CTCS: 2-(4-chlorosulfonyl -phenyl) ethyl trichlorosilane; BMPA: 2-bromo-2-methylpropionic acid) [41]

Ding, et al. [42], have the presented the use of regular shaped magnetite nanoparticle (MNP) (20-30 nm) to support the catalysts and ligand for ATRP comparing with unsupported catalysts. In the MNP-supported system, *N, N, N'',N''*-tetraethyldiethylenetriamine (TEDETA) ligand and Cu catalyst were first tethered onto the MNP surface and they were then used in a living/controlled radical polymerization of MMA (Figure 8). It was found that the MNP-supported catalyst mediated a living/controlled radical polymerization of MMA as effectively as unsupported catalysts. The catalysts immobilized on the large particles, resulting in the polymers with uncontrolled molecular weights and high polydispersity even in the presence of an excess amount of CuBr. The fresh and reused supported catalyst effectively mediated the chain extension of MMA. This supported catalyst did not need free deactivator or ligands and thus the resulting residual catalyst concentration in the resulting polymer was low.

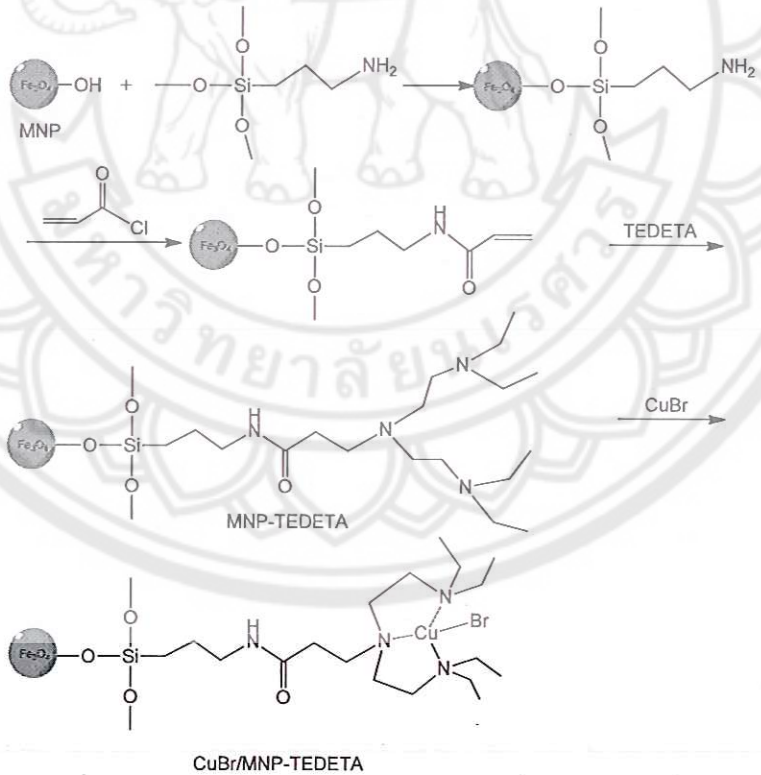

Figure 8 Immobilization of *N,N,N'', N''*-tetraethyldiethylenetriamine (TEDETA) ligand and Cu catalyst onto MNP surface [42]

Xu, et al. [43], have the presented the surface modification of MNP through the growth of poly(2-hydroxyethyl methacrylate) (PHEMA) brushes *via* ATRP from the surface-immobilized initiators. The PHEMA-grafted MNP was then functionalized with nitrilotriacetate-Ni^{2+} to yield magnetic beads for selective capture polyhistidine-tagged (His-tagged) protein from cell extracts (Figure 9). The first step is the coating MNP with silica to prevent oxidation and dissolution of the particle. The ATRP initiators were then immobilized onto the silica surface *via* silanization (Figure 10). HEMA monomer was polymerized from the immobilized initiators to give PHEMA-grafted MNP. Subsequently, the polymer brushes further reacted with succinic anhydride (SA) and N_{α}, N_{α}-bis(carboxymethyl)-L-lysine hydrate (aminobutyl NTA). It was found that the particles can rapidly isolate multilayers of His-tagged protein directly from a cell extract with high purity. The the polymer brushes having 50 nm thickness can reduce diffusion limitations and allow protein capture within 5 min. Moreover, the brush-modified particles afford high protein recoveries and can be reused if desired.

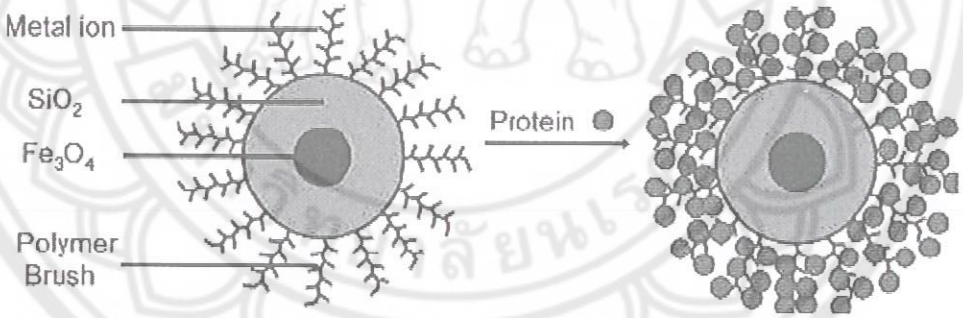

Figure 9 Schematic diagram of PHEMA brush-modified beads and the protein binding [43]

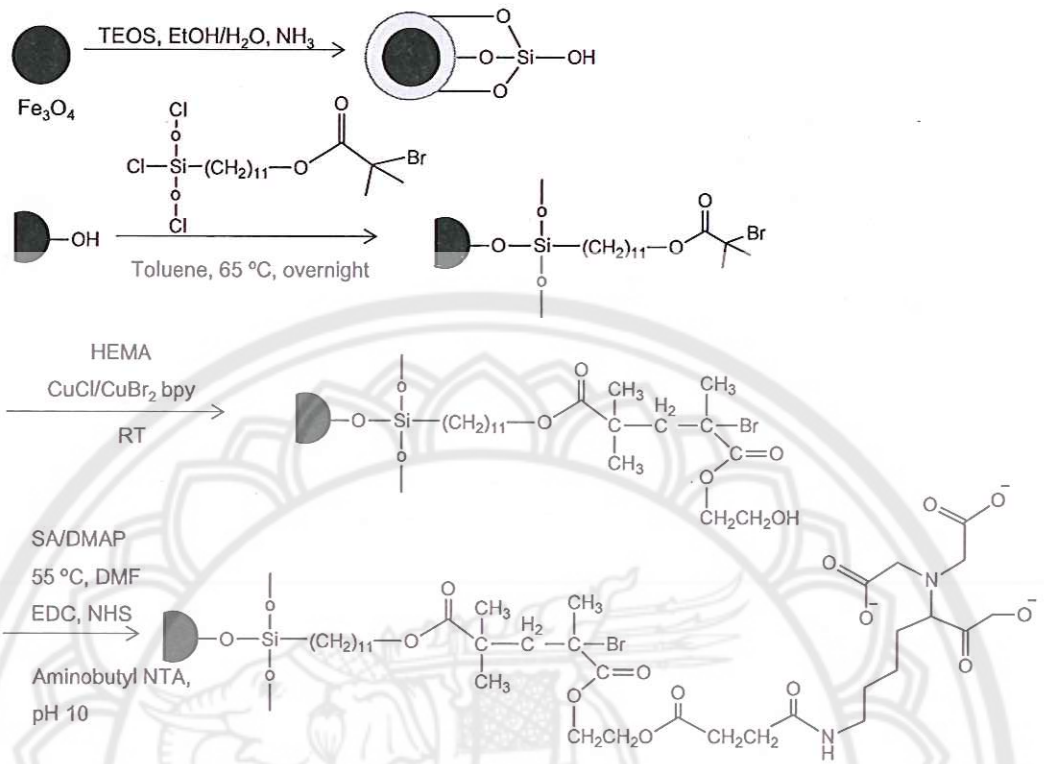

Figure 10 Surface modification of MNP with PHEMA brush [43]

Yu, et al. [44], have presented surface modification of silica nanoparticles with the copolymer between poly (methacryloxypropyl- trimethoxysilane) (PMPTS) and poly(2,2,3,3,4,4,4-heptafluorobutyl methacrylate) (PHFBMA) by two-step surface-initiated ATRP (SI-ATRP) (Figure 11). It was found that the polymerization of PHFBMA second block from PMPTS-grafted surface was well controllable. The good controllability might be greatly influenced by the polymerization conditions including the initiator concentration, the molar ratio of monomer and initiator and the polymerization temperature. The results showed that all the molecular weight, the surface roughness, and the water contact angel (WCA) of the SiO_2/PMPTS-b-PHFBMA nanoparticle increased with the increase of the monomer conversion. Therefore, the superhydrophobicity was attributed to both the existence of PHFBMA and surface roughening effects.

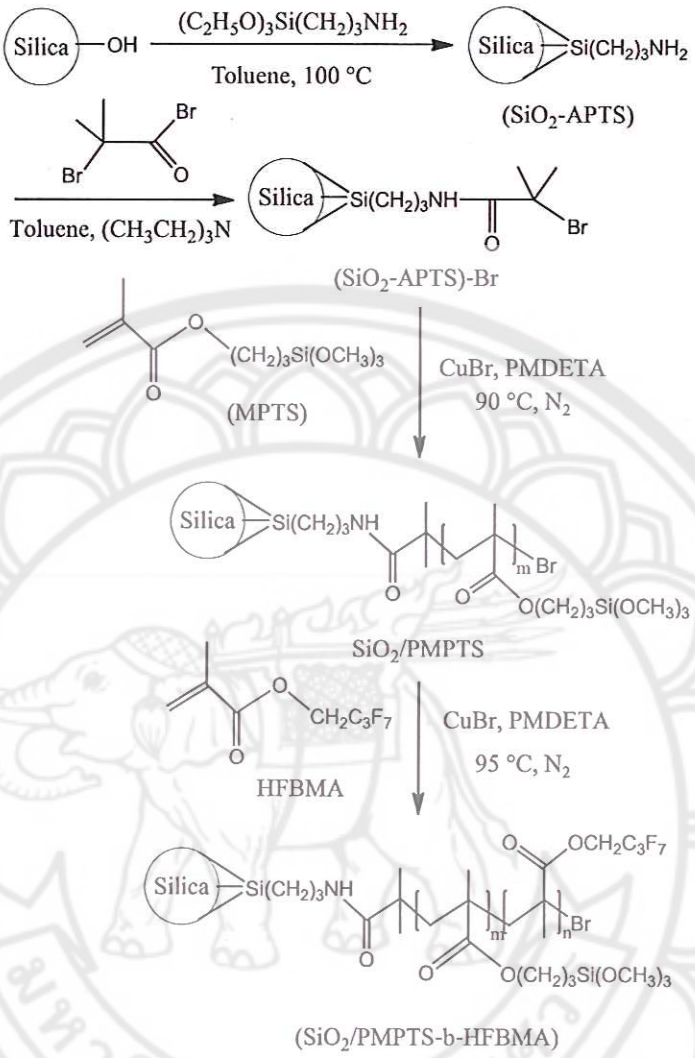

Figure 11 Synthetic Scheme for surface modification of silica nanoparticle with PMPTS-b-PHFBMA copolymer [44]

Polyelectrolyte

Polyelectrolytes are defined as polymer chains composed of monomer units having ionizable groups. Their most prominent features are a high solubility, in most cases in water or polar solvent, and strong adsorbing capacity at oppositely charged surfaces [45]. The properties of polyelectrolyte are thus similar to both electrolytes (salts) and polymers, and are sometimes called polysalts. Similar to salts, their solutions are electrically conductive. Similar to polymers, their solutions are often viscous. Charged molecular chains, commonly present in soft matter systems, play a

fundamental role in determining structure, stability and the interactions of various molecular assemblies [46].

Polyelectrolytes can be divided into 'weak' and 'strong' types. A 'strong' polyelectrolyte is one which dissociates completely in solution for most reasonable pH values (Figure 12). A 'weak' polyelectrolyte, by contrast, has a dissociation constant (pK_a or pK_b) in the range of ~2 to ~10, meaning that it will be partially dissociated at intermediate pH [47]. Thus, weak polyelectrolytes are not fully charged in solution, and moreover their fractional charge can be modified by changing the solution pH, counterion concentration, or ionic strength. Some examples of weak polyelectrolytes are shown in Figure 13 [48].

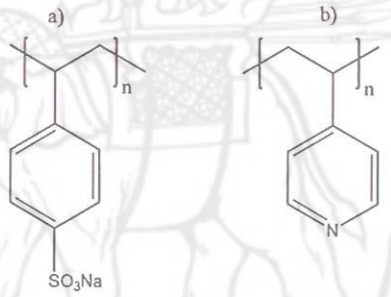

Figure 12 Some examples of strong polyelectrolytes

a) poly(styrene sulfonic acid) (PSS)

b) poly(vinylpyridine) (PVP) [47]

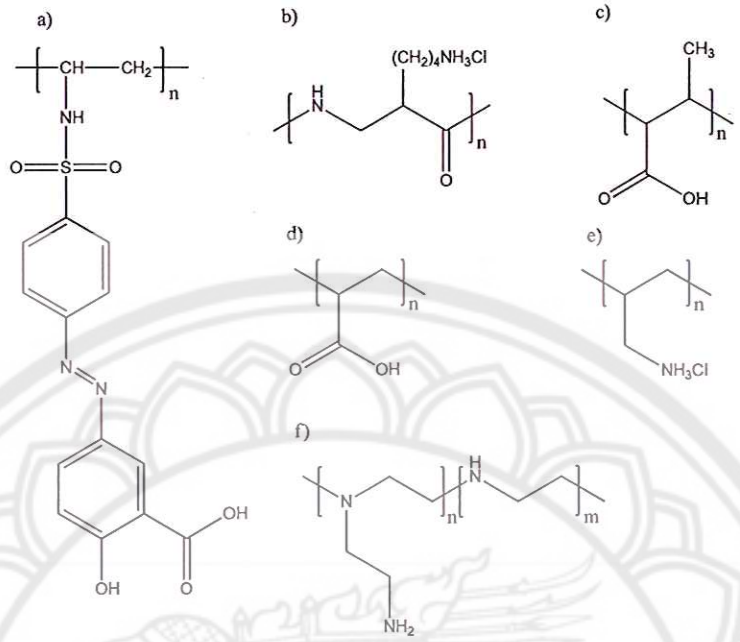

Figure 13 Some examples of weak polyelectrolytes

a) **poly{1-[4-(3-carboxy-4 hydroxyphenylazo)benzenesulfonamido]-1,2-ethanediyl} (PAZO),**
b) **poly(L-lysine hydrochloride) (PLL),**
c) **poly(methacrylic acid) (PMA),**
d) **poly(acrylic acid) (PAA),**
e) **polyallylamine hydrochloride (PAH),**
f) **poly(ethylenimine) (PEI)** [48]

1. Polyelectrolytes in solution

A positively or negatively charged polyelectrolyte is called a polycation (polybase) or a polyanion (polyacid), respectively. If positive and negative charges are on the same chain, the polyelectrolyte is called a polyampholyte (e.g. proteins). The degree of charge depends on the particular polyelectrolyte and ranges from a small fraction to 100% of the monomer units. Polyelectrolytes are soluble in water, although their backbone is often hydrophobic. Their solubility is related to the gain in entropy when counterions are released in water.

Surface modification of materials with polyelectrolyte

Surface coating of materials with polyelectrolytes has been extensively studied over the past decade. They can exhibit interesting stimuli-responsive behaviors associated with their large electrostatic potentials. Depending on their nature, polyelectrolytes can respond to external stimuli, such as pH, ionic strength or temperature. They have thus been widely employed for the immobilization of biomolecules or other applications. In this report, literature reviews in the topic of surface modification of materials with carboxylic acid groups has been focused.

Fulghum, et al. [49], have reported the synthesis of ternary polymer particle composed of a spherical colloidal particle core (polystyrene), coated with multilayers of poly(diallyl dimethyl ammonium chloride) (PDADMAC)/poly(acrylic acid)(PAA) polyelectrolytes prepared *via* the layer-by-layer (LbL) deposition process. The multilayer intermediate shell was then grafted with poly(methyl methacrylate) (PMMA) brush *via* surface-initiated ATRP of the PS core. They found that the layer of PAA had a zeta potential of -45 mV. This negatively charge surface of the particles was sufficient for selective adsorption of positively charged PDADMAC to form multi layer surface. Moreover, polydispersity (PDI) and molecular weight of PMMA determined from a sacrificial initiator were 1.4 and 73,000 g/mol, respectively.

Berger, et al. [50], have reported the polymerization of stimuli-responsive bicomponent polymeric Janus particles (JPs). In the first step, PAA or poly(N-isopropylacrylamide) (PNIPAm) was immobilized on one side of silica particles using a "grafting from" approach surface-initiated ATRP (Figure 14). In the second step, poly(2-vinylpyridine)(P2VP) was then immobilized through a "grafting to" method by reaction between reactive terminating groups of polymer chains and functional groups on the particle surface. A very interesting pH-dependent aggregation behavior of biocomponent PAA-P2VP JPs was observed. The JPs appeared from large aggregates about 4-10 μm in diameter in the range of $2 < pH < 5$. This was probably because PAA ($iep^{PAA} = 2.3$) and P2VP ($iep^{PVP} = 7.3$) chains were negatively and positively charged, respectively; the charges of polymers were thus compensated. In Regime II ($5.5 < pH < 7.5$), the singular particles were observed in solution in a range of $5.5 < pH < 7.5$ because PAA and P2VP were negatively charged and almost uncharged, respectively. Further increase of pH value up to 9.2 led to the formation of small

aggregate composed almost of 2 JPs. However, the apparent value of zeta potential of JPs decreased from -50 mV down to -40 mV when the solution pH increased from 7.5 up to 9.2, respectively.

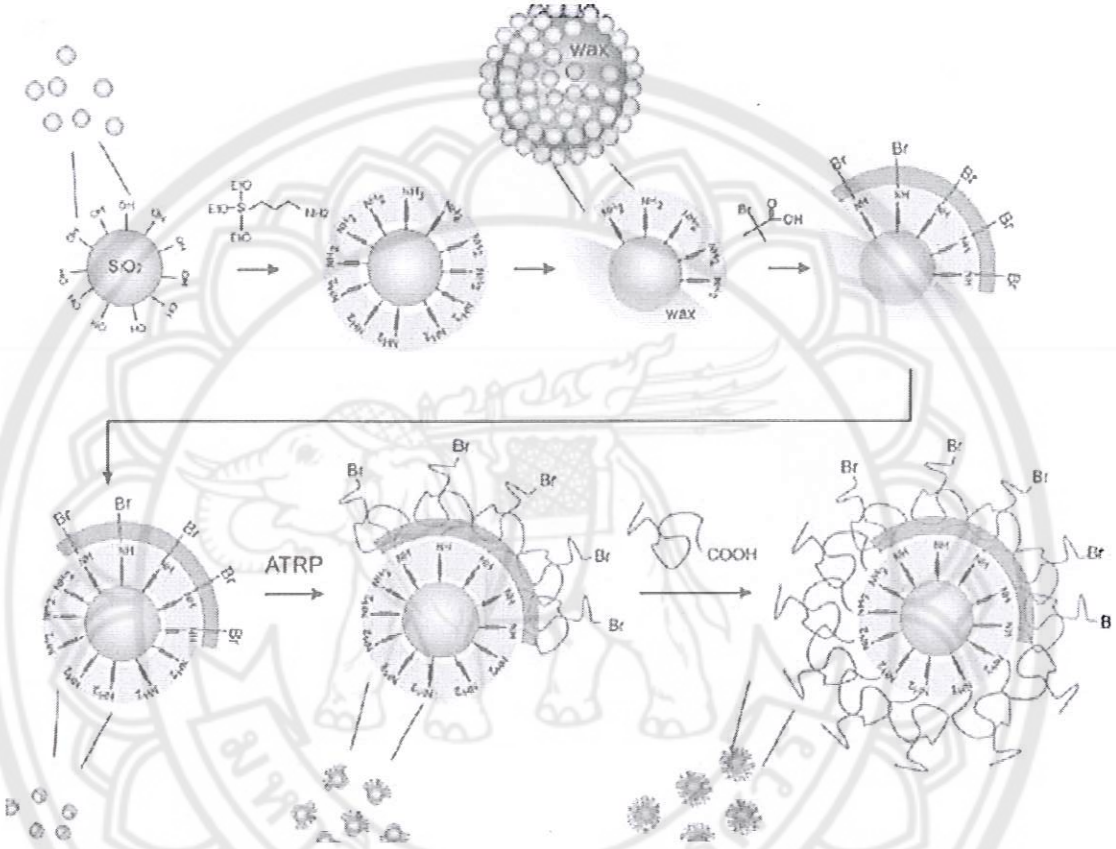

Figure 14 The synthesis of bicomponent Janus particles by "grafting from" and "grafting to" approaches [50]

Chen, et al. [51], have demonstrated a novel approach for preparing narrowly dispersed polymer/magnetite nanocomposite particles with well-controlled surface and particle size. In the first step, oleic acid-modified MNPs were synthesized *via* a co-precipitation method and then embedded into the polystyrene (PS) core by miniemulsion polymerization to obtain magnetic polystyrene lattices (MPL) (Figure 15). Then, PAA was then grafted on the MPL by photoemulsion polymerization to obtain the magnetic spherical polyelectrolyte brushes (MSPB). The brush thickness and the grafting density of PAA chains on the MPL surface were tunable by

can simultaneously block non-specific physical interactions of the remaining unreacted functional groups of the PAA brushes. The subsequent attachment of streptavidin was only through specific recognition of biotin. Thus, the problem of non-specific binding was greatly reduced. In addition, BSA as a polypeptide may also offer a biocompatible environment for immobilizing other biomolecules. This method can be readily expanded to immobilize a wide range of antigens or ligands for advanced biomedical applications.

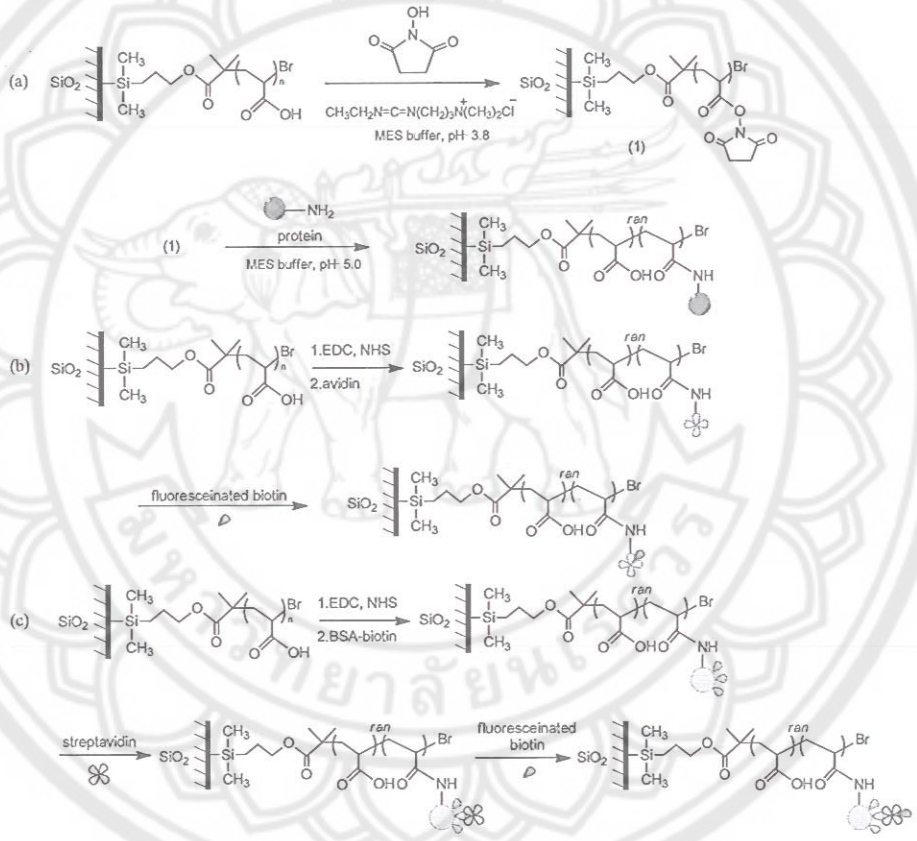

Figure 16 (a) BSA immobilization on PAA brushes by EDC/NHS coupling, (b) biotin immobilization on PAA brushes through avidin–biotin interaction and (c) biotin immobilization on PAA brushes using BSA as a linkage (EDC: *N*-(3-dimethylaminopropyl)-*N*-ethylcarbodiimide hydrochloride; NHS: *N*-(hydroxyl-succinimide) [17]

Furthermore, Rutnakornpituk, et al. [52], have presented a "grafting from" strategy to modify MNP surfaces with poly(*t*-BA) *via* ATRP, followed by a hydrolysis of *t*-BA groups to obtain PAA and finally immobilization of folic acid (FA) on their surfaces (Figure 17). FA was successfully activated with ethylene diamine (EDA) to obtain primary amine-terminated folic acid derivative. This logical strategy enhanced the reactivity of FA to efficiently react with carboxylic acid overexpressed on the surface of PAA-coated MNPs through amidization reaction. Moreover, PAA on MNP surface can also provide stabilization mechanisms through both steric and electrostatic repulsion. This novel nanocomplex was hypothetically viable to efficiently graft other affinity molecules on their surfaces and might be suitable for use as an efficient drug delivery vehicle particularly for cancer treatment.

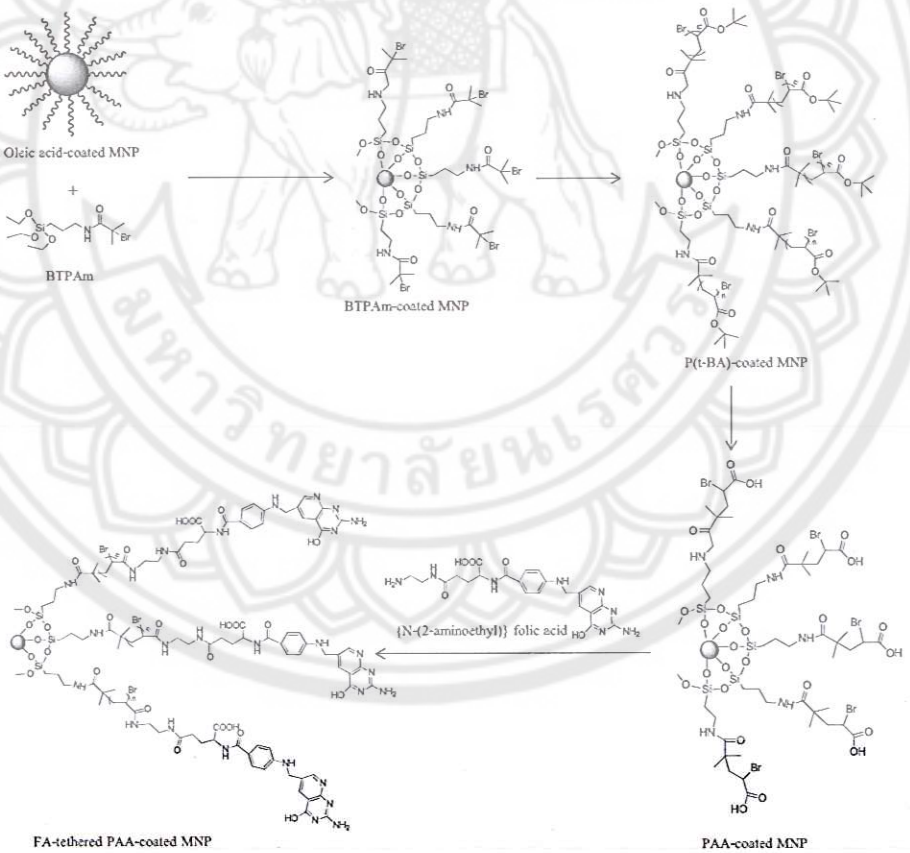

Figure 17 Surface functionalization of MNP with PAA and its immobilization with folic acid [52]

A class of pH-responsive zwitterionic diblock copolymers consisting of weak polyacids and polybases has also been proposed. Bo and coworker [53] have reported the synthesis of double hydrophilic block copolymer composed of PAA and poly(4-vinylpyridine) (P4VP) (PAA-*b*-P4VP) *via* ATRP method. Water-soluble micelles with PAA core and P4VP corona were observed at low (acidic) pH, while micelles with P4VP core and PAA corona were formed at high (basic) pH (Figure 18). Both types of PAA-*b*-P4VP micelles were used for encapsulation and two-way pH-induced release of hydrophobic anti-cancer metalloporphyrins. It was found that metalloporphyrins encapsulated by the micelles with PAA core and P4VP corona (formed at low pH) could be released upon increasing pH, while those entrapped by the micelles with P4VP core and PAA shell (formed at high pH) could be released upon decreasing pH. This behavior originated from the two-way pH-induced disruption of the PAA-*b*-P4VP micelles. Moreover, micelles with P4VP core were found to entrap a significantly larger amount of metalloporphyrins than the micelles with PAA core. This phenomenon was associated with the axial coordination between the transition metals of metalloporphyrins and the pyridine groups.

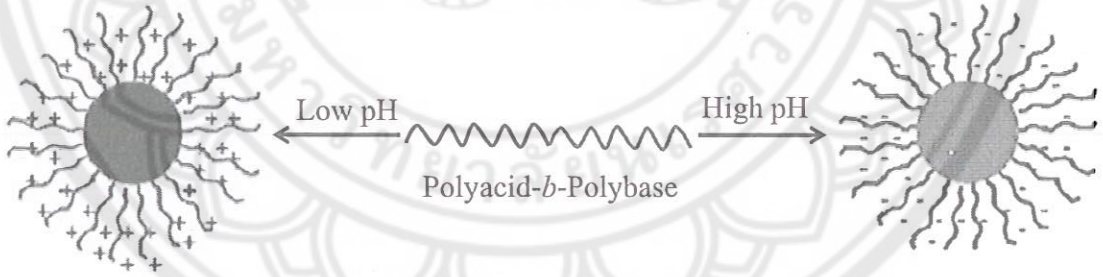

Figure 18 pH-modulated micellar self-assembly behavior of PAA-*b*-P4VP zwitterionic diblock copolymer [53]

CHAPTER III

RESEARCH METHODOLOGY

This chapter deals with the detailed methodology to modify MNP surface with PAA homopolymer or PAA/PEGMA copolymer with various molar ratios in order that the degree of negative charges on their surface can be tuned. The particles were prepared by a thermal decomposition reaction of iron(III) acetylacetonate, $(Fe(acac)_3$, as an iron precursor in benzyl alcohol to obtain narrow-size distribution nanoparticle. They were then surface modified using a "grafting from" strategy *via* atom transfer radical polymerization (ATRP) of *tert*-butyl acrylate (*t*-BA) and poly(ethylene glycol) methyl ether methacrylate (PEGMA), followed by deprotection of *t*-butyl groups of P(*t*-BA) in acidic dispersions to obtain poly(acrylic acid) (PAA)- or PAA/PEGMA-coated MNP. Molar ratio of PEGMA and PAA was adjusted to obtain various degrees of negative charge on the particle surface. Thus, a four-step method to prepare the surface-modified MNP is following;

1. Synthesis of MNP *via* thermal decomposition of $Fe(acac)_3$
2. Synthesis of 2-bromo-2-methyl- *N*-(3-(triethoxysilyl)propyl) propanamide (BTPAm)-coated MNP, the particle immobilized with an ATRP initiator
3. Synthesis of P(*t*-BA) homopolymer or P(*t*-BA)PEGMA copolymer on the MNP surface *via* ATRP (Figure 19)
4. Deprotection of *t*-butyl groups of P(*t*-BA) to obtain PAA homopolymer or PAA/PEGMA copolymer grafted on MNP surface (Figure 20)
5. Measurement of the numbers of carboxyl groups on the MNP surface

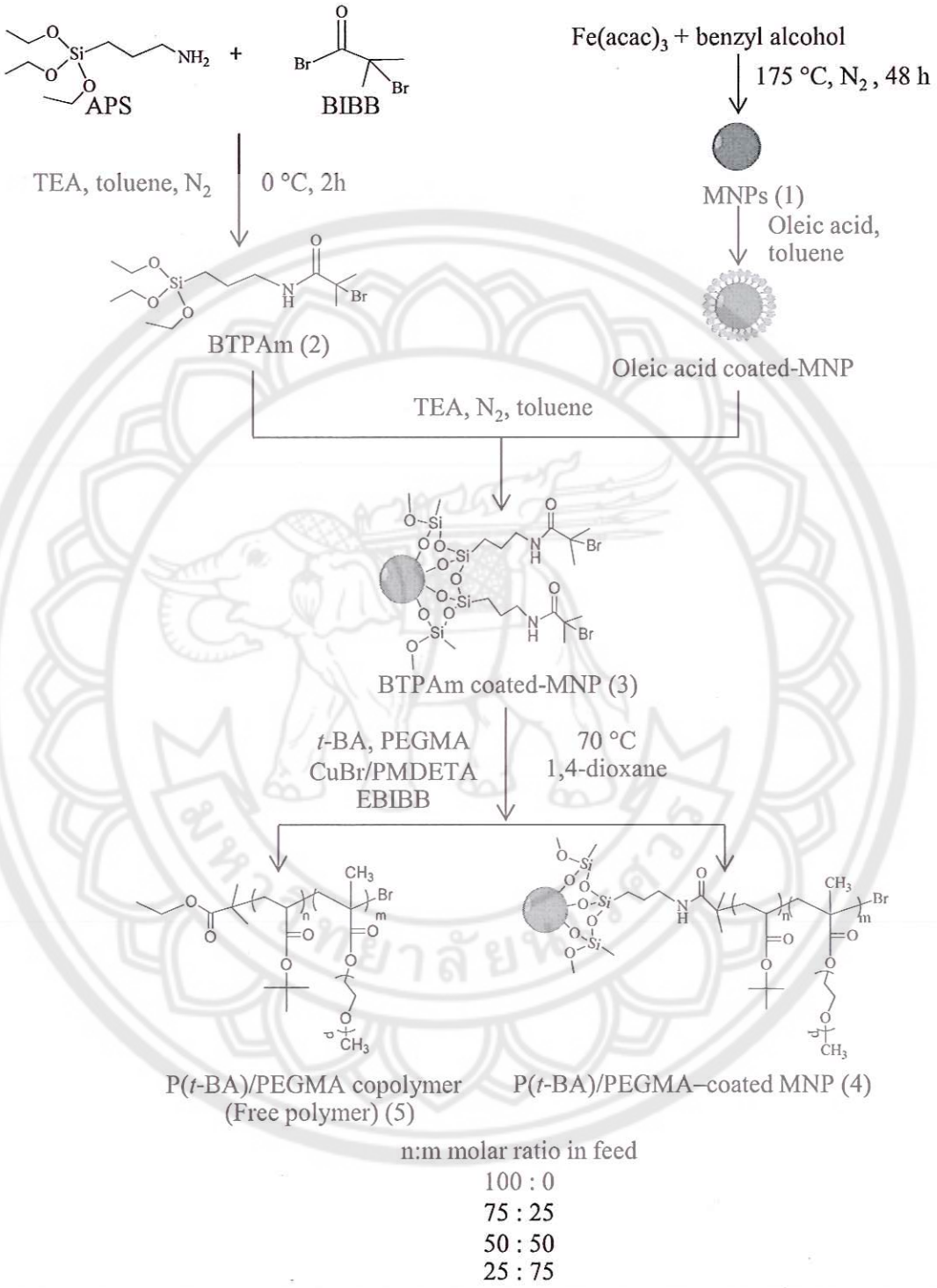

Figure 19 Synthesis of MNP grafted with P(*t*-BA) homopolymer or P(*t*-BA)/PEGMA copolymer

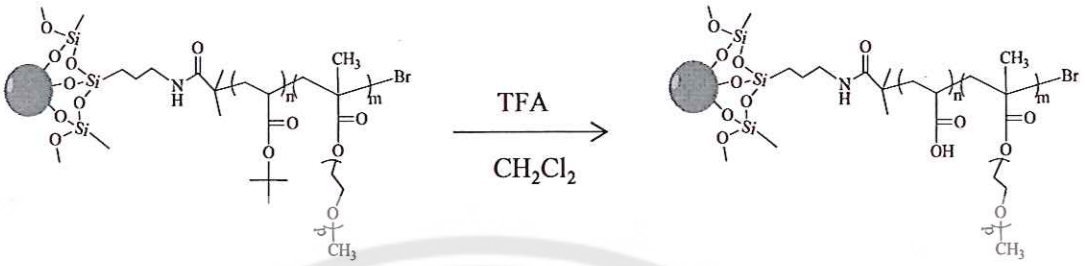

P(*t*-BA)/PEGMA–coated MNP PAA/PEGMA–coated MNP

Figure 20 Deprotection of *t*-BA groups in P(*t*-BA) grafted on MNP surface in acidic solution

Equipments

1. Magnetic stirrer (Fisher Scientific, United State of America)
2. Rotary Evaporator (Buchi B-171, Switzerland)
3. High vacuum pump (Edward)
4. Centrifuge (Scanspeed)
5. Mechanical stirrer (VELP Sciencetifica)
6. Ultrasonic (Branson 820006)
7. pH meter (HORIBA F-21)

Materials

1. 99% Iron (III) acetylacetonate ($Fe(acac)_3$) Acros
2. 98% Benzyl alcohol, Laboratory reagent
3. 99% 3-aminopropyl triethoxysilane (APS), Acros
4. 97% Triethylamine (TEA), Carto Erba
5. 98% 2-bromoisobutyryl bromide (BIBB), Acros
6. 98% ethyl-2-bromoisobutyrate (EBiB), Aldrich
7. 98% Copper (I) bromide (CuBr), Acros
8. 99% (*N,N,N′,N′′,N′′*-pentamethyldiethylenetriamine (PMDETA), Acros,
9. 99% stabilized *tert*-butyl acrylate (*t*-BA), Acros
10. Poly(ethylene glycol)methyl methacrylate (PEGMA), M_n = 300, Aldrich
11. 99.5% Dichloromethane, CH_2Cl_2, Merck
12. 99% extra pure Trifluoroacetic acid (TFA) $C_2HO_2F_3$, Acros

13. chloroform-d, 99.8 atom % D, $CDCl_3$, Aldrich
14. Toluene, A.R.grade, Lab Scan
15. 1,4-dioxane, A.R.grade, Lab Scan
16. Oleic acid, Fluka
17. *N,N*-dimethyl formamide (DMF), A.R.grade , Lab Scan

Methodology

1. Synthesis of magnetite nanoparticle (MNP)

MNP was synthesized following the procedure previously reported [54]. $Fe(acac)_3$ (5 g, 14.05 mmol) was thermally decomposed in benzyl alcohol (70 ml) at 175 °C under nitrogen atmosphere for 48 h. During this process, the initial red-brown color of the mixture changed to dark black, indicating the formation of MNP. Then, the resulting dark suspensions were precipitated by thoroughly washing with distilled ethanol and distilled CH_2Cl_2 and subsequently dried at room temperature *in vacuo*. The resultant products were obtained as black powder and were characterized using FT-IR. To prepare oleic acid-coated MNP dispersion in toluene, oleic acid (4 ml) was slowly dropped into the dispersion of MNP (0.8 g) in toluene (20 ml) and the mixture was ultrasonicated for 3 h under nitrogen atmosphere.

2. Synthesis of BTPAm-coated MNP, the particle immobilized with an ATRP initiator

BTPAm (Figure 19) was prepared by a coupling reaction between APS and BIBB. The solution of BIBB (0.1 ml, 0.8 mmol) in toluene (10 ml) was slowly added into the solution of APS (0.18 ml, 0.8 mmol) and TEA (0.12 ml, 0.8 mmol) in toluene (10 ml). The mixture was magnetically stirred for 2 h at 0°C under nitrogen atmosphere and then for another 24 h at room temperature. TEA salt, which was the reaction by-product, was precipitated out during the reaction. It was removed by filtration and the filtrate was evaporated to remove the unreacted TEA under reduce pressure.

The as-synthesized BTPAm was added in the dispersion containing oleic acid-coated MNP and TEA in toluene. The condensation of triethyloxysilane of BTPAm on the MNP surface was set at room temperature for 24 h under nitrogen

atmosphere. The suspension was precipitated in methanol and washed with toluene repeatedly to remove oleic acid and ungrafted BTPAm from the suspension and then dried at room temperature *in vacuo*. The resulting product appeared as fine black powder.

3. Surface-initiated atom transfer radical polymerization of P(*t*-BA) homopolymer or P(*t*-BA)/PEGMA copolymer on MNP (Figure 19)

In the present work, MNPs grafted with P(*t*-BA) homopolymer and P(*t*-BA)/PEGMA copolymer with various molar ratios of each composition (75:25, 50:50, 25:75 molar ratio of P(*t*-BA)/PEGMA, respectively) were prepared. An example for synthesizing 50:50 molar ratio of P(*t*-BA)/PEGMA on MNP surface was explained. Other copolymer-MNP complexes were prepared in a similar fashion with corresponding amounts of reagents used (Table 1). In the typical procedure, BTPAm-coated MNP (0.1 g), *t*-BA (1.45 ml, 0.01 mol), PEGMA (2.86 ml, 0.01 mol) and EBiB (0.03 ml, 0.0002 mol), used as an sacrificial initiator, were mixed in 1,4-dioxane (2.5 ml, 60%w/v) by ultrasonication for 15 min. Then, the mixture solution was degassed by ultrasonication for 10 min and it was again degassed by freeze-pump-thaw cycles. PMDETA (0.04 ml, 0.0002 mol), Cu(I)Br (0.03 g, 0.01 mol) and DMF (0.22 ml, 5%v/v), used as an internal standard, were added into the solution under nitrogen atmosphere, and it was then stirred at 90°C at a given time to commence ATRP reactions. The P(*t*-BA)/PEGMA-coated MNP was removed from the dispersion by precipitation with diethyl ether, centrifugation at speed of 35,000 rpm for 4 min together with the use of an external magnet and dried *in vacuo*.

Table 1 Molar ratio of the reagents used for copolymerization of P(*t*-BA) and PEGMA *via* ATRP from MNP surface

Reagent	Molar ratio of the reagent used (mol)			
	Types of the copolymer on MNP surface			
	100:0 P(*t*-BA)-PEGMA	75:25 P(*t*-BA)-PEGMA	50:50 P(*t*-BA)-PEGMA	25:75 P(*t*-BA)-PEGMA
P(*t*-BA)	100	75	50	25
PEGMA	-	25	50	75
CuBr	1	1	1	1
PMDETA	1	1	1	1
EBIB	1	1	1	1

4. Deprotection of *t*-butyl groups of P(*t*-BA) to obtain PAA homopolymer or PAA/PEGMA copolymer grafted on MNP surface (Figure 20)

P(*t*-BA)- or P(*t*-BA)/PEGMA-coated MNP (0.05 g) was re-suspended in CH_2Cl_2 (20 ml) containing 0.5 M TFA (0.742 ml). The mixture was then stirred at room temperature for 24 h. During the reaction, the resulting PAA- or PAA/PEGMA-coated MNP were gradually precipitated in CH_2Cl_2. They was washed with CH_2Cl_2 together with the use of an external magnet and dried *in vacuo*.

5. Measurement of –COOH groups on the MNP surface.

1.50 mg of the polymer-grafted MNP was dispersed in 5 ml of a 0.005 M NaOH solution with stirring. The aqueous dispersion was then titrated with 0.005 M HCl solution.

Characterization

1. Fourier transform infrared spectrophotometry (FTIR)

FTIR experiments were performed on a Perkin-Elmer Model 1600 Series FTIR Spectrophotometer. Solid samples were made by a pressed disc method after mixing dried solid samples with KBr.

2. Nuclear magnetic resonance spectroscopy (NMR)

^{1}H-NMR spectra were recorded by a Bruker AC 200-MHz spectrometer at room temperature in $CDCl_3$.

3. Transmission electron microscopy (TEM)

Samples for TEM analysis were prepared by drop-casting the samples onto a carbon coated copper grid and the images were taken using a Philips Tecnai 12 operated at 120 kV equipped with a Gatan model 782 CCD camera

4. Thermogravimetric analysis (TGA).

TGA thermograms were recorded on SDTA 851 Mettler-Toledo Toledo at the temperature ranging between 25 and 600°C at a heating rate of 20°C/min under oxygen atmosphere.

5. Vibrating sample magnetometry (VSM)

Magnetic properties of the particles were determined using a Standard 7403 Series at Lakeshore vibrating sample magnetometer (VSM).

6. Photocorrelation spectroscopy (PCS)

PCS was performed on NanoZS4700 nanoseries Malvern instrument at 25°C. The solvents were filtered using nylon syringe filters with a pore size of 0.2 μm before use. The dispersions were sonicated for 15 min before each measurement.

7. Gel permeation chromatography (GPC)

The apparent molecular weights and molecular weight distributions were measured by gel permeation chromatography (GPC) (Spectra System AS1000 autosampler) using THF as eluent at 35°C.

8. Conductometric titration

Determination of numbers of carboxylic groups on the particle surface was carried out using Seveneasy conductometer (Metter Toledo Bmblt 8603 Swchwerzenbach).

CHAPTER IV

RESULTS AND DISCUSSION

The aim of this work was to modify magnetite nanoparticle (MNP) surface with poly(*tert*-butyl acrylate) (P(*t*-BA)) homopolymer or P(*t*-BA)/poly(ethylene glycol) methyl ether methacrylate (PEGMA) copolymer *via* an atom transfer radical polymerization (ATRP) reaction using a "grafting-from" technique, followed by deprotection of *t*-butyl groups in an acidic dispersion to obtain poly(acrylic acid)(PAA) homopolymer or PAA/PEGMA copolymer-coated MNP. Molar ratio of PAA and PEGMA was tuned in order that various degrees of negative charges on the particle surface were obtained. Moreover, the polymers grafted on the particle surfaces are thought to provide both steric and electrostatic stabilizations and dispersibility of the particles in aqueous media due to the presence of the charges from PAA and polymeric brushes from PEGMA.

In the current work, MNP was first synthesized *via* a thermal decomposition reaction of $Fe(acac)_3$ to obtain narrow-size distribution nanoparticles. Then, an initiator for ATRP was covalently bonded onto the surface of the MNP through the combination of a ligand exchange reaction and a condensation of triethoxysilane to obtain the ATRP initiating sites on their surface, followed by a copper-mediate ATRP reaction of *t*-BA monomer or the mixture of *t*-BA and PEGMA oligomer to obtain P(*t*-BA) homopolymer or P(*t*-BA)/PEGMA copolymer, respectively, grafted on the MNP surface. PAA on the particle surfaces was obtained by deprotection of *t*-butyl groups of P(*t*-BA) in an acidic dispersion. The degree of negative charges due to the presence of carboxylate functional groups should be adjusted by varying the molar ratio of PAA to PEGMA in the reactions. Therefore, this chapter involves the detailed results and discussion in the following topics;

1. Synthesis of magnetite nanoparticle (MNP) (Figure 20)
2. Synthesis of BTPAm, an ATRP initiator, and its grafting onto MNP surface (Figure 24)

3. Synthesis of P(*t*-BA) homopolymer (Figure 26) and P(*t*-BA)/PEGMA copolymer initiated from MNP surface *via* ATRP reactions (Figure 28)

4. Deprotection of *t*-butyl groups of P(*t*-BA) to obtain PAA homopolymer or PAA/PEGMA copolymer grafted on MNP surface (Figure 36 and 37)

5. Measurement of the numbers of carboxyl groups on the MNP surface.

Synthesis of magnetite nanoparticle (MNP)

MNP was synthesized following the procedure previously reported [54]. $Fe(acac)_3$ was used as iron precursor and benzyl alcohol as a reducing agent and reaction solvent. Fe^{3+} of $Fe(acac)_3$ was partially reduced to Fe^{2+} by OH group in benzyl alcohol to obtain the mixture of Fe^{2+}/Fe^{3+} of magnetite (Fe_3O_4 or $Fe_2O_3.FeO$). During this process, the initial red-brown complex of $Fe(acac)_3$ changed to black upon heating to 175 °C for 48 h, indicating the formation of MNP. After removing the reaction by-product, the resultant black solid was characterized by FT-IR to elucidate its functional groups. According to FT-IR in Figure 21, a characteristic absorption peak of the Fe-O bond appears at 587 cm^{-1}. No signal of organic compounds was observed in the spectrum indicating the absence of organic moiety in bare MNP.

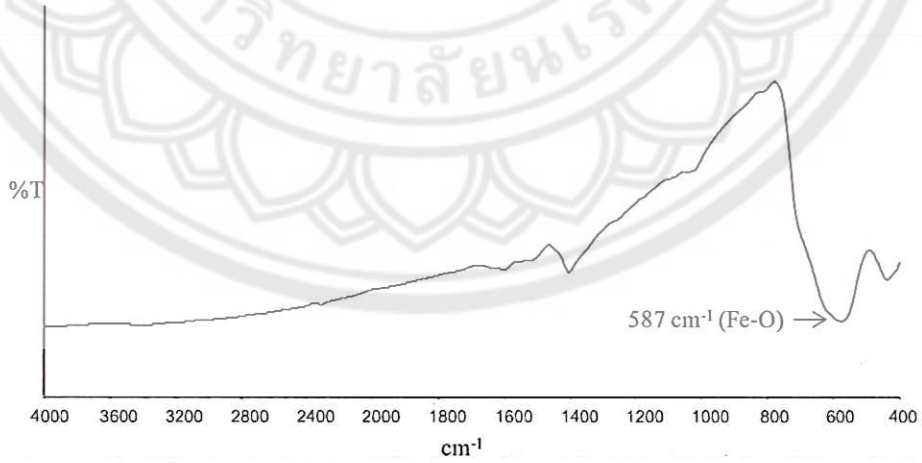

Figure 21 FT-IR spectrum of MNP synthesized *via* a thermal decomposition reaction of $Fe(acac)_3$ in benzyl alcohol

The as-prepared MNP was resuspended in toluene and it was directly cast on a TEM grid. It was found that the particles were well organized because they were somewhat uniformed in size and the particle size was in the range of 5-11 nm with the average of 7.78 ± 1.58 nm in diameter (Figure 22).

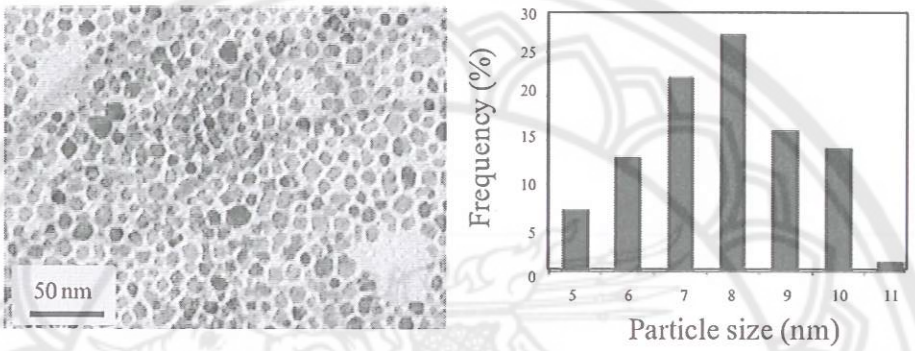

Figure 22 A TEM image of bare magnetite nanoparticle (MNP) and its size distribution

Synthesis of BTPAm, an ATRP initiator, and its grafting onto MNP surface

BTPAm, an ATRP initiator, was prepared by a coupling reaction between aminopropyl triethoxysilane (APS) with 2-bromoisobutyryl bromide (BIBB) through an amidization reaction. Functional groups and chemical structure were characterized *via* FT-IR (Figure 23) and ^{1}H-NMR (Figure 24), respectively.

Figure 23 shows FT-IR spectra of APS (Figure 23A), BIBB (Figure 23B) and BTPAm (Figure 23C). According to Figure 23C, the spectrum of BTPAm exhibits its characteristic signals of Si-O stretching at 1112-1026 cm^{-1}, of N-H bending at 1532 cm^{-1}, N-H- stretching at 3345 cm^{-1} and -NH-CO- carbonyl stretching at 1658 cm^{-1}. These characteristic signals well correspond to FT-IR spectra of APS (Figure 23A) and BIBB (Figure 23B). All assigned functional groups of BTPAm were detailed in Table 2.

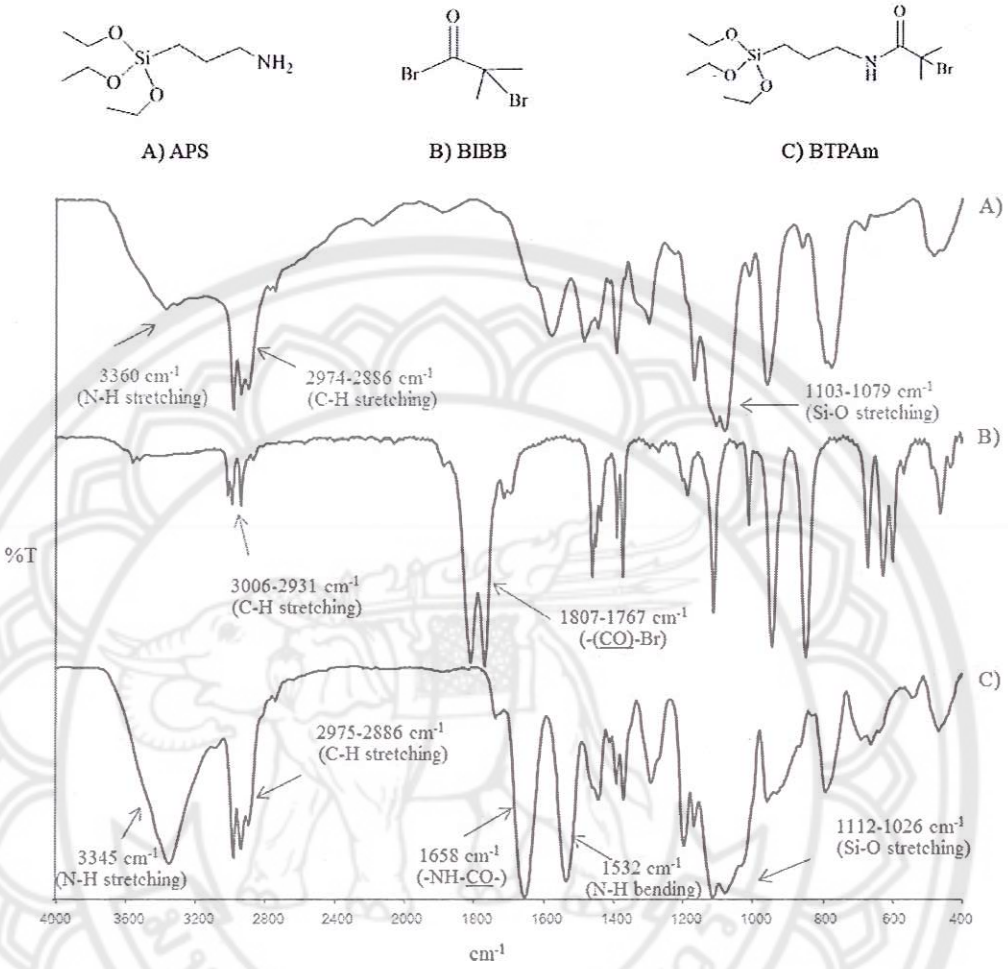

Figure 23 FT-IR spectra of A) 3-aminopropyl triethoxysilane (APS), B) 2 bromoiso-butyryl bromide (BIBB) and C) 2-bromo-2-methyl-*N*-(3-triethoxysilyl) propanamide (BTPAm)

Table 2 Functional group annotation of BTPAm (Figure 23)

Wavenumber (cm^{-1})	Designated functional groups
3345	N-H stretching
2975-2886	C-H stretching
1658	Amide (-(NH)-(CO) stretching
1532	N-H bending
1112-1026	Si-O stretching

Figure 24 shows ^{1}H NMR spectrum of BTPAm in comparison with APS (Figure 24A) and BIBB (Figure 24B) starting reagents. In good agreement with FT-IR results, a distinctive shift of the ^{1}H NMR signal corresponding to methylene protons adjacent to NH group (from 2.50 ppm of signal *a* to 3.22 ppm of signal *a'*) indicated the formation of BTPAm. In addition, slight shifts of other signals such as methylene protons of signal *b* (1.45 ppm) to signal *b'* (1.62 ppm), and methyl protons of signal *f* (2.50 ppm) to signal *f'* (2.40 ppm) also confirmed the formation of BTPAm.

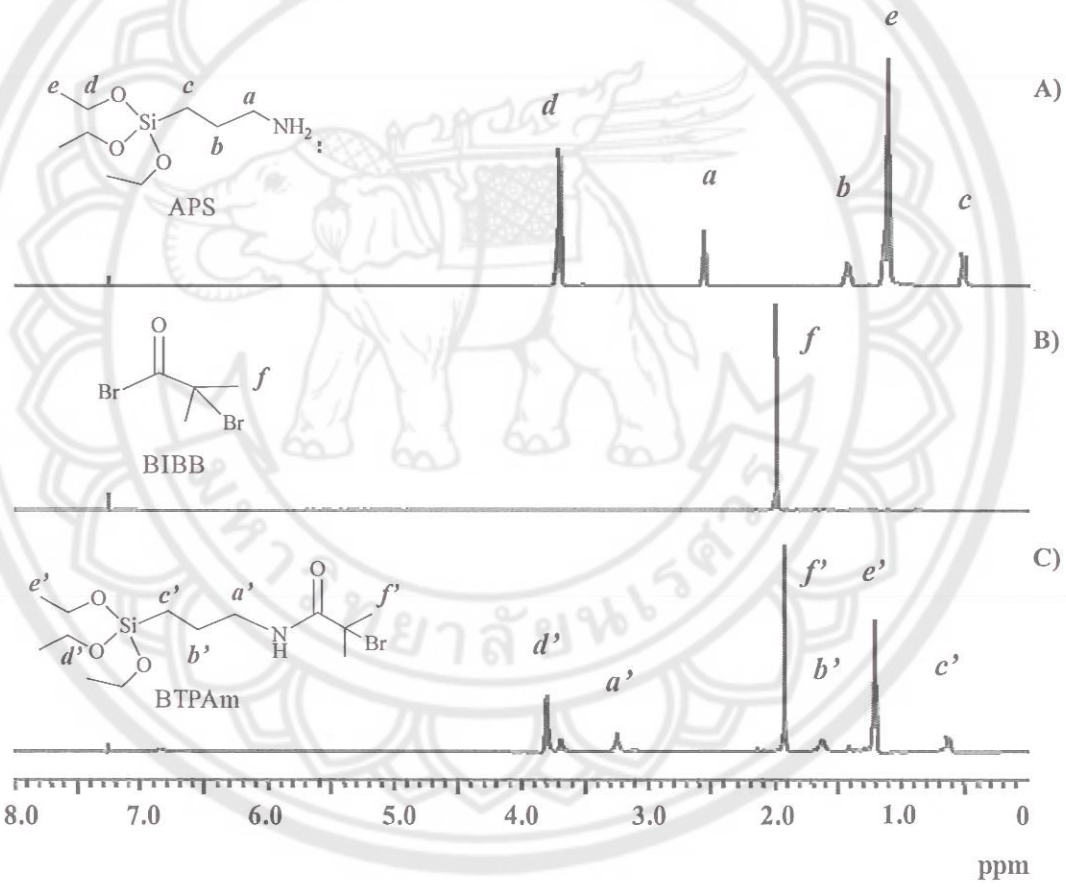

Figure 24 ^{1}H NMR spectra of A) 3-aminopropyl triethoxysilane (APS), B) 2-bromoisobutyryl bromide (BIBB) and C) 2-bromo-2-methyl-*N*-(3-triethoxysilyl) propanamide (BTPAm) (solvent; $CDCl_3$)

To immobilize the as-synthesized BTPAm onto MNP surface, bare MNP was first coated with oleic acid to form dispersible MNP in toluene. BTPAm was then

covalently bonded onto the oleic acid-coated MNPs through the combination of a ligand exchange reaction and condensation of triethoxysilane to obtain the particle with ATRP initiators on its surface.

The functional groups of BTPAm-coated MNP were performed using an FT-IR technique. Comparing with the FT-IR spectra of MNP (Figure 25A) and BTPAm (Figure 25B), Figure 25C exhibits FT-IR characteristic absorption peaks of BTPAm-coated MNP; 1648 cm^{-1} (-NH-CO- carbonyl stretching), 1111-1019 cm^{-1} (Si-O stretching), 1529 cm^{-1} (N-H bending) and 3341 cm^{-1} (N-H stretching) (Figure 25C). In combination with a strong and broad signal of Fe-O bonds (586 cm^{-1}), this evidenced that BTPAm was complexed to MNP surfaces. All designated functional groups of BTPAm-coated MNPs were detailed in Table 3.

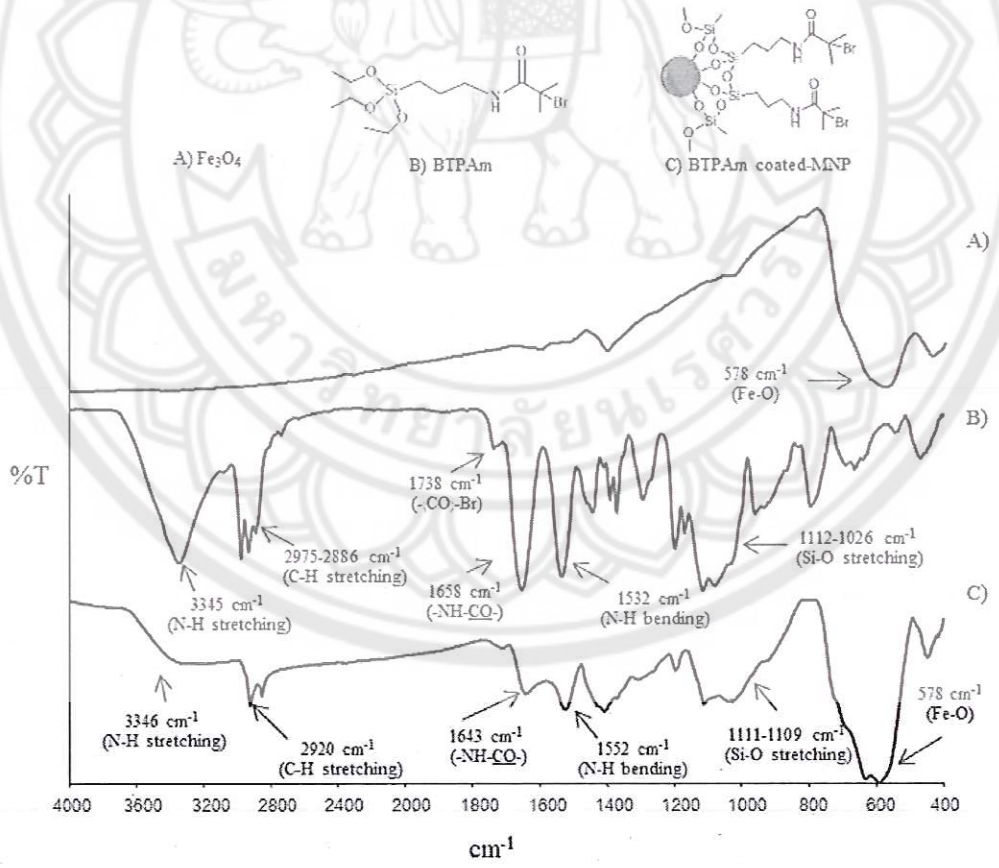

Figure 25 FT-IR spectra of A) bare MNP, B) BTPAm and C) BTPAm-coated MNP

Table 3 Functional group annotation of BTPAm-coated MNP (Figure 25)

Wavenumber (cm^{-1})	Designated functional groups
3345	N-H stretching
2920-2852	C-H stretching
1643	-NH-CO- (amide) stretching
1552	NH bending
1111-1019	Si-O stretching
578	Fe-O

Figure 26 depicts a TEM image of the particles coated with BTPAm and their size distribution. The particle size ranged between 5-11 nm with an average diameter of 8.18 ± 1.50 nm.

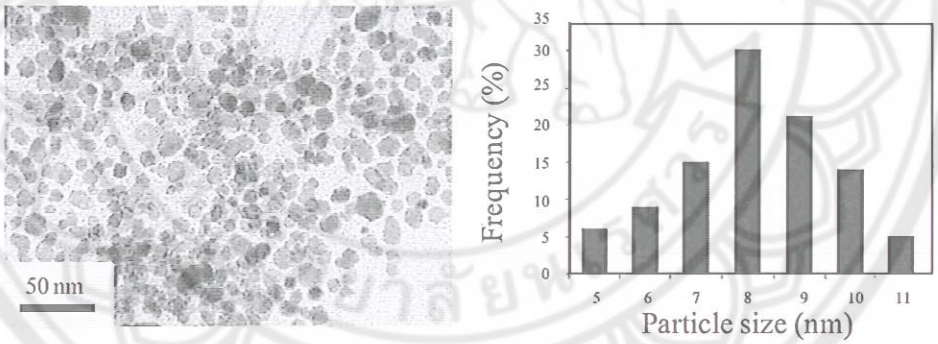

Figure 26 A TEM image of BTPAm-coated MNP and its size distribution

Synthesis of P(*t*-BA) homopolymer and P(*t*-BA)/PEGMA copolymer initiated from MNP surface *via* ATRP reactions

1. Synthesis of P(*t*-BA) homopolymer initiated from MNP surface *via* ATRP reactions

BTPAm, the ATRP active species grafted on the particle surfaces, was thought to be able to trigger ATRP reaction. Reactivation of the dormant species enabled for P(*t*-BA) chains to gradually, but steadily, grow again. It is thus

hypothesized that controlled molecular weight and low polydispersity index of P(*t*-BA) on MNP surfaces should be gained. However, P(*t*-BA) grafted on the particle surface was not detectable *via* NMR technique due to inherent magnetic properties of MNP; utilization of "sacrificial initiator" was adopted to monitor the reaction progress. In the present work, EBiB was selected as a sacrificial initiator. Therefore, it is hereafter assumed that the propagating rate of the polymer from an EBiB free initiator and BTPAm, the MNP-supported initiator, were comparable. It is hence assumed that molecular weight and molecular weight distribution of the free polymer initiated from the sacrificial initiator and the polymer grafted on the particle surface were comparable.

The structure of the obtained P(*t*-BA) was confirmed by ^{1}H NMR spectroscopy. The sample was removed from the reaction without removal of *t*-BA monomer; the signals of the monomer were thus observed in the spectrum. From Figure 27, distinctive shifts of ^{1}H NMR signals corresponding to the protons on the backbone chain indicated the formation of P(*t*-BA), such as the shifts from 6.05-5.99 ppm of signal *c* to 2.16 ppm of signal *c'*, from 5.70 ppm of signal *b* and 6.28 ppm of signal *d* to 1.75 ppm of signal *b'*. In addition, a slight shift of methyl protons of signal *a* (1.48 ppm) to signal *a'* (1.46 ppm) also confirmed the formation of P(*t*-BA).

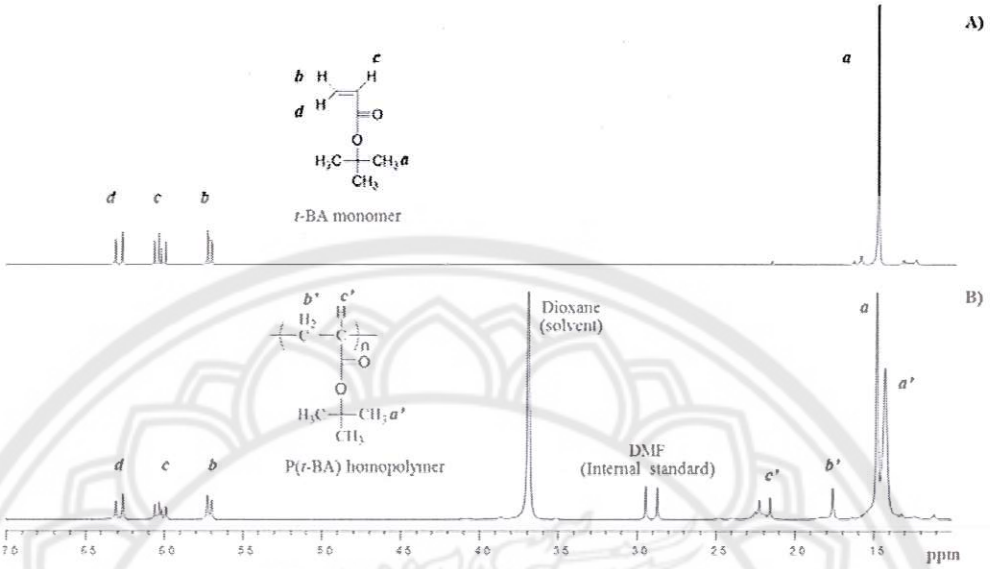

Figure 27 ^{1}H NMR spectra of A) *t*-BA monomer and B) P(*t*-BA) homopolymer prepared *via* ATRP in dioxane with the use of DMF as an internal standard (solvent; $CDCl_3$)

The conversion *vs* time plot of P(*t*-BA) homopolymer (100/0 of P(*t*-BA)/PEGMA) is illustrated in Figure 28. It was determined from ^{1}H NMR spectra and can be calculated from the following equation (1);

$$\% \text{ Conversion} = \left(1 - \frac{[M_t]}{[M_O]}\right) \times 100 \qquad (1)$$

Where $[M_0]$ = integration ratio of the monomer peak / DMF peak at initial time ($t = 0$)

$[M_t]$ = integration ratio of the residual monomer peak / DMF peak at time t.

Examples of NMR spectra at various ATRP reaction times and the calculation of percent conversions are illustrated in Appendix A. Kinetic studies of the polymerization of P(*t*-BA) homopolymer (100/0 of P(*t*-BA)/PEGMA) were plotted as a function of reaction time to exhibit that the reaction was initially fast and its propagation rate decreased after 4 h of the reaction (240 min) (Figure 28). The first-order reaction during first 4 h of ATRP reaction corresponding to 52 % reaction conversion, indicating a constant concentration of active radical species. Moreover,

the rate of monomer conversion started to deviate from linearity at higher monomer conversion (after 48 h reaction), indicating the presence of irreversible terminations.

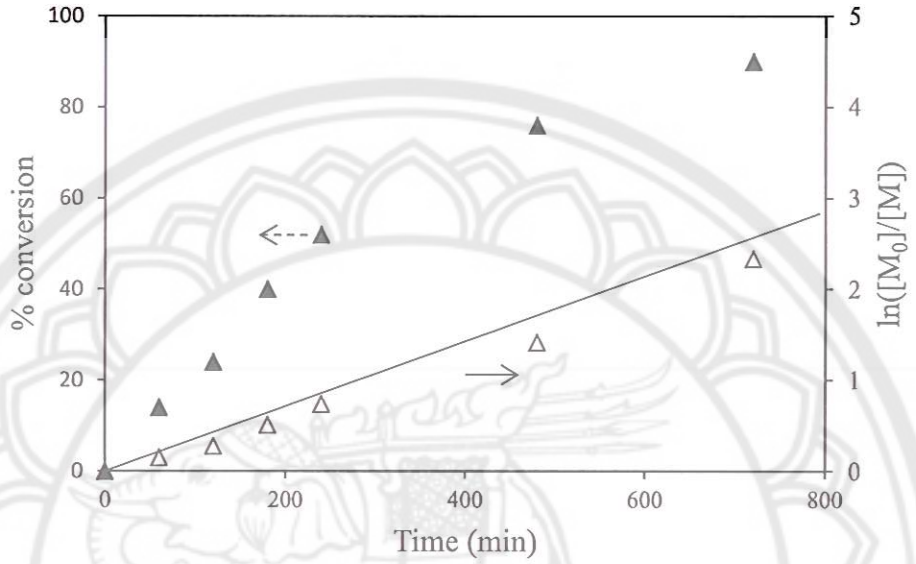

Figure 28 Kinetic plots of ATRP of P(*t*-BA) homopolymer; % conversion *vs* time plot (▲) and ln([M_0]/[M]) *vs* time plot (Δ)

Figure 29 shows an FT-IR spectrum of P(*t*-BA)-coated MNP (Figure 28C) comparing with those of BTPAm-coated MNP (Figure 29A) and *t*-BA monomer (Figure 29B). The success of grafting the P(*t*-BA) homopolymer was indicated from the presence of a sharp and strong carbonyl signal at 1729 cm^{-1} (-CO-O- stretching). In addition, the vibration of *t*-butyl groups in P(*t*-BA) as indicated by a doublet at 1390 and 1365 cm^{-1} (C-H bending) is also clearly observed in the spectrum, indicating the existence of the polymer in the complexes. Moreover, a broad and strong characteristic signal of Fe-O bonds from MNP cores was obviously apparent (598 cm^{-1}). All assigned functional groups of *t*-BA monomer were detailed in Table 4 and those of P(*t*-BA)-coated MNP were shown in Table 5.

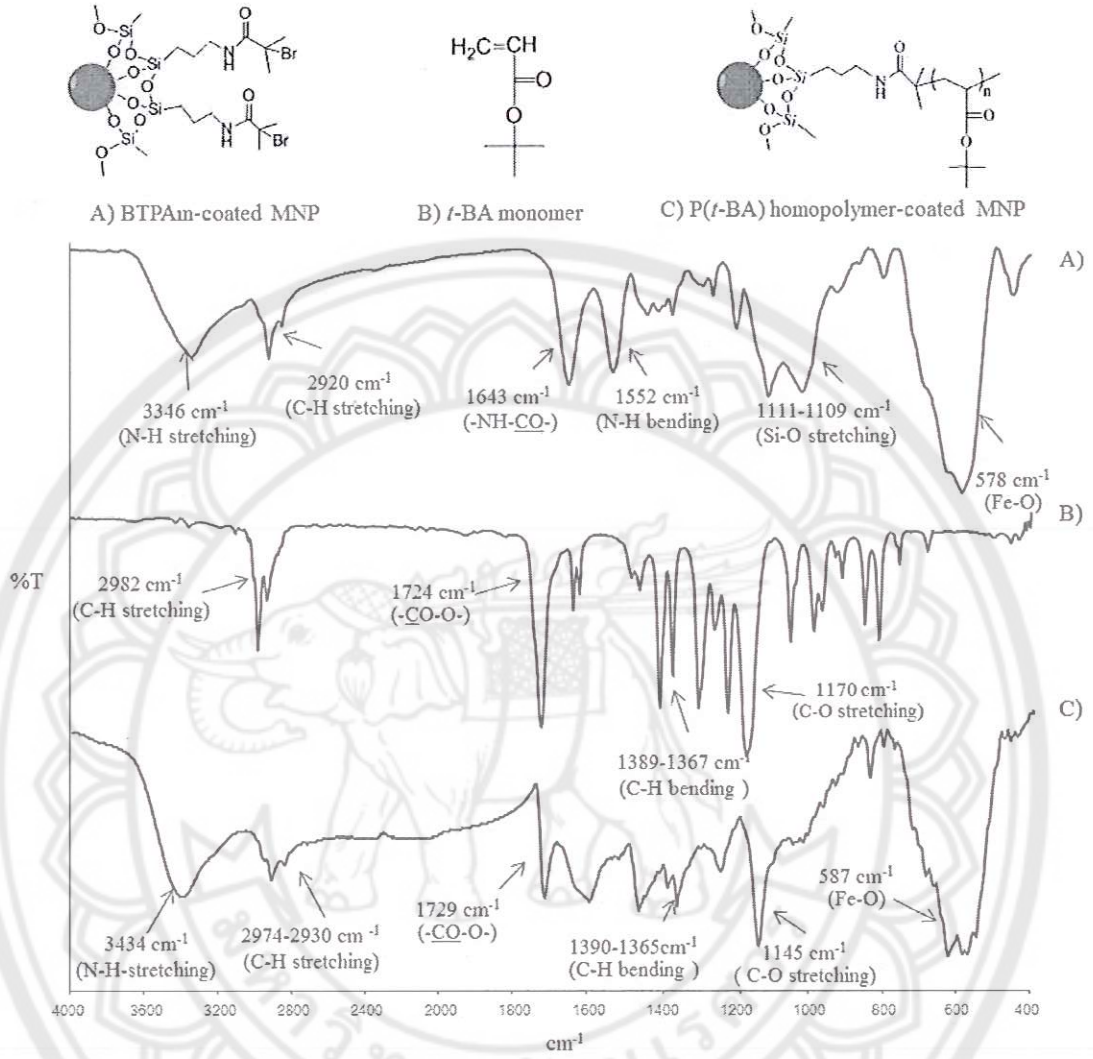

Figure 29 FT-IR spectra of A) BTPAm-coated MNP, B) *t*-BA monomer and C) P(*t*- BA) homopolymer-coated MNP

Table 4 Functional group annotation of *t*-BA monomer (Figure 29B)

Wavenumber (cm^{-1})	Designated functional groups
2982	C-H stretching
1724	-(CO)-O- (ester) stretching
1389-1367	C-H bending

Table 5 Functional group annotation of P(*t*-BA)-coated MNP (Figure 29C)

Wavenumber (cm^{-1})	Designated functional groups
3434	N-H stretching
2982	C-H stretching
1729	-(CO)-O- (ester) stretching
1390-1365	C-H bending
587	Fe-O

A TEM image of P(*t*-BA)-coated MNPs was depicted in Figure 30. The particle size was in the range of 5-11 nm with the average of 8.28 ± 1.42 nm in diameter. It should be noted that P(*t*-BA)-coated MNPs were not well dispersible in water due to the presence of hydrophobic P(*t*-BA) coating on the particle surface: the TEM sample was thus prepared from MNP-toluene dispersion.

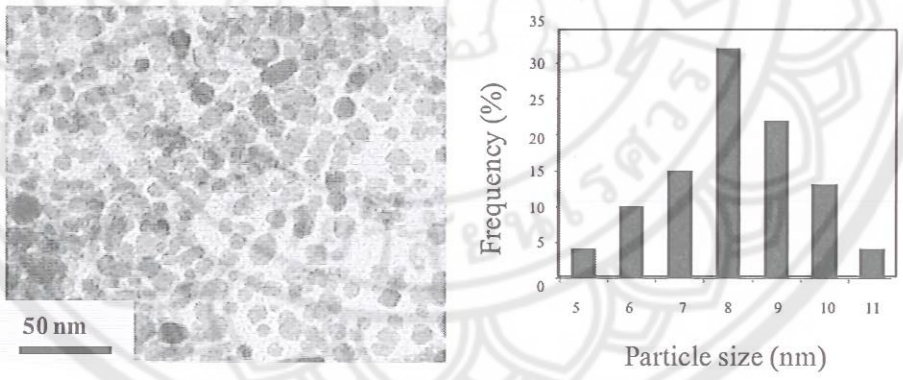

Figure 30 A TEM image of P(*t*-BA)-coated MNP and its size distribution. The TEM sample was prepared from MNP-toluene dispersion

2. Synthesis of P(*t*-BA)/PEGMA copolymers initiated from MNP surface *via* ATRP reactions

In this section, P(*t*-BA) and PEGMA with various molar compositions (75/25, 50/50 and 25/75, respectively) were statistically copolymerized on MNP surface *via* ATRP reaction. PEGMA on MNP surface allows the particles to well

suspend in water, while P(*t*-BA) was used as a precursor of poly(acrylic acid)(PAA). Direct synthesis of well-defined PAA brushes have not far been achieved by ATRP due to the chelating capacity of the monomer to the metal catalyst, resulting in deactivation of the catalyst [55]. Therefore, in this work, surface-initiated ATRP of P(*t*-BA)/PEGMA copolymer was first performed and *t*-butyl groups in P(*t*-BA) moiety on MNP surface would be then deprotected to eventually obtain PAA/PEGMA-grafted MNP.

In ATRP reactions, P(*t*-BA)/PEGMA copolymer grafted on MNP was prepared in a similar fashion to those of P(*t*-BA) homopolymer grafted on MNP with corresponding amounts of reagents used (Table 1/chapter III). The structural characterization of the obtained P(*t*-BA)/PEGMA copolymers was confirmed by ^{1}H NMR spectroscopy. A representative ^{1}H NMR spectrum is demonstrated in Figure 31. The shifts of signal *a* (5.72-5.75 ppm) and *b* (6.27-6.34 ppm) of *t*-BA monomers and signal *e* (5.58 ppm) and *f* (6.14 ppm) of PEGMA to signal *a'* and *e'* of methylene protons in the backbone indicated the formation of the copolymer. In addition, the shifts of signal *c* (5.99-6.08 ppm) to *c'* (2.18 ppm) and signal *g* (1.96 ppm) to *g'* (1.26 ppm) also confirmed the occurrence of the copolymerization. In good agreement with this, the appearance of signal *d'* of methyl protons in *t*-butyl groups in P(*t*-BA) (spectra C, D and E) also designated the formation of the copolymer.

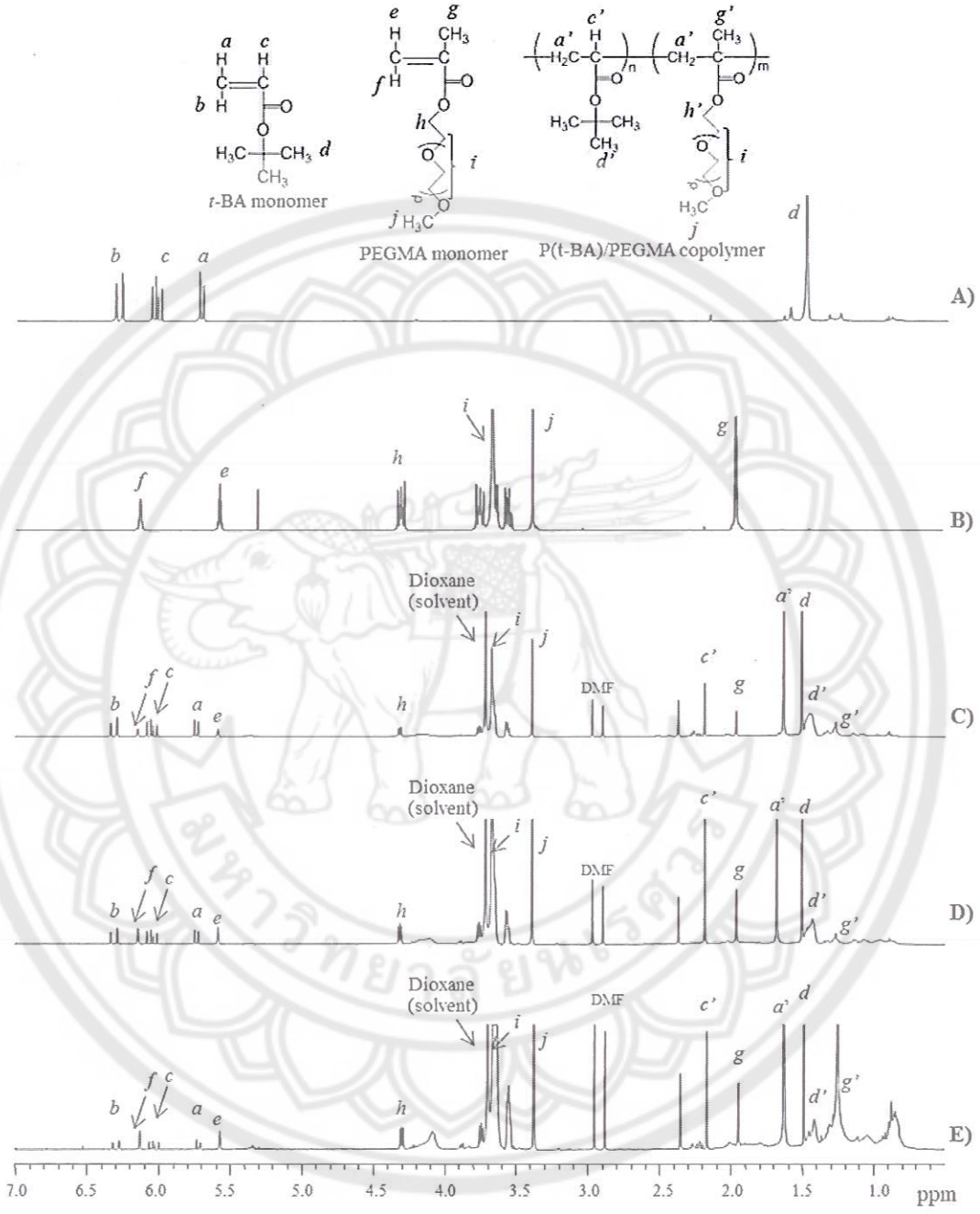

Figure 31 ^{1}H NMR spectra of A) *t*-BA monomer, B) PEGMA, P(*t*-BA)/PEGMA copolymer prepared *via* ATRP in dioxane with the use of DMF as an internal standard, having molar ratio of P(*t*-BA)/PEGMA C) 75/25, D) 50/50 and E) 25/75 (solvent: $CDCl_3$)

Percent monomer conversion of the copolymerization having different molar ratio of P(*t*-BA)/PEGMA was determined from ^{1}H NMR spectra using the procedure similarly to those of the P(*t*-BA) homopolymer. Figure 32-34 show individual monomer conversion and first-order kinetic plots using an equimolar monomer feed; P(*t*-BA)/PEGMA molar ratios are 75/25, 50/50 and 25/75, respectively. From all three copolymerizations, it can be seen that P(*t*-BA) and PEGMA were consumed rapidly at the beginning period and slow at the ending period during the copolymerization. It was apparent that PEGMA was consumed more quickly than P(*t*-BA) as indicated by the higher monomer conversion of PEGMA than that of P(t-BA) at the same reaction time. For example, in the copolymerization of P(*t*-BA)/PEGMA copolymer with 75/25 molar ratio, the conversion of PEGMA was 88%, while that of P(t-BA) was only 64% at 3 h of ATRP reaction (Figure 32).

In all cases, the consumption rate of PEGMA followed the first-order reaction only a short period of time with high monomer conversions as compared to that of P(*t*-BA), indicating the high reactivity of PEGMA in the reaction. For instance, in Figure 33, the consumption rate of PEGMA obeyed the first-order relationship during first 2 h of ATRP, corresponding to 78% monomer conversion, whereas those of P(*t*-BA) showed the first-order reaction during 3 h, corresponding to 64% monomer conversion. When the reaction was prolonged, the monomer consumption deviated from linearity, indicating that the rate of the ATRP was not directly proportional to the monomer concentration. This was probably due the premature termination of active radicals during the copolymerization due to the decrease of the monomer concentration. This phenomenon could be confirmed by the rather broad polydispersity indices for a controlled/living radical polymerization (Table 6).

In addition, it was also observed that increasing PEGMA molar ratio in the copolymer seemed to promote the rate of ATRP reaction. For example, at 2 h of ATRP reaction, PEGMA conversions reached 58% in the 75/25 P(*t*-BA)/PEGMA copolymer and, when PEGMA content in the copolymer increased, PEGMA conversions was 78% in the case of 50/50 P(t-BA)/PEGMA copolymer and 91% in the case of 25/75 P(*t*-BA)/PEGMA copolymer. The accelerated rate of monomer conversion was also observed in P(*t*-BA) as increasing PEGMA composition in the

copolymer. This was attributed to the increase of the solution polarity due to the increment of PEGMA concentrations in the mixture, resulting in the suitable reaction condition for the proceeding of copolymerization obtained.

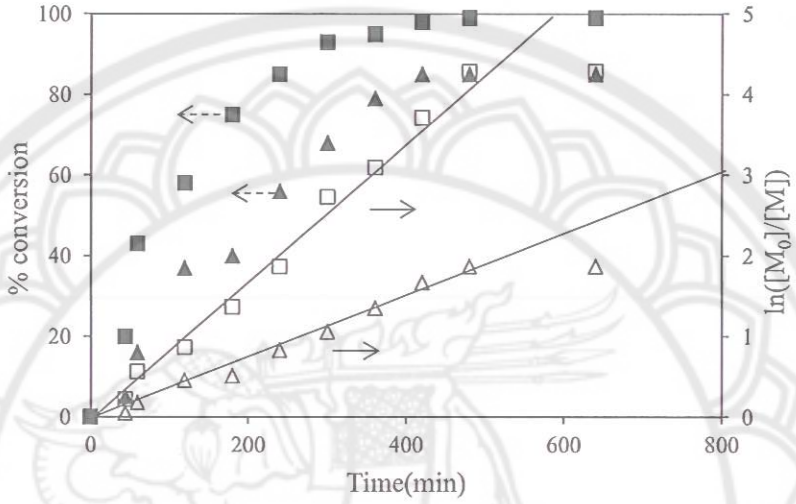

Figure 32 The percent conversion *vs.* time plots and ln([M_0]/[M]) *vs.* time plots of ATRP of P(*t*-BA)/PEGMA copolymer (75/25 molar ratio); P(*t*-BA) (▲, △) and PEGMA (■, □)

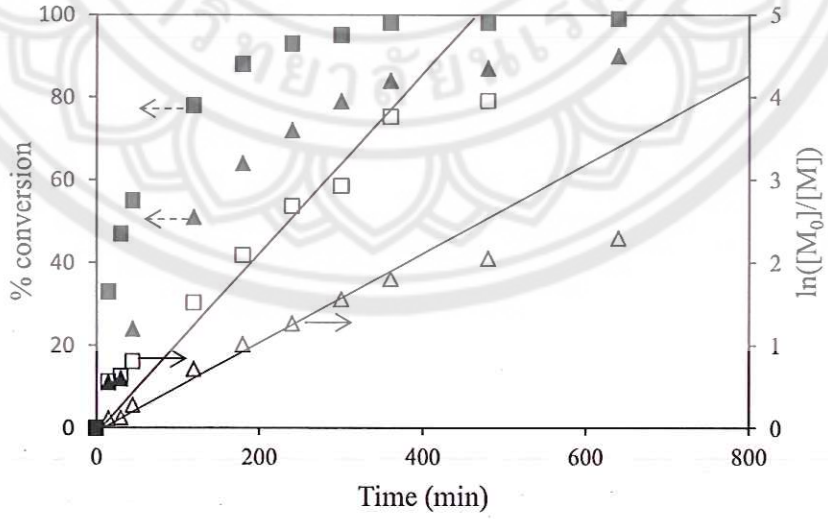

Figure 33 The percent conversion *vs.* time plots and ln([M_0]/[M]) *vs.* time plots of ATRP of P(*t*-BA)/PEGMA copolymer (50/50 molar ratio); P(*t*-BA) (▲, △) and PEGMA (■, □)

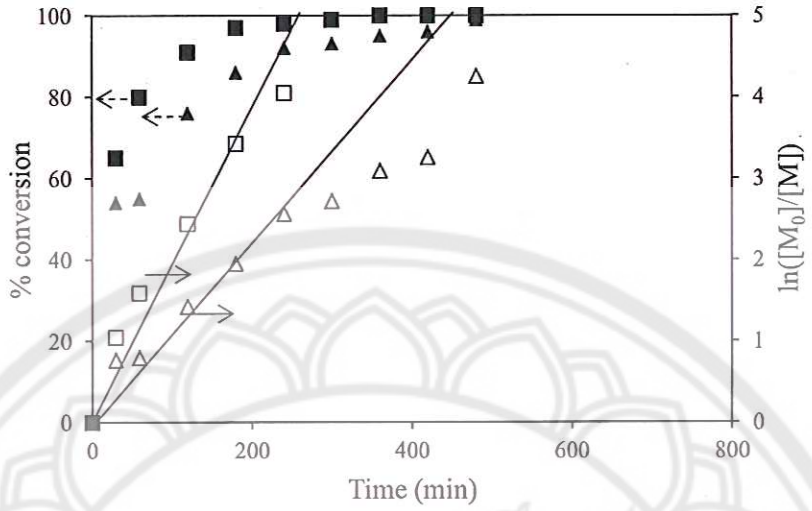

Figure 34 The percent conversion *vs.* time plots and ln([M_0]/[M]) *vs.* time plots of ATRP of P(*t*-BA)/PEGMA copolymer (25/75 molar ratio); P(*t*-BA) (▲, △) and PEGMA (■, □)

Table 6 reports the molecular weight ($\overline{M}_n$) and the molecular weight distribution (Polydispesity index, PDI) of P(*t*-BA)/PEGMA copolymer (50/50 molar ratio) at four different time intervals during the ATRP copolymerization. It was found that $\overline{M}_n$ gradually increased as the reaction conversions increased, indicating the growth of the copolymer chains, and this was also confirmed from GPC results. Their experimental $\overline{M}_n$ (from GPC) at different time intervals were comparable to those of the theoretical ones calculated according to the equation shown in the footnote of Table 6 and an example of the calculation is illustrated in Appendex A.

Table 6 Monomer conversion, molecular weight and molecular weight distribution of P(*t*-BA)/PEGMA copolymer (50/50 molar ratio) using $[P(t\text{-BA})]_0/[PEGMA]_0/[EBiB]_0/[CuBr]_0/[PMDETA]_0$ in 50/50/1/1/1 molar ratio in 1,4-dioxane at 90 °C

Entry	Reaction time (h)	Conversion [a]		$\overline{M}_n$ [b](exp) (g/mol)	$\overline{M}_n$ [c](theo) (g/mol)	PDI[b]
		P(t-BA)	PEGMA			
1	0.25	11	33	5,898	5,655	1.3
2	0.75	24	55	13,604	9,788	1.5
3	2	51	78	18,300	14,968	1.6
4	4	72	93	21,419	18,564	1.8

[a]Determined from ^{1}H NMR spectroscopy (monomer depletion monitored relative to DMF, which was used as an internal standard). [b]Measured *via* GPC (calibrated with polystyrene standard). [c] $\overline{M}_{n,th} = ([P(t\text{-BA})]_0/[EBiB]_0 \times conv._{P(t\text{-BA})} \times M_{P(t\text{-BA})}] + ([PEGMA]_0/[EBiB]_0 \times conv._{PEGMA} \times M_{PEGMA}])$ (The calculation is shown in Appendix A)

Table 6 summarizes the percent conversion and the estimated composition of each copolymer that would be then used for further studies. The ATRP reactions were ceased at a given time corresponding to the selected percent conversion (Figure 28, 32, 33 and 34). These selected conversions were based on the fact that their conversions were less than 65% in order to lessen feasible reaction termination due to the depletion of monomer concentration in the mixture. Copolymer compositions were calculated from the feed composition of the monomers and taking its percent conversion into account. Thus, % P(*t*-BA) in the copolymer was estimated from the following equation:

$$\%\ P(t\text{-BA})\ \text{in the copolymer} = \frac{[\%\ Conv._{P(t\text{-BA})} \times \%\ feed_{t\text{-BA}}]}{[\%\ Conv._{P(t\text{-BA})} \times \%\ feed_{t\text{-BA}} + \%\ Conv._{PEGMA} \times \%\ feed_{PEGMA}]}$$

where $\%conv._{P(t\text{-BA})}$ is %conversion of P(*t*-BA)

$\%Conv._{PEGMA}$ is %conversion of PEGMA

$feed_{PEGMA}$ is molar of PEGMA in feed

$feed_{t\text{-BA}}$ is molar of *t*-BA in feed

Percent PEGMA in the (co)polymer was calculated in a similar fashion and the results were shown in Table 7. It was found that P(*t*-BA)/PEGMA molar ratios in the copolymers were comparable to the feed compositions. Interestingly, percentage of PEGMA in the copolymers was found to be slightly higher than its percent feeding in every composition. This result agrees well with the conversion *vs* time plots (Figure 32-34) indicating the higher reaction reactivity of PEGMA than that of P(*t*-BA).

Table 7 Reaction conversions and the compositions of P(*t*-BA)/PEGMA copolymer for use in further studies

Type of copolymer	% Conversion[a] of		% in the copolymer[b]	
	P(*t*-BA)	PEGMA	P(*t*-BA)	PEGMA
100:0 P(*t*-BA)/PEGMA	52	0	100	0
75:25 P(*t*-BA)/PEGMA	37	58	66	34
50:50 P(*t*-BA)/PEGMA	42	64	40	60
25:75 P(*t*-BA)/PEGMA	54	65	22	78

[a] Reaction conversion was calculated from ^{1}H NMR

[b] % P(*t*-BA) in the copolymer = [% $Conv._{P(t\text{-BA})}$ × % $feed_{t\text{-BA}}$]/[% $Conv._{P(t\text{-BA})}$ × % $feed_{t\text{-BA}}$ + % $Conv._{PEGMA}$ × % $feed_{PEGMA}$]

% PEGMA in the copolymer was calculated in a similar fashion (The calculation is shown in Appendix A)

Figure 35 shows FT-IR spectra of P(*t*-BA)/PEGMA copolymer-coated MNPs having the copolymer molar ratio of 75/25, 50/50 and 25/75, respectively (Figure 35D-

F). FT-IR spectra of BTPAm-coated MNP, *t*-BA monomer and PEGMA oligomer were also provided for comparison in Figure 35A-C, respectively. The success of the grafting reaction of the copolymers onto the particle surface was signified by the presence of the sharp and strong signals of ester groups of PEGMA and *t*-BA repeating units; ~1728-1717 cm^{-1} (-CO-O-) and 1147-1100 cm^{-1} (C-O stretching) (Figure 35D-F). In addition, the symmetric vibration of *t*-butyl groups (C-H bending) in P(*t*-BA) as indicated by a doublet ranging between 1400-1366 cm^{-1} was also clearly observed in the spectra. In all cases, a broad and strong characteristic signal of Fe-O bonds from MNP cores was obviously apparent (~597-586 cm^{-1}). The assigned functional groups of PEGMA oligomer were detailed in Table 8 and those of P(*t*-BA)/PEGMA copolymer-coated MNP were shown in Table 9.

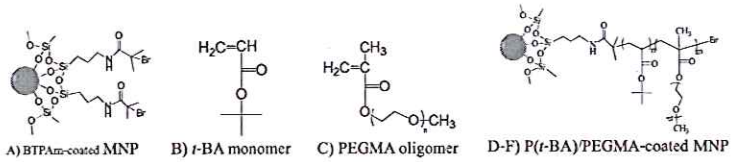

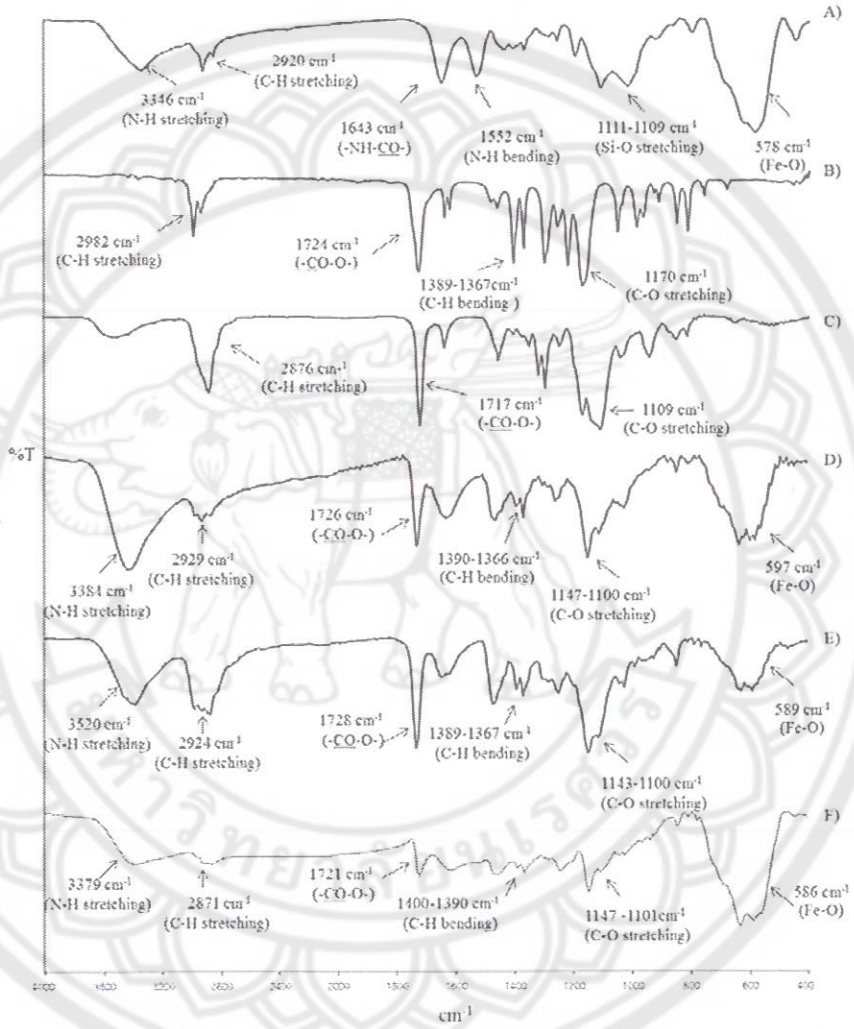

Figure 35 FT-IR spectra of A) BTPAm-coated MNP, B) *t*-BA monomer, C) PEGMA oligomer and P(*t*-BA)/PEGMA-coated MNPs having D) 75/25, E) 50/50 and F) 25/75 molar ratios of P(*t*-BA)/PEGMA

Table 8 Functional group annotation of PEGMA oligomer (Figure 35C)

Wavenumber (cm^{-1})	Designated functional groups
2876	C-H stretching
1717	-(CO)-O- stretching
1109	C-O stretching

Table 9 Functional group annotation of P(*t*-BA)/PEGMA copolymer-coated MNP (Figure 35D-F)

Wavenumber (cm^{-1})	Designated functional groups
3520-3379	N-H stretching
2929-2817	C-H stretching
1400-1366	C-H bending
1728-1717	-(CO)-O- stretching
1147-1100	C-O stretching
597-586	Fe-O

TEM images and the particle size distribution of P(*t*-BA)/PEGMA-coated MNPs (75/25, 50/50 and 25/75 molar ratios) were depicted in Figure 35. The particle size was in the range of 5-10 nm with the average of 8.07 ± 1.4 nm in diameter. The particles were well dispersed in water due to the presence of hydrophilic PEGMA on their surface. Hence, the TEM samples were prepared from MNP-aqueous dispersions. However, some nano-scale clustering of these particles were observed and this was attributed to the existence of hydrophobic P(*t*-BA) coating on the particle surface. Furthermore, it was also observed that increasing PEGMA-to-P(*t*-BA) ratio in the copolymer enhanced dispersibility of the particles in water.

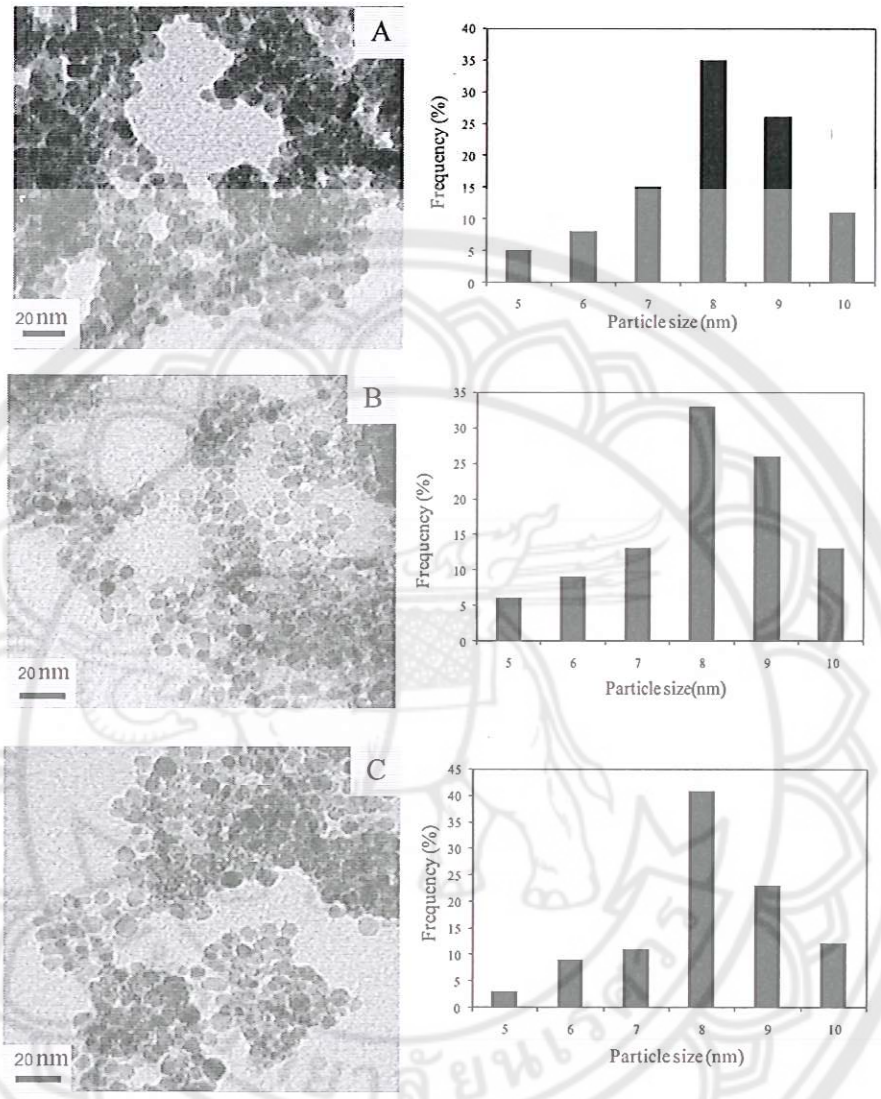

Figure 36 TEM images and particle size distribution of P(t-BA)/PEGMA-coated MNPs having molar ratio of P(*t*-BA)/PEGMA of A) 75/25, B) 50/50 and C) 25/75, respectively. The TEM samples were prepared from MNP-aqueous dispersion

Deprotection of *t*-butyl groups of P(*t*-BA) to obtain PAA homopolymer or PAA/PEGMA copolymer grafted on MNP surface

P(*t*-BA)- and P(*t*-BA)/PEGMA-coated MNPs (75/25, 50/50 and 25/75 molar ratio) were then used for further studies in deprotection of *t*-butyl groups of P(*t*-BA)

on the particle surfaces. After the deprotection, it was anticipated that PAA- and PAA/PEGMA- coated MNPs should be obtained.

FT-IR spectra in Figure 37 illustrate the functional groups of P(*t*-BA) homopolymer-coated MNP before and after deprotection reactions. It evidences the transformation from a sharp and strong peak of carbonyl groups of esters (1729 cm^{-1}) to a broad and strong peak (1671 cm^{-1}) of carboxylic acid functional groups. The shift of C-O bond stretching signals of esters (1145 cm^{-1}) to those of carboxylic acid (1206 cm^{-1}) was another evidence of the occurrence of the deprotection reaction. In addition, the depletion of the doublet signals (1390-1365 cm^{-1}) of C-H bending of *t*-butyl groups in combination with the presence of a broad and strong signal of O-H stretching (3428 cm^{-1}) was another supportive result indicating the formation of PAA on the particle surface.

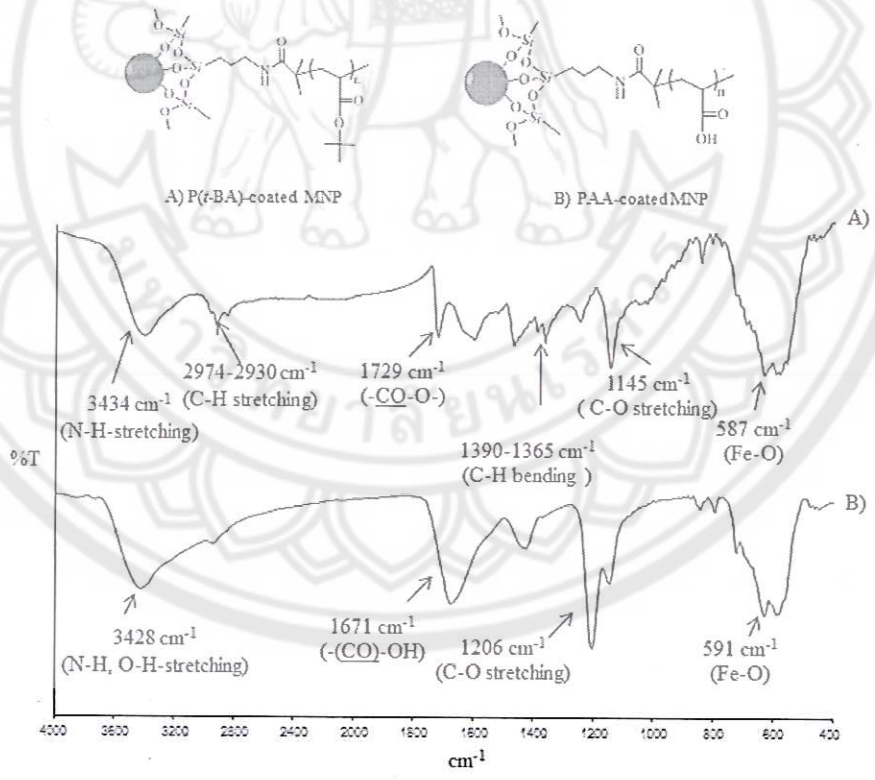

Figure 37 FT-IR spectra of A) P(*t*-BA) homopolymer-coated MNP (before deprotection) and B) PAA homopolymer-coated MNP (after deprotection)

Table 10 Functional group annotation of PAA homopolymer-coated MNP (Figure 37B)

Wavenumber (cm^{-1})	Designated functional groups
3428	O-H stretching
1671	-(CO)-OH stretching
1206	C-O stretching
591	Fe-O

Turning now to the case of MNPs coated with P(*t*-BA)/PEGMA copolymers, similar results to the case of P(*t*-BA) homopolymer-coated MNP were apparent; the transformation of ester groups in P(*t*-BA) to carboxylic acid groups in PAA was observed after the deprotection reaction. Figure 38 shows FT-IR spectra of MNPs coated with P(*t*-BA)/PEGMA copolymers (before deprotection) and PAA/PEGMA copolymers (after deprotection) with various molar ratio of each component.

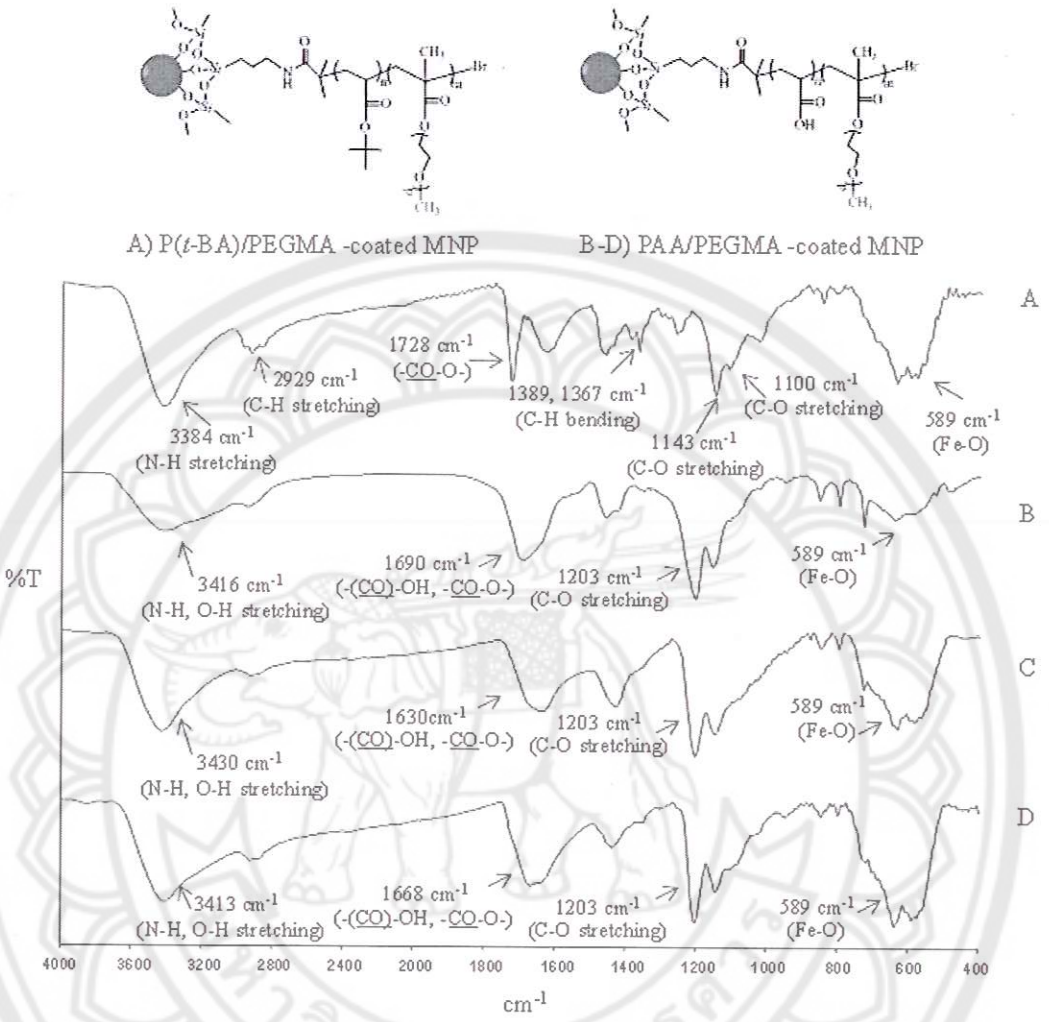

Figure 38 FT-IR spectra of A) P(*t*-BA)/PEGMA-coated MNPs (before deprotection) and PAA/PEGMA-coated MNPs (after deprotection) having molar ratio of P(*t*-BA)/PEGMA of B) 75/25, C) 50/50 and D) 25/75, respectively

Table 11 Functional group annotation of PAA/PEGMA copolymer-coated MNP (Figure 38B-D)

Wavenumber (cm^{-1})	Designated functional groups
3430-3413	N-H, O-H stretching
1690-1630	-(CO)-OH, -(CO)-O stretching
1203	C-O stretching
589	Fe-O

TEM images and the particle size distribution of PAA- and PAA/PEGMA-coated MNPs (75/25, 50/50 and 25/75 molar ratios) were depicted in Figure 39. The particle size was in the range of 5-10 nm with the average of 8.07 ± 1.4 nm in diameter. The particles were well dispersed in water due to the presence of PEGMA and polyelectrolyte PAA on their surface. It is worth to inform that the presence of PAA on MNP surface significantly promoted their dispersibility in water as compared to those containing P(*t*-BA) (before deprotection), in which some nano-scale clustering was apparent (Figure 36).

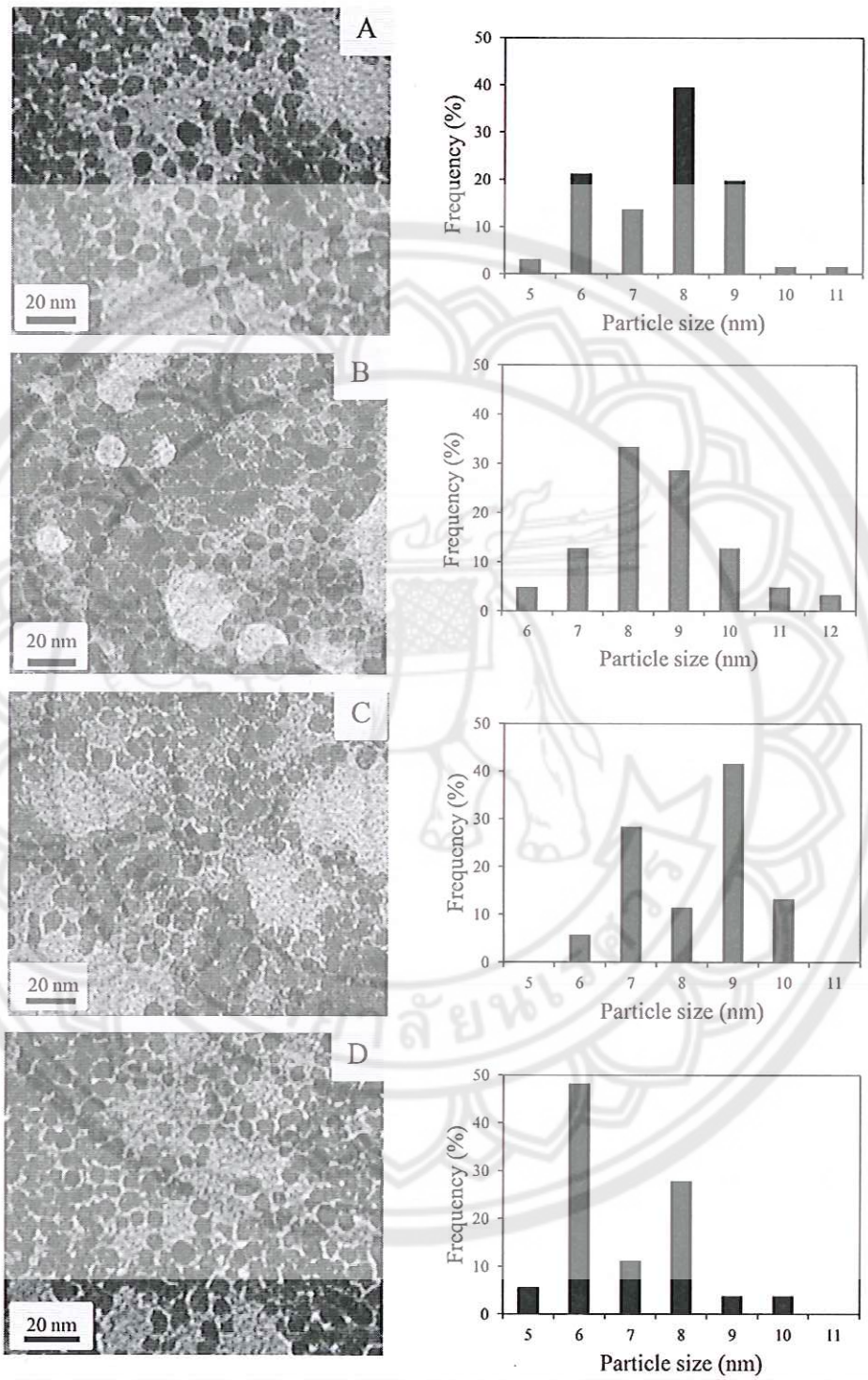

Figure 39 TEM images and particle size distribution of PAA- and PAA/PEGMA-coated MNPs having molar ratio of PAA/PEGMA of A) 100/0, B) 75/25, C) 50/50 and D) 25/75, respectively. The TEM samples were prepared from MNP-aqueous dispersion

Hydrodynamic diameter and zeta potential of the PAA-coated MNP and PAA/PEGMA-coated MNP were determined as a function of pH of aqueous solutions *via* photocorrelation spectroscopy (PCS). It is known that carboxylic acid functional groups of PAA can be ionized and essentially form carboxylate anions in alkaline solutions. The dependence of the change of the solution pH on hydrodynamic size and surface charges of the polymer-coated MNPs was thus attracted our attention.

In the case of the PAA homopolymer-coated MNP (Figure 40), it was found that as increasing the solution pH, their hydrodynamic diameter gradually decreased in the range of acidic pH (pH 1-5) and rapidly decreased as the dispersion pH was continuously increased up to 11. It was rationalized that ionization of carboxylic acids on the particle surface took place at high pH, resulting in the formation of carboxylate ions on their surface (Figure 41). The negative charges of carboxylate ions led to additional electrostatic repulsion toward neighboring particles and thus prevented massive flocculation (Figure 42).

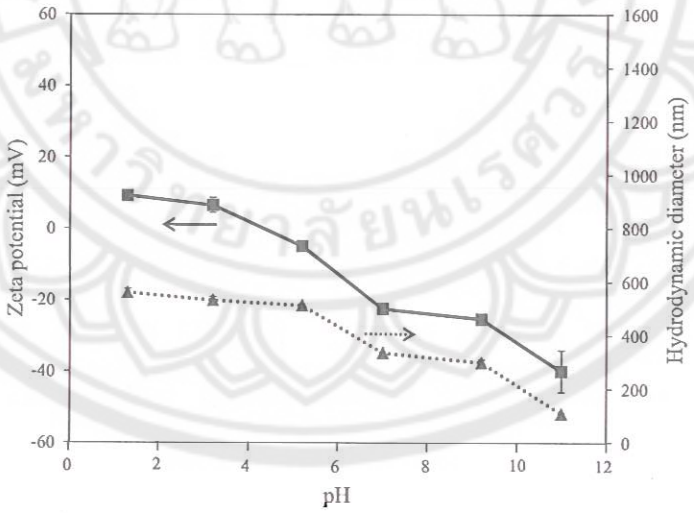

Figure 40 The effect of pH change of the PAA-coated MNP in aqueous dispersions on hydrodynamic diameter and zeta potential (surface charge)

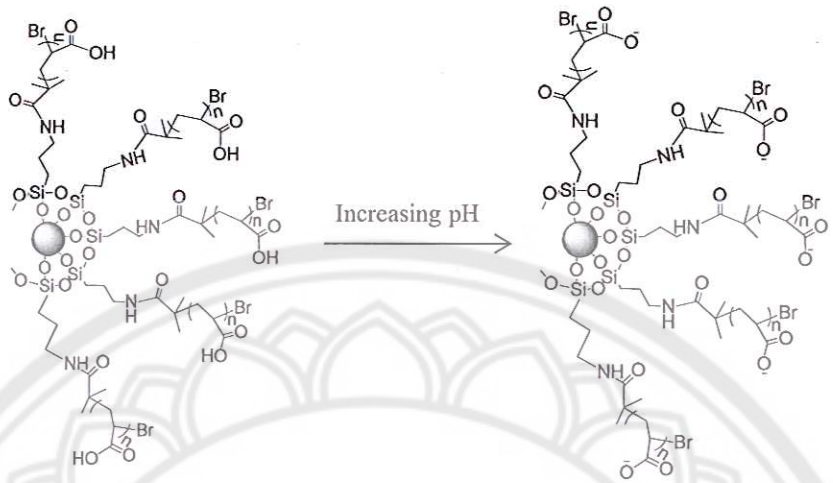

Figure 41 Formation of carboxylate ions on MNP surfaces at basic pH of PAA-coated MNPs

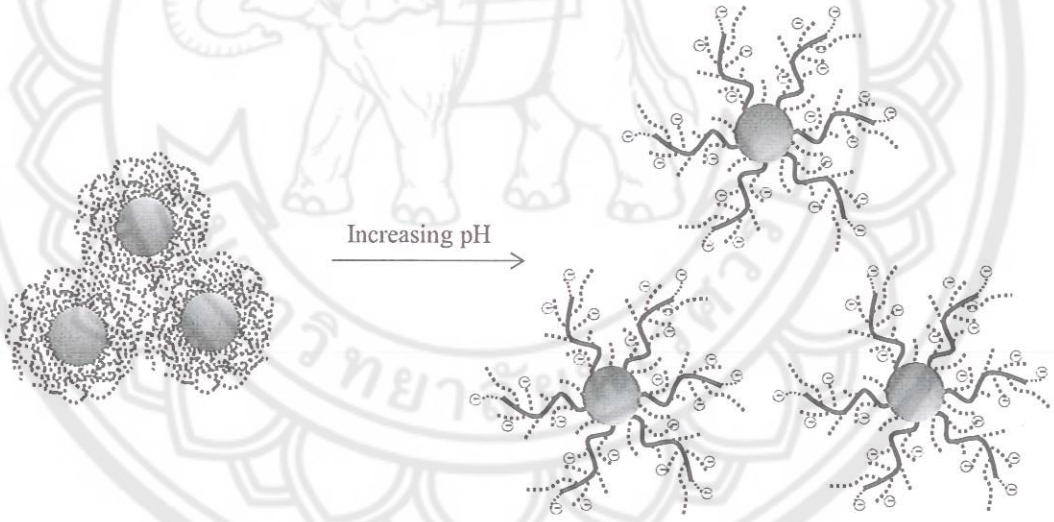

Figure 42 Electrostatic repulsion of PAA-coated MNPs at basic pH

In the case of the PAA/PEGMA copolymer-coated MNP (Figure 43A-C), the pH dependence of the dispersions on zeta potential showed similar behavior to the case of PAA homopolymer-coated MNP; their surface charges became more negative as increasing pH of the dispersions. Their surface charges ranged between +40 and -50 mV. Electrostatic stabilization of the complexes was apparently enhanced in the range of high acidic or basic pHs due to the repulsion of the same charges of the polymers coating on the particle surface, resulting in the promotion of the particle dispersibility

in water and the formation of the particles having relatively small hydrodynamic size (Figure 44). Interestingly, the hydrodynamic diameter of the copolymer-coated MNP drastically increased up to about 1 μm (~1100-1400 nm) at pH between 5 and 7. This was probably due to the presence of PEGMA on their surface, resulting in the formation of entanglement of the dangling brush of PEGMA which might overcome the electrostatic repulsion at the pH close to the point of zero charge (PZC) of the complexes (Figure 44,45). It should be noted that this phenomenon was not observed in the PAA homopolymer-coated MNP. TEM experiments also showed a supportive result to this explanation as indicated by the presence of some micro-scale aggregation of multiple nanoparticles (Figure 46). These microclusters were not apparent in the TEM images of the PAA homopolymer-coated MNP (Figure 38). Hydrodynamic diameters and zeta potentials of PAA- or PAA/PEGMA- coated MNPs in aqueous dispersions at different pH were summarized in Table 12.

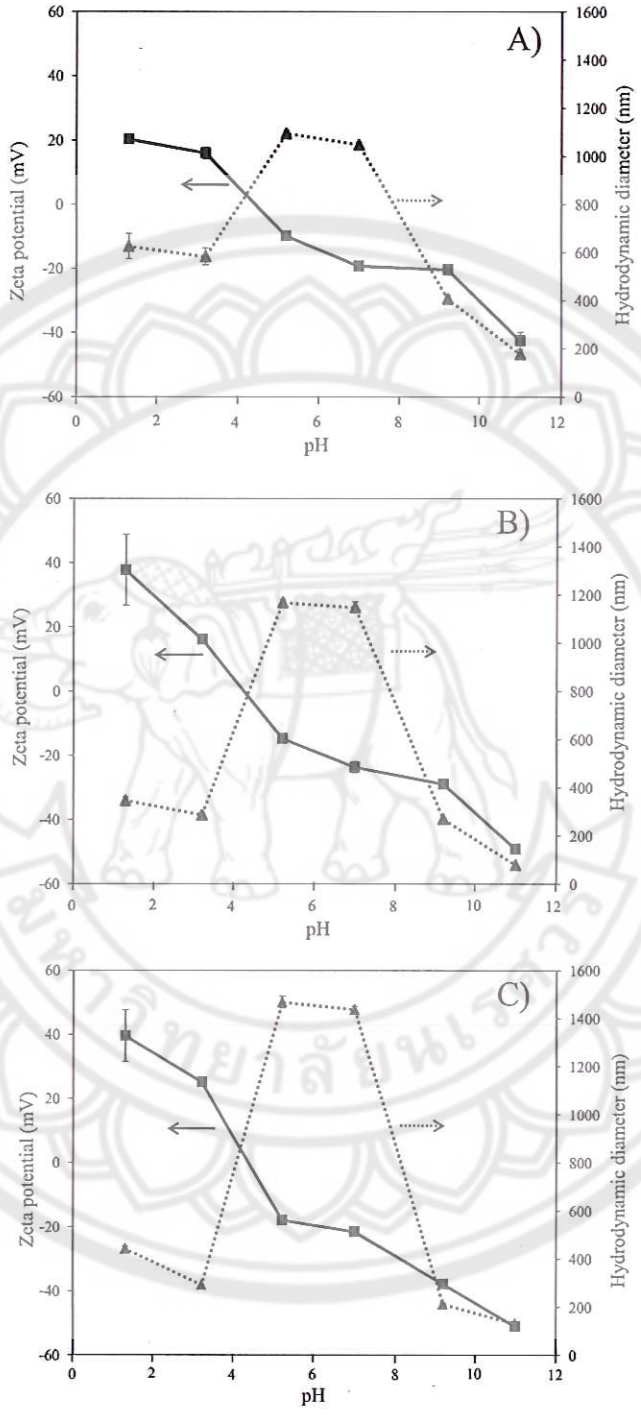

Figure 43 The effect of pH change of PAA/PEGMA-coated MNP in aqueous dispersions on hydrodynamic diameter and zeta potential (surface charge). PAA/PEGMA molar ratios in the copolymers were A) 75/25, B) 50/50 and C) 25/75, respectively.

Table 12 Hydrodynamic diameter and zeta potentials of PAA- or PAA/PEGMA-coated MNP in aqueous dispersions at different pHs

	pH	Hydrodynamic diameter (nm)	Zeta potential (mV)
PAA-coated MNP	1.3	561 ± 14	9.3 ± 0.2
	3.2	532 ± 13	6.5 ± 2.1
	5.2	514 ± 5	-4.9 ± 1.1
	7.0	337 ± 3	-22.4 ± 1.4
	9.2	300 ± 10	-25.3 ± 0.4
	11	109 ± 3	-49.9 ± 5.9
75/25 PAA/PEGMA-coated MNP	1.3	625 ± 53	20.3 ± 0.9
	3.2	583 ± 35	16.0 ± 1.8
	5.2	1095 ± 11	-9.8 ± 0.9
	7.0	1048 ± 11	-19.2 ± 0.3
	9.2	408 ± 14	-20.3 ± 0.6
	11	178 ± 7	-42.5 ± 2.7
50/50 PAA/PEGMA-coated MNP	1.3	347 ± 12	37.7 ± 11.0
	3.2	287 ± 6	16.2 ± 0.7
	5.2	1169 ± 11	-14.7 ± 1.2
	7.0	1149 ± 22	-23.6 ± 1.8
	9.2	270 ± 7	-28.8 ± 0.4
	11	80 ± 1	-49.1 ± 0.7
25/75 PAA/PEGMA-coated MNP	1.3	444 ± 10	39.6 ± 8.1
	3.2	293 ± 2	25.2 ± 0.5
	5.2	1468 ± 25	-17.9 ± 0.8
	7.0	1438 ± 13	-21.4 ± 0.3
	9.2	213 ± 5	-37.7 ± 0.7
	11	131 ± 5	-51.0 ± 0.3

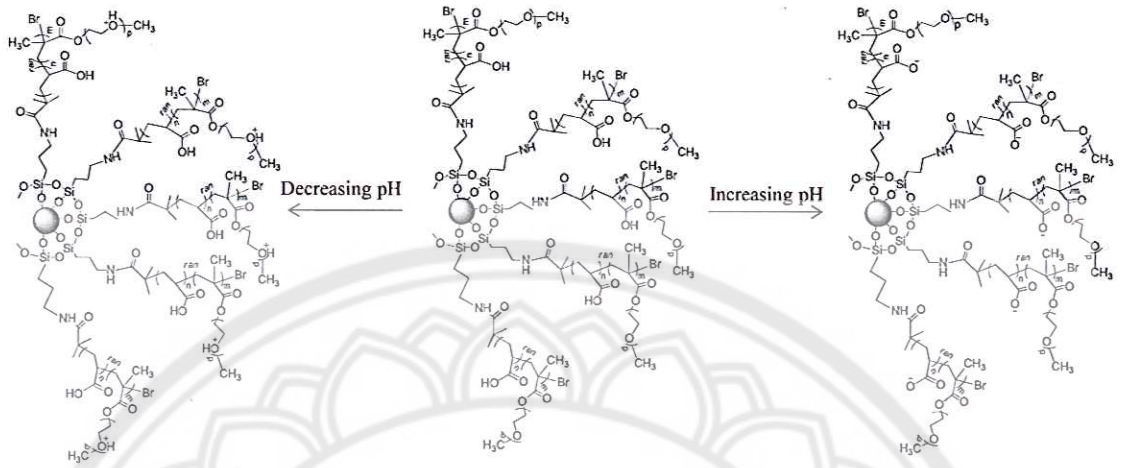

Figure 44 Formation of carboxylate ions on MNP surfaces at basic pH of PAA/PEGMA-coated MNPs

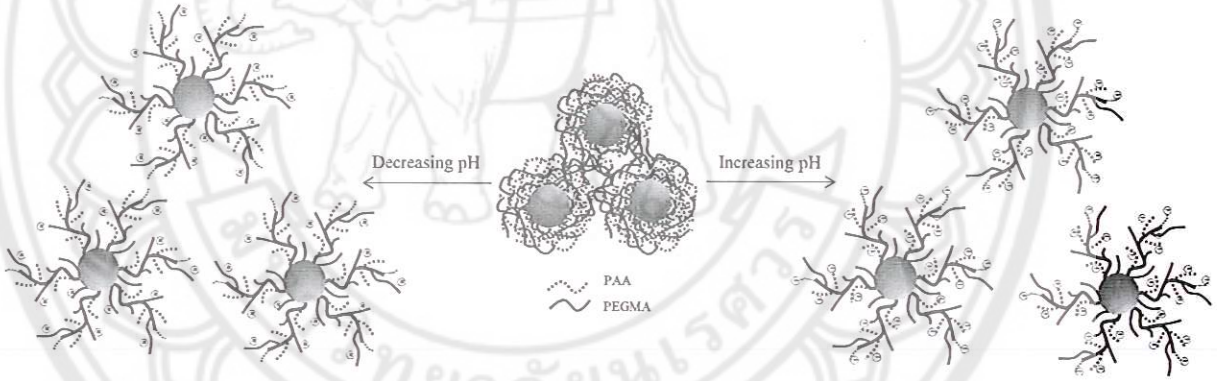

Figure 45 Electrostatic repulsion of PAA/PEGMA-coated MNPs at acidic and basic pH

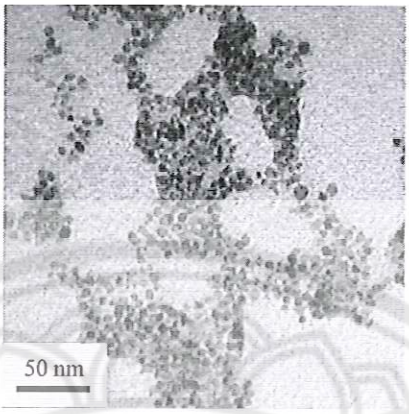

Figure 46 TEM image of PAA/PEGMA-coated MNPs showing the presence of some nanoaggregation

To determine percentage of each component in the complexes in each step of the reactions, the complexes were characterized *via* TGA to investigate their mass loss in comparison with bare MNP and MNP coated with BTPAm. It should be noted that the particles were isolated from unreacted BTPAm and the monomer using an external magnet together with centrifugation. TGA was conducted in a temperature range of 0 to 600 °C under oxygen atmosphere. It was assumed that the weight of the complexes remaining at 600 °C (% char yield) was the weight of Fe completely oxidized. The weight loss of the complexes was thus attributed to the decomposition of organic components including BTPAm linker and the polymers that complexed to the particle surfaces. Hence, % char yield of bare MNP and BTPAm-coated MNP were first determined to obtain percentage of BTPAm in the complexes. To determine the amount of BTPAm in each complex, the ratio of MNP core to BTPAm was determined (12.4:1, respectively), and this ratio was used to estimate % BTPAm in other complexes. Hence, % polymers in the complexes can be calculated and an example of calculation is shown in Appendix A.

The TGA curve of bare MNP (Figure 47a) showed weight loss of 12 % (88 % char yield) upon heating to 600 °C. This was attributed to the decomposition of residual benzyl alcohol which might remain on their surface. TGA thermogram of BTPAm-coated MNP (Figure 47b) showed the decomposition temperature ranging between 200 and 400 °C with the weight loss of 19 % (81 % char yield) at 600 °C,

originating from the decomposition of grafted BTPAm on the MNP surface. According to TGA thermogram (Figure 47b) and Table 13, the BTPAm contents in BTPAm-coated MNP was about 7 %.

In the cases of the P(*t*-BA)- and P(*t*-BA)/PEGMA-coated MNP (75/25, 50/50 and 25/27, respectively), TGA thermograms show a large range of the decomposition of the polymers between 150 and 450 °C and the contents of the polymers were in the range of 23-36% (Table 13). After the deprotection reaction of *t*-butyl groups, percentage of organic components in the PAA- and PAA/PEGMA-coated MNP (75/25, 50/50 and 25/27, respectively) (Figure 47) significantly dropped to 5-21% due to the removal of *t*- butyl groups from the polymeric layer of the particles.

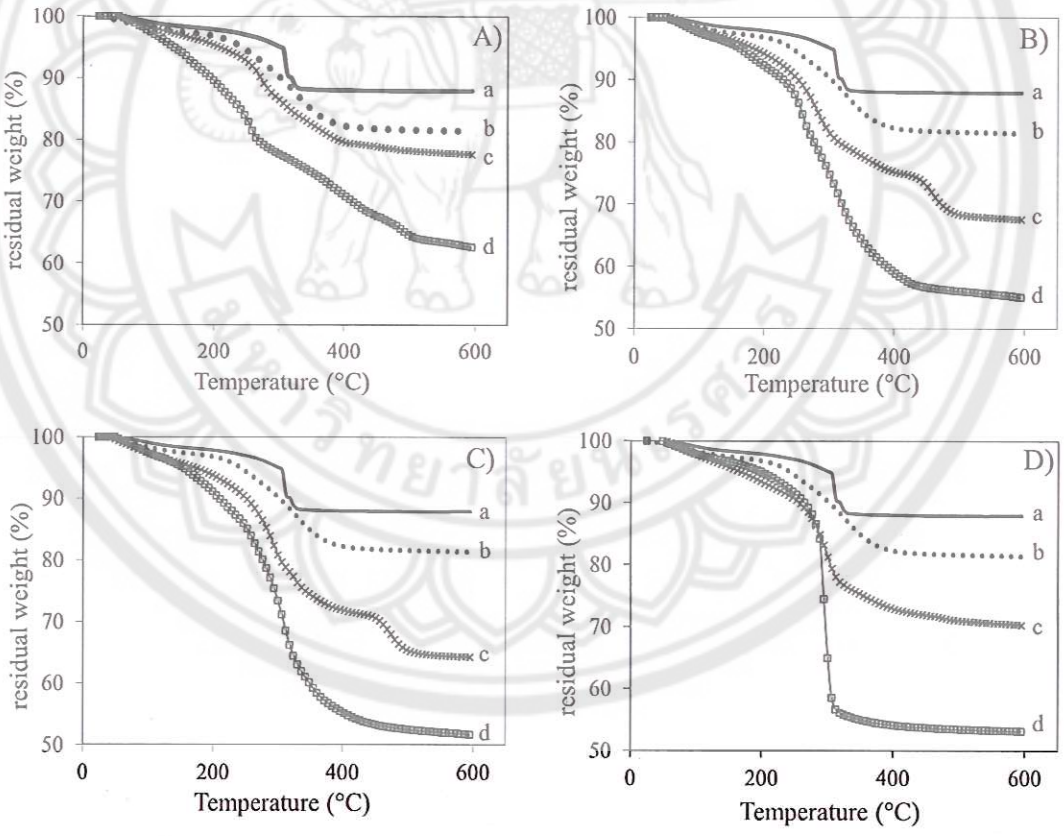

Figure 47 TGA thermograms of polymer-coated MNPs having molar ratio of P(*t*-BA)/PEGMA of A) 100/0, B) 75/25, C) 50/50 and D) 25/75, respectively; a) bare MNP, b) BTPAm-coated MNP, c) P(*t*-BA)-coated MNP and d) PAA-coated MNP

Table 13 Percentage of each component in the complexes prepared in solution system

Type of complex	% Char yield [a]	% in the complex			
		MNP	BTPAm	P(*t*-BA)/PEGMA	PAA/PEGMA
bare MNP	88	100	-	-	-
BTPAm-coated MNP	81	93	7	-	-
P(*t*-BA)/PEGMA -coated MNP					
(100/0)	63	71	6	23	-
(75/25)	55	63	5	32	-
(50/50)	52	59	5	36	-
(25/75)	53	60	5	35	-
PAA/PEGMA -coated MNP					
(100/0)	78	88	7	-	5
(75/25)	68	77	6	-	17
(50/50)	64	73	6	-	21
(25/75)	70	80	6	-	14

[a] Determined *via* TGA technique

Magnetic properties of MNP complexes were investigated *via* a vibration sample magnetometer (VSM). *M-H* curves of bare MNPs, BTPAm-coated MNPs and PAA/PEGMA-coated MNP (100/0, 75/25, 50/50 and 25/75, respectively) were presented in Figure 48. They showed superparamagnetic behavior at room temperature as indicated by the absence of magnetic remanence (M_r) and coercitivity (H_c) upon removing an external applied magnetic field. From the results in Figure 48, the decrease of saturation magnetization (M_s) from 56 emu/g of bare MNP to 52 of BTPAm-coated MNP was attributed to the existence of a thin layer of BTPAm on the

Table 14 Saturation magnetization (M_s) of PAA/PEGMA-coated MNPs and their Precursors

Sample	M_s [a] (emu/g sample)
Bare MNP	56
BTPAm-coated MNP	52
100:0 PAA/PEGMA-coated coated MNP	44
75:25 PAA/PEGMA-coated coated MNP	42
50/50: PAA/PEGMA-coated coated MNP	35
25/75 PAA/PEGMA-coated coated MNP	24

[a] Estimated from the saturation magnetization (M_s) at 10,000 G from VSM technique

Measurement of the numbers of carboxyl groups on the MNP surface

The amounts of carboxyl groups presenting on the particle surface were quantitatively determined by a conductometric titration. Figure 49A shows the conductometric titration curve of the reaction between NaOH and HCl having a V-shape (Blank). During the titration, the reaction that takes place in the titration vessel is following [56]:

$$Na^+ + OH^- \xrightarrow{H^+ \; Cl^-} H_2O + Cl^- + Na^+ \qquad (2)$$

In the region I, before the end point, OH^- is removed from the solution by reaction with H^+, and Cl^- is added to the solution. The conductance of the solution decreases prior to the end point. After the end point (region II), no OH^- is available to react, and the conductance of the solution increases as a result of the additional of H^+ and Cl^-.

In the case of the titration of HCl with –COOH groups on the particle surface, the conductometric titration curve exhibits three regions (Figure 49B). Before the

titration of -COOH groups on the MNP surface, the –COOH groups grafted on the MNP surface was dispersed in an excess of NaOH solution. Thus, the reaction that takes place in the vessel is following:

$$-COO^- + H^+ \xrightarrow{Na^+\ OH^-} -COO^- + Na^+ + H_2O + Na^+OH^-_{excess} \quad (3)$$

In the region I of the titration, because basicity of excess OH^- in the solution is stronger than that of $–COO^-$, the OH^- in the solution was first neutralized when HCl was titrated (4).

$$Na^+_{excess} + OH^-_{excess} \xrightarrow{H^+\ Cl^-} H_2O + Na^+ + Cl^- \quad (4)$$

In the region II, when the OH^- in the solution was completely neutralized, the H^+ ions reacted with the $–COO^-$ groups on the MNP surface. After the $–COO^-$ groups on the MNP surface were completely reacted with H^+ ions, the solution conductivity sharply increase due to the excess of H^+ and Na^+ (region III). The measurement of the amounts of –COOH groups on the surface of the (co)polymer-grafted MNP was estimated from the following equation [57]:

$$[Acid] = \frac{V \times M \times N_A}{SC} \quad (5)$$

where, [Acid] is the number of carboxyl groups per gram sample (molecules/g)

V is the consumption volume of HCl solution in the second region (region II) of the conductometric titration (L)

M is the molar concentration of polyelectrolyte (mol/L)

N_A is Avogadro's constant (6.022×10^{23} molecules/mol)

SC is the solid content or the sample (g)

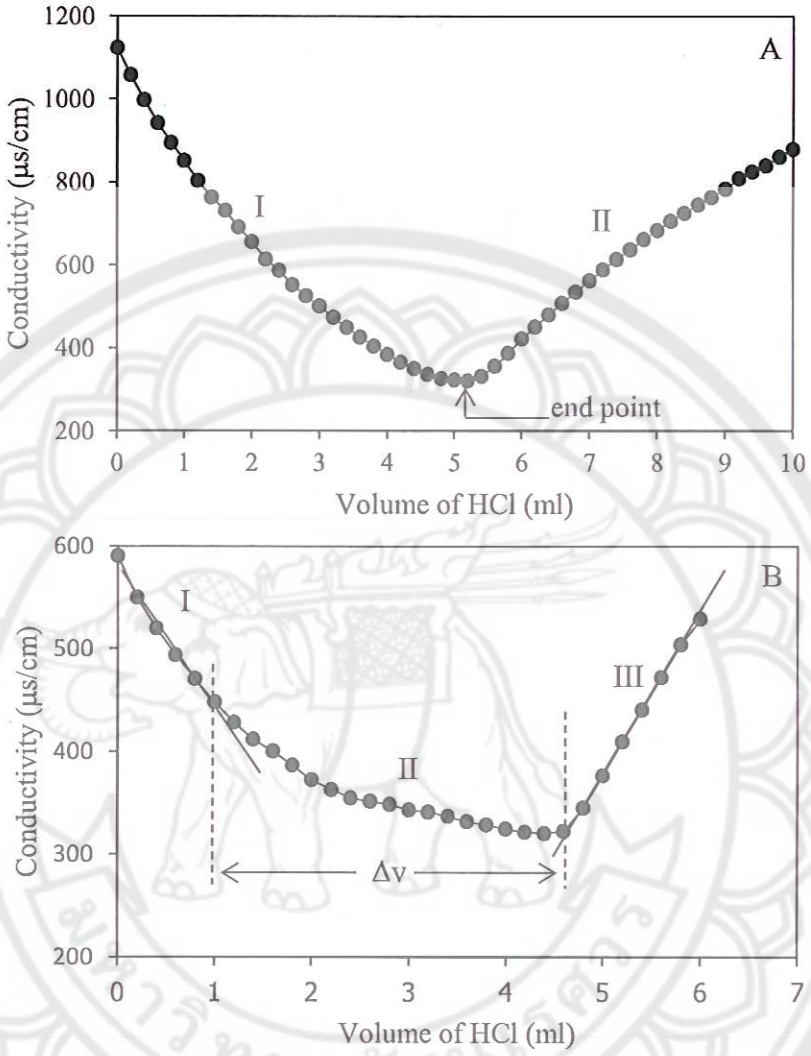

Figure 49 The examples of the conductometric titration curves, A) the titration curve of HCl with NaOH and B) the titration curve of HCl with carboxyl groups on the PAA-coated MNP surface

Figure 50 exhibits the grafting density of –COOH groups on the surface of the (co)polymer-grafted MNP. It was found that grafting density of –COOH groups consistently increased from 37 to 52 molecules/nm^2 as the percentage of PAA in the copolymer increased from 25% to 100%, respectively. These values of the grafting density in the molecules/nm^2 basis correspond to 7,400 and 10,400 molecules of –COOH groups per particle, respectively. Examples of the calculation of the grafting density of –COOH on the MNP surface are shown in Appendix A. This implied that

the grafting density of –COOH groups presenting in the MNP surface can be fine-tuned by simply modulating molar ratio of loaded monomers in the copolymerization.

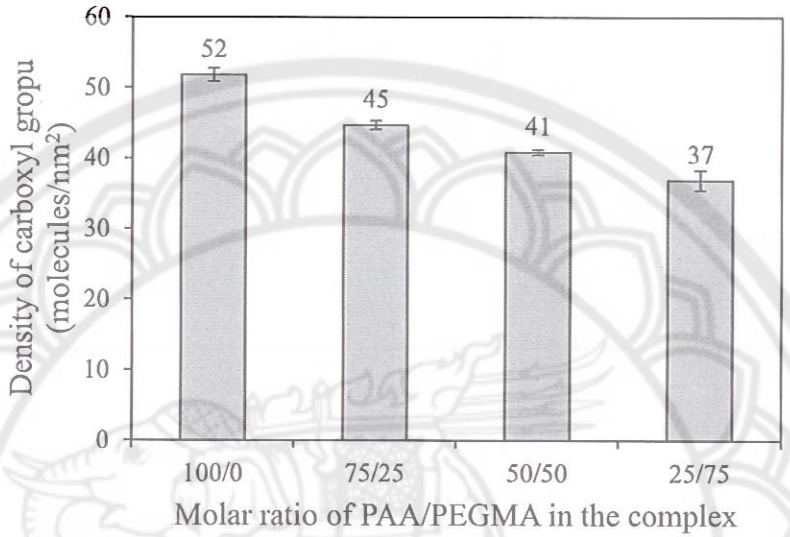

Figure 50 Grafting density of carboxyl groups on MNP surface coated with PAA/PEGMA copolymers

CHAPTER V

CONCLUSIONS

This work presented a "grafting-from" method to modify MNP surfaces with P(*t*-BA) and PEGMA statistical copolymer *via* ATRP reaction, followed by acid deprotection of t-butyl groups to obtain PAA/PEGMA-coated MNP. The systematic adjustment of molar ratio of P(*t*-BA) to PEGMA in the loading was carried out in the will of fine tuning of the properties of the PAA/PEGMA-coated MNP such as responsiveness to the pH change and water dispersibility.

In the surface modification of MNP *via* ATRP, it was found that the reaction reactivity of PEGMA was higher than that of P(*t*-BA). In addition, increasing PEGMA composition in the copolymerization seemed to promote the rate of ATRP reaction under the condition used in this work (1:1 CuBr:PMDETA mol:mol in dioxane at 90°C). The molecular weight gradually increased as the reaction conversions increased, indicating the steady growth of the (co)polymer chains in a controllable fashion.

After the deprotection of *t*-butyl groups in P(*t*-BA) moiety, PAA-or PAA/PEGMA-coated MNP showed pH-sensitive properties. In the PAA-coated MNP, increasing pH of the solution resulted in the increase in negative charge of the particle and the decrease in its hydrodynamic size. In the PAA/PEGMA-coated MNP, the presence of PEGMA was thought to influence the hydrodynamic size of the complex probably due to its interparticle entanglement. The presence of negative charge on the particle surface enhanced the particle dispersibility in polar solvent. TEM indicated that the particles were well dispersible in water due to the presence of hydrophilic PAA and PEGMA on the MNP surface as compared to those containing P(*t*-BA), in which some nano-scale clustering was apparent. Both TGA and VSM results indicated the presence of the copolymer in the complexes.

The presence of hydrophilic PAA and PEGMA on MNP surfaces not only promoted the particle dispersibility in water, but the carboxyl groups can also be used for further functionalizations with biomolecules of interest. Therefore, this novel

magnetically guidable nanocomplex with tunable loading density of carboxyl groups on its surface might be applicable for use as a capture of positively charged bioentities or as an intermediate for covalent coupling with biomolecules containing affinity functional groups.

REFERENCES

REFERENCES

[1] Dong, H., Huang, J., Koepsel, R. R., Ye, P., Russell, A.J. and Matyjaszewski. (2011). Recyclable antibactreial magnetic nanoparticles grafted with quaternized poly(2-(dimethylamino)ethyl methacrylate) brushes. **Journal of The American Chemical Society**, 12, 1305-1311.

[2] Kang, S. M and Choi, I, S. (2009). Bioconjugation of poly(poly(ethylene glycol)methacrylate)-coated iron oxide magnetic nanopartcles for magnetic capture of target proteins. **Macromolecular Research**, 17, 259-264.

[3] Liu, C., Guo, J., Yang, W., Hu, J., Wang, C. and Fu, S. (2009). Magnetic mesoporous silica microspheres with thermo-sensitive polymer shell for controlled drug release. **Journal of Materials Chemistry**, 19, 4764-4770.

[4] Zhou, J., Meng, L., Lu, Q., Fu, J. and Huang, X. (2009). Superparamagnetic submicro-megranates: Fe_3O_4 nanoparticles coated with highly cross-linked organic/inorganic hybrids. **Chemical Communications**, 6370-6372.

[5] Ahmad, H., Rahman, M. A. and Miah, A. J. (2008). Magnetic and temperature-sensitive composite polymer particles and adsorption behavior of emulsifiers and trypsin. **Macromolecular Research**, 16, 637-643.

[6] Xia, H., Zhang, C. and Wang, Q. (2001). Study on ultrasonic induced encapsulating emulsion polymerization in the presence of nanoparticles. **Journal of Applied Polymer Science**, 80, 1130–1139.

[7] Huang, J., Koepsel, R. R., Murata, H., Wu, W., Lee, S. B., Kowalewski, T., Russell, A.J. and Matyjaszewski, K. (2008). Nonleaching antibacterial glass Ssurfaces via "Grafting Onto": The effect of the number of quaternary ammonium groups on biocidal activity. **Langmuir**, 23, 6785-6795.

[8] Pothayee, N., Balasubramaniam, S., Davis, R. M., Riffle, J. S., Carroll, M. R. J., Woodward, R. C. and Pierre, T.G. S. (2011). Synthesis of 'ready-to-adsorb' polymeric nanoshells for magnetic iron oxide nanoparticles via atom transfer radical polymerization. **Polymer**, 52, 1356-1366.

[9] Matyjaszewski, K., Dong, H. Jakubowski, W., Pietrasik, J. and Kusumo, A. (2007). Grafting from surfaces for "Everyone": ARGET ATRP in the presence of air. **Langmuir**, 23, 4528-4531.

[10] Mu, B., Wang, T., Wu, Z., Shi, H., Xue, D. and Liu, P. (2011). Fabrication of functional block copolymer grafted superparamagnetic nanoparticles for targeted and controlled drug delivery. **Colloids and Surfaces A: Physicochemical and Engineering Aspects**, 375, 163-168.

[11] Hawker, C. J., Bosman, A. W. and Harth, E. (2005). New polymer synthesis by nitroxide mediated living radical polymerizations. **Chemical Reviews**, 101, 3661-3688.

[12] Boyer, C., Bulmus, V., Davis, T. P., Ladmiral, V., Liu, J. and Perrier, S. (2009). Bioapplications of RAFT. **Chemical Reviews**, 109, 5402-5436.

[13] Matyjaszewski, K. and Xia, J. (2001). Atom transfer radical polymerization. **Chemical Reviews**, 101, 2921-2990.

[14] Braunecker, W. A. and Matyjaszewski, K. (2007). Controlled/living radical polymerization: Features, developments, and perspective. **Progress in Polymer Science**, 32, 93-146.

[15] Dobrynin, A.V. and Rubinstein, M. (2005). Theory of polyelectrolytes in solutions and at surfaces. **Progress in Polymer Science**, 30, 1049-1118.

[16] Mu, B., Liu, P., Tang, Z., Du, P. and Dong, Y. (2011). Temperature and pH dual-responsive cross-linked polymeric nanocapsules with controllable structures via surface-initiated atom transfer radical polymerization from templates. **Nanomedicine: Nanotechnology, Biology, and Medicine**, 1-8.

[17] Dong, R., Krishnan, S., Baird, B. A., Lindau, M. and Ober, C. K. (2007). Patterned biofunctional poly(acrylic acid) brushes on silicon surfaces. **Biomacromolecules**, 8, 3082-3092.

[18] Kusumo, A., Bombalski, L., Lin, Q., Matyjaszewski, K., Schneider, J. W. and Tilto, R. D. (2007). High capacity, charge-selective protein uptake by polyelectrolyte brushes. **Langmuir**, 23, 4448-4454.

[19] Lei, Z. and Bi, S. (2007). Preparation and properties of immobilized pectinase onto the amphilic PS-b-PAA diblock copolymers. **Journal of Biotechnology**, 128, 112-119.

[20] Cullen, S. P., Liu, X., Mandel, I. C., Himpsel, F. J. and Gopalan, P. (2007). Polymaric brushes as functional templates for immobolozing ribonuclease A: study of binding kinetics and activity. **Langmuir**, 24, 913-920.

[21] **Classes of magnetic materials**. (October 20, 2009). Retrieved May 25, 2011, from http://www.irm.umn.edu/hg2m/hg2m_b/hg2m_b.html

[22] **Magnetism**. (2011). Retrieved, May 26, 2011, from http://www.splung.com/content/sid/3/page/magnetism

[23] **Types of magnetism**. Retrieved May 26, 2011, from http://www.doitpoms.ac.uk/tlplib/ferromagnetic/printall.php

[24] **The Hysteresis Loop**. Retrieved May 26, 2011, from http://www.ndted.org/EducationResources/CommunityCollege/MagParticle/Physics/HysteresisLoop.htm

[25] Lambert, R., Riaz, F. and Little, D. **Hysteresis Loop**. Retrieved May 26, 2011, from http://www.egglescliffe.org.uk/physics/chur/palaeomag/palaeomag.html

[26] Mohapatra, M. and Anand, S. (2010). Synthesis and applications of nano-structured iron oxides/hydroxides-a review. **International Journal of Engineering, Science and Technology**, 2, 127-146.

[27] Ravikumar, C. and Bandyopadhyaya, R. (2011). Mechanistic study on magnetite nanoparticle formation by thermal decomposition and coprecipitation routes. **The Journal of Physical Chemistry C**, 115, 1380-1387.

[28] Kang, Y. S., Risbud, S., Rabolt, J. F. and Stroeve, P. (1996). Synthesis and characterization of nanometer-size Fe_3O_4 and γ-Fe_2O_3 particles. **Chemistry of Materials**, 8, 2209-2211.

[29] Sun, S. and Zeng, H. (2002). Size-Controlled Synthesis of Magnetite Nanoparticles. **Journal of the American Chemical Society**, 124, 8204-8205.

[30] Daou, T. J., Pourroy, G., Begin-Colin, S., Greneche, J. M., Ulhaq-Bouillet, C., Legare, P., Bernhardt, P., Leuvrey, C. and Rogez, G. (2006). Hydrothermal

synthesis of monodisperse magnetite nanoparticles. **Chemistry of Materials,** 18, 4299-4404.

[31] Koneracka, M., Antosova, A., Zavisova, V., Lancz, G., Gazova, Z., Siposova, K., Jurikova, A., Csach, K., Kovac, J., Tomasovicova, N., Fabian, M. and Kopcansky, P. (2010). Characterization of Fe_3O_4 magnetic nanoparticles modified with dextran and investigation of their interaction with protein amyloid aggregates. **Acta Physica Polonica A,** 110(5), 983-985.

[32] Huong, N. Y., Giang, L. T. K., Binh, N. T. and Minh, L. Q. (2009). Surface modification of iron oxide nanoparticles and their conjunction with water soluble polymers for biomedical application. **Journal of Physics: Conference Series,** 187, 1-5.

[33] Mahmoudi, M., Simchi, A., Imani, M., Milani, I. S. and Stroeve, P. (2008). Optimal design and characterization of superparamagnetic iron oxide nanoparticles coated with polyvinyl alcohol for targeted delivery and imaging. **The Journal of Physical Chemistry B,** 112, 14470-14481.

[34] Aqil, A., Vasseur, S., Duguet, E., Passirani, C., Benoit, J. P., Roch, A., Muller, R., Jerome, R. and Jerome, C. (2008). PEO coated magnetic nanoparticles for biomedical application. **European Polymer Journal,** 44, 3191-3199.

[35] Dozier, D., Palchoudhury, S. and Bao, Y. (2010). Synthesis of iron oxide nanoparticles with biological coatings. **Iron Oxide Nanoparticles,** 7, 16-18.

[36] Sun, S., Zemg, H., Robinson, D. B., Rice, P. M., Wang, S. X. and Li, G. (2004). Monodisperse MFe_2O_4 (M) Fe, Co, Mn) Nanoparticles. **Journal of the American Chemical Society,** 126, 273-279.

[37] Poca, A. G., Marco, J. F., Morales, M. P. and Serna, C. J. (2007). Effect of nature and particle size on properties of uniform magnetite and maghemite nanoparticles. **The Journal of Physical Chemistry C,** 111, 18577-18584.

[38] Zhou, Y., Wang, S., Ding, B. and Yang, Z. (2008). Modification of magnetite nanoparticles via surface-initiated atom transfer radical polymerization (ATRP). **Chemical Engineering Journal,** 138, 578-585.

[39] Fuchs, A. V. (2010). **The Eacapsulation of Gold Nanoparticles Using RAFT, ATRP and Miniemulsion Polymerization Techniques**. Bachelor thesis, BH., Queensland University of Technology, Australia.

[40] Oh, J. K. and Park, J. M. (2010). Iron oxide-based superparamagnetic polymeric nanomaterials: Design, preparation, and biomedical application. **Progress in Polymer Science**, 659, 1-22.

[41] Xu, F. J., Neoh, K. G. and Kang, E. T. (2009). Bioactive surfaces and biomaterials via atom transfer radical polymerization. **Progress in Polymer Science**, 34, 719-761

[42] Ding, S., Xing, Y., Radosz, M. and Shen, Y. (2006). Magnetic nanoparticle supported catalyst for atom transfer radical polymerization. **Macromolecules**, 39, 6399-6405.

[43] Xu, F., Geiger, H. J., Baker, G. L. and Gruening, M. L. (2011). Polymer brush-modified magnetic nanoparticles for His-Tagged protein purification. **Langmuir**, 27, 3106-3112.

[44] Yu, H. and Luo, Z. (2011). Novel superhydrophobic silica/poly(siloxane-fluoroacrylate) hybrid nanoparticles prepared via surface-initiated ATRP and their surface pProperties: the effects of polymerization conditions. **Journal of Polymer Science Part: A: Polymer chemistry**, 49, 174-184.

[45] Ulrich, S., Laguecir, A. and Stoll, S. (2005). Complexation of a weak polyelectrolyte with a charged nanoparticle. Solution properties and polyelectrolyte stiffness influences. **Macromolecules**, 38, 8939-8949

[46] Wikipedia .(June 7, 2011). **Polyelectrolyte**. Retrieved May 26, 2011, from http://en.wikipedia.org/wiki/Polyelectrolyte

[47] Borisov, O. and Ballauff, M. (2006). Polyelectrolyte brushes. **Current Opinion in Colloid & Interface Science**, 11, 316–323.

[48] Burke, S. E. and Barrett, C. J. (2004). Controlling the physicochemical properties of weak polyelectrolyte multilayer films through acid/base equilibria. **Pure and Applied Chemistry**, 76, 1387–1398.

[49] Fulghum, T. M., Patton, D. L. and Advincula, R. C.(2006). Fuzzy ternary particle systems by surface-initiatial atom transfer radical polymerization from Layer-by-Layer colloidal core-shell macroinitiator particles. **Langmuir**, 22, 8397-8402.

[50] Berger, S., Synytska, A., Ionov, L., Eichhorn, K. and Stamm, M. (2008). Stimuli-responsive bicomponent polymer Janus particles by "grafting from"/ "grafting to" approaches. **Macromolecules**, 41, 9669-9676.

[51] Chen, K., Zhu, Y., Zhang, Y, Li, L., Lu, Y. and Guo, X. (2011). Synthesis of magnetic spherical polyelectrolyte brushes. **Macromolecules**, 44, 632-639.

[52] Rutnakornpituk, M., Puangsin, N., Theamdee, P., Rutnakornpituk, B. and Wichai, U. (2011). Poly(acrylic acid)-grafted magnetic nanoparticle for conjugation with folic acid. **Polymer**, 52, 987-995.

[53] Bo, Q. and Zhao, Y. (2006). Double-hydrophilic block copolymer for encapsulation and two-way pH change-induced release of metalloporphyrins. **Journal of Polymer Science: Part A: Polymer Chemistry**, 44, 1734–1744.

[54] Sun, Y., Ding, X., Zheng, Z., Cheng, X., Hu, X. Peng, Y. (2007). Surface initiated ATRP in the synthesis of iron oxide/polystyrene core/shell nanoparticles. **European Polymer Journal**, 43, 762–772.

[55] Rowe, M. D., Hammer, B. G. and Boyes, S. (2008). Synthesis of surface-initiated stimuli-responsive diblock copolymer brushes utilizing a combination of ATRP and RAFT polymerization techniques. **Macromolecules**, 41, 4147-4157.

[56] Braun, R. D. (1982). Introduction to Chemical Analysis. **McGraw-Hill**, 329-335

[57] Musyanovych, A., Rossmanith, R., Tontsch, C. and Landfester, K. (2007). Effect of hydrophilic comonomer and surfactant type on the colloidal stability and size distribution of carboxyl- and amino-functionalized polystyrene particles prepared by miniemulsion polymerization. **Langmuir**, 23, 5367-5376.

APPENDIX

APPENDIX A CALCULATIONS

Calculations of percent conversion of the homo- and copolymerization

Percent conversion of the homo-copolymerization was calculated from integration ratio of the residual monomer peak/ DMF peak as an internal standard (Figure 49).

Example P(*t*-BA)/PEGMA 50/50:

At 0 h ; P(*t*-BA), PEGMA and DMF have integration area 4.72, 4.88 and 1.78, respectively.

At 0.25 h ; P(*t*-BA), PEGMA and DMF have integration area 2.43, 1.89 and 1.03, respectively.

Thus, % conversion of PEGMA and ABA can be calculated from the following equations:

$$\% \text{ conversion} = \left(1 - \frac{[M]}{[M_o]}\right) \times 100;$$

$[M_0]$ = Integration ratio of P(*t*-BA),PEGMA/ DMF were used as an initial concentration

$[M_0]$ of P(*t*-BA) = 4.72/1.78 = 2.65

$[M_0]$ of PEGMA = 4.88 /1.78 = 2.74

$[M]$ = Concentration of integration ratio of P(*t*-BA),PEGMA/ DMF at 0.25 h reaction

$[M]$ of P(*t*-BA) = 2.43/1.03 = 2.36

$[M]$ of PEGMA = 1.89/1.03 = 1.83

$$\% \text{ conversion of P(}t\text{-BA) at 0.25 h} = \left(1 - \frac{[2.36]}{[2.65]}\right) \times 100$$

$$= 10.94 \approx 11$$

$$\% \text{ conversion of PEGMA at 0.25 h} = \left(1 - \frac{[1.83]}{[2.74]}\right) \times 100$$

$$= 33.21 \approx 33$$

The percent conversion of P(*t*-BA)/PEGMA copolymer at other molar ratios (100/0, 75/25 and 25/75, respectively) were calculated in a similar fashion

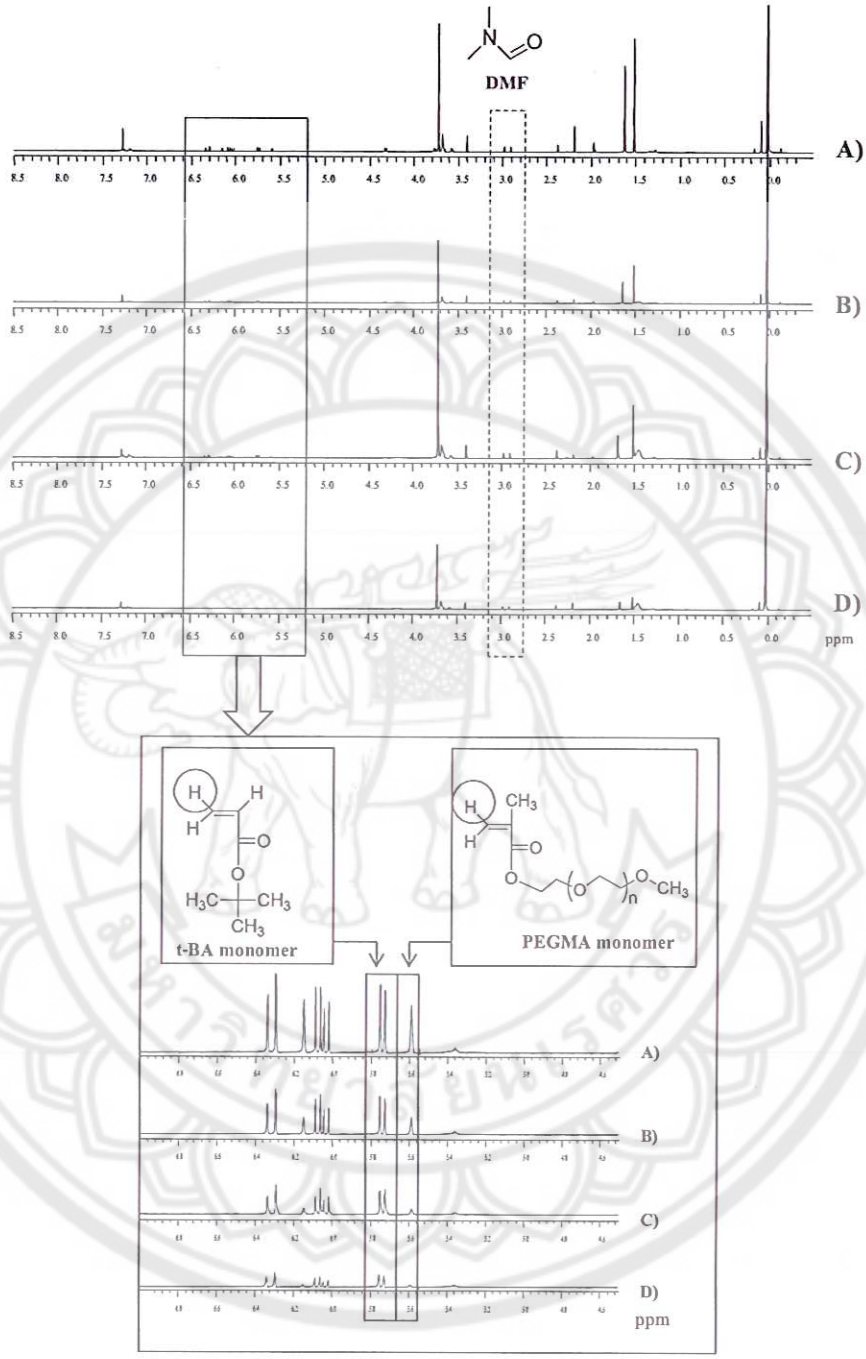

Figure 51 ^{1}H NMR spectra of 50:50 P(*t*-BA): PEGMA copolymer as calculation their %conversion A) 0 h, B) 0.25 h (15 min), C) 0.50 h (30 min) and D) 0.75 h (45min)

Calculation of molecular weight of 50/50 P(*t*-BA)/PEGMA copolymer

Molecular weight of 50/50 P(*t*-BA)/PEGMA copolymer were calculated from the following equation:

$$M_{n,th} = ([P(t\text{-BA})]_0/[EBiB]_0 \times conv._{P(t\text{-BA})} \times M_{P(t\text{-BA})}] + ([PEGMA]_0/[EBiB]_0 \times conv._{PEGMA} \times M_{PEGMA})$$

M_n of 50/50 P(*t*-BA)/PEGMA copolymer at 2 h = ((0.5/1)×51×128.17(g/mol)) + ((0.5/1)×78×300(g/mol))

= 14968 g/mol

The Molecular weight of 50/50 P(*t*-BA)/PEGMA copolymer at other time were calculated in a similar fashion

Calculation of percentage of P(*t*-BA) and PEGMA in the copolymer

50/50 P(*t*-BA)/PEGMA copolymer were calculated from the feed composition of the monomers and taking percent conversion into account. Thus, % P(*t*-BA) and PEGMA in the copolymer was estimated from the following equation:

$$\%\ P(t\text{-BA})\ \text{in the copolymer} = \frac{[\%\ Conv._{P(t\text{-BA})} \times \%\ feed_{t\text{-BA}}]}{[\%\ Conv._{P(t\text{-BA})} \times \%\ feed_{t\text{-BA}} + \%\ Conv._{PEGMA} \times \%\ feed_{PEGMA}]}$$

$$= \frac{[42\times0.5\ ]}{[(42\times0.5) + (64\times0.5)\ ]}$$

% P(*t*-BA) in the copolymer = 40

% PEGMA in the copolymer = 60

In the same way, the % conversion of P(*t*-BA)/PEGMA copolymer at various molar ratios (100/0, 75/25 and 25/75, respectively) were calculated as above equation.

Calculations of percentage of the composition in the polymer-MNP complex determined via thermogravimetric analysis (TGA) technique

1. Calculation of % yield magnetite nanoparticles (Fe_3O_4)

$$\%\ \text{yield} = \frac{\text{mole of } Fe_3O_4}{\text{mole of } Fe(acac)_3}$$

$Fe(acac)_3$ molecular weight = 353.17 g/mol

Fe_3O_4 molecular weight = 231.4 g/mol

weight of $Fe(acac)_3$ = 5 g

$$\therefore \text{ mole of } Fe(acac)_3 = \frac{5\,(g)}{353.17\,(g/mol)}$$

$$= 0.0142 \text{ mol}$$

Fe of $Fe(acac)_3$ 1 mol to obtain Fe of Fe_3O_4 3 mol

$$\text{If } Fe(acac)_3\ 0.0142 \text{ mol to obtain } Fe_3O_4 = \frac{3\,(mol) \times 0.0142\,(mol)}{1\,(mol)}$$

$$= 0.0130 \text{ mol}$$

$$\text{Therefore \% yield of } Fe_3O_4 = \frac{13.7 \times 60.7}{35.5}$$

$$= 91.5\ \%$$

2. Calculation of % Fe_3O_4 and % components in complexes

$$\%\ Fe_3O_4 \text{ in complexes} = \frac{\%\ Fe_3O_4 \text{ in polymer-coated MNP} \times 100}{\%\ Fe_3O_4 \text{ in MNP}}$$

values of % Fe_3O_4 in polymer-coated MNP from TGA technique

- % Fe_3O_4 in MNP = 88 %
- % Fe_3O_4 in BTPAm-coated MNP = 81%
- % Fe_3O_4 in 100/0 P(*t*-BA)/PEGMA-coated MNP = 63 %
- % Fe_3O_4 in 75/25 P(*t*-BA)/PEGMA-coated MNP = 55 %
- % Fe_3O_4 in 50/50 P(*t*-BA)/PEGMA-coated MNP = 52 %
- % Fe_3O_4 in 25/75 P(*t*-BA)/PEGMA-coated MNP = 53 %
- % Fe_3O_4 in 100/0 PAA/PEGMA-coated MNP = 78 %
- % Fe_3O_4 in 75/25 PAA/PEGMA-coated MNP = 68 %
- % Fe_3O_4 in 50/50 PAA/PEGMA-coated MNP = 64 %
- % Fe_3O_4 in 25/75 PAA/PEGMA-coated MNP = 70 %

2.1 Bare MNP (Percent char yield = 87.95%)

% Fe_3O_4	= (87.95/87.95) ×100	= 100 %

2.2 BTPAm-coated MNP complexes (Percent char yield = 81.39 %)

% Fe_3O_4	= (81.39/87.95) ×100	= 92.54 %
% BTPAm	= 100-92.54 %	= 7.46 %

(weight ratio of Fe_3O_4 : BTPAm = 12.4 : 1.0)

2.3 100/0 P(*t*-BA)/PEGMA-coated MNP (Percent char yield = 62.58 %)

% Fe_3O_4	= (62.58/87.95) ×100	= 71.15%
% BTPAm	= (1×71.15)/12.47	= 5.74 %
% copolymer in complexes	= 100-(71.15+5.74)	= 23.11 %

2.4 75/25 P(*t*-BA)/PEGMA -coated MNP (Percent char yield = 55.03 %)

% Fe_3O_4	= (55.03/87.95) ×100	= 62.57%
% BTPAm	= (1× 62.57)/12.4	= 5.04 %
% copolymer in complexes	= 100-(62.57+5.04)	= 32.38 %

2.5 50/50 P(*t*-BA)/PEGMA -coated MNP (Percent char yield = 51.71%)

% Fe_3O_4	= (51.71/87.95) ×100	= 58.79%
% BTPAm	= (58.79)/12.4	= 4.74 %
% copolymer in complexes	= 100-(58.79+4.74)	= 36.46 %

2.6 25/75 P(*t*-BA)/PEGMA -coated MNP (Percent char yield = 53.15 %)

% Fe_3O_4	= (53.15/87.95) ×100	= 60.43 %
% BTPAm	= (1×60.43)/12.4	= 4.87 %
% copolymer in complexes	= 100-(60.43+4.87)	= 34.70 %

2.7 100/0 PAA/PEGMA -coated MNP (Percent char yield = 77.61 %)

% Fe_3O_4	= (77.61/87.95) ×100	= 88.24 %
% BTPAm	= (1×88.24)/12.4	= 7.12 %
% copolymer in complexes	= 100-(88.24+7.12)	= 4.64 %

2.8 75/25 PAA/PEGMA -coated MNP (Percent char yield = 67.55 %)

% Fe_3O_4	= (67.55/87.95) ×100	= 76.80%
% BTPAm	= (1×76.80)/12.4	= 6.19 %
% copolymer in complexes	= 100-(76.80+6.19)	= 17 %

2.9 50/50 PAA/PEGMA -coated MNP (Percent char yield = 64.30%)

% Fe_3O_4	= (64.30/87.95) ×100	= 73.11%
% BTPAm	= (1×73.11)/12.4	= 5.89 %
% copolymer in complexes	= 100-(73.11+5.89)	= 20.99 %

3.0 25/75 P(*t*-BA)/PEGMA -coated MNP (Percent char yield = 70.28 %)

% Fe_3O_4	= (70.28/87.95) ×100	= 79.91 %
% BTPAm	= (1×79.91)/12.4	= 6.44 %
% copolymer in complexes	= 100-(79.91+6.44)	= 13.65 %

Examples of the measurement of the numbers of carboxyl groups on the MNP surface

The conductometric black titration was use for determination of number of carboxylic groups on the MNP surface, which can be calculated from the following equation,

$$[Acid] = \frac{V \times M \times N_A}{SC}$$

where, [Acid] is the number of carboxyl group (molecules/g)

V is the consumption volume of HCl solution in the second region (region II) of the conductometric titration (L)

M is the molar concentration of polyelectrolyte (mol/L)

N_A is Avogadro's constant (6.022×10^{23} molecules/mol)

SC is the solid content or the sample (g)

From TEM analysis, particle diameter is 8 nm.

Surface area = $4\pi r^2$, where r = 4 nm

Thus, surface area of a single particle = $4 \times 22/7 \times 4^2$ =201 nm^2

Volume = $4/3\pi r^3$, where r = 4 nm

Thus, volume of a single particle = $4/3 \times 22/7 \times 4^3$ = 268 nm^3

Because density of magnetite = 5.26 g/cm^3 [1-2] = mass/volume

Mass of a single particle $= 5.26\ g/cm^3 \times 268\ nm^3$

$= 1.41 \times 10^{-18}\ g$

Example PAA/PEGMA 50/50:

$$[Acid] = \frac{((5.2-1.6)\times10^{-3}\,L)\times(0.005 mol/L)\times(6.022\times10^{23}\,molecules/mol)}{1.50\times10^{-3}\,g}$$

$= 7.2264\times10^{21}$ molecules/g

$= 7.2264\times10^{21}$ molecules/ 7.09×10^{17} particles

$\approx$ 10,192 molecules/particle

$\approx$ 10,192 molecules/201 nm^2

$\approx$ 52 molecules/nm^2

In the same way, the calculation of carboxylic group of PAA/PEGMA copolymer at various molar ratios (100/0, 75/25 and 25/75, respectively) were calculated as above equation (Table 1).

Table 15 Results of conductometric titration of PAA/PEGMA copolymer at various molar ratios

sample	Conductometric back titration	
	Amount of carboxyl groups per	
	Particle*	nm^2*
PAA/PEGMA-coated MNP 100/0	10,400	52
PAA/PEGMA-coated MNP 75/25	9,000	45
PAA/PEGMA-coated MNP 50/50	8,200	41
PAA/PEGMA-coated MNP 25/75	7,400	37

*Determined from the average values from the experiment

References

[1] Tebble RS, Craik DJ. Magnetic Materials, Wiley-Interscience, London, 1969.

[2] Cornell RM, Schertmann U. The Iron Oxides: Structure, Properties, Reactions, Occurrence and Uses, VCH Publishers, Weinheim, 1996.

APPENDIX B FT-IR spectra

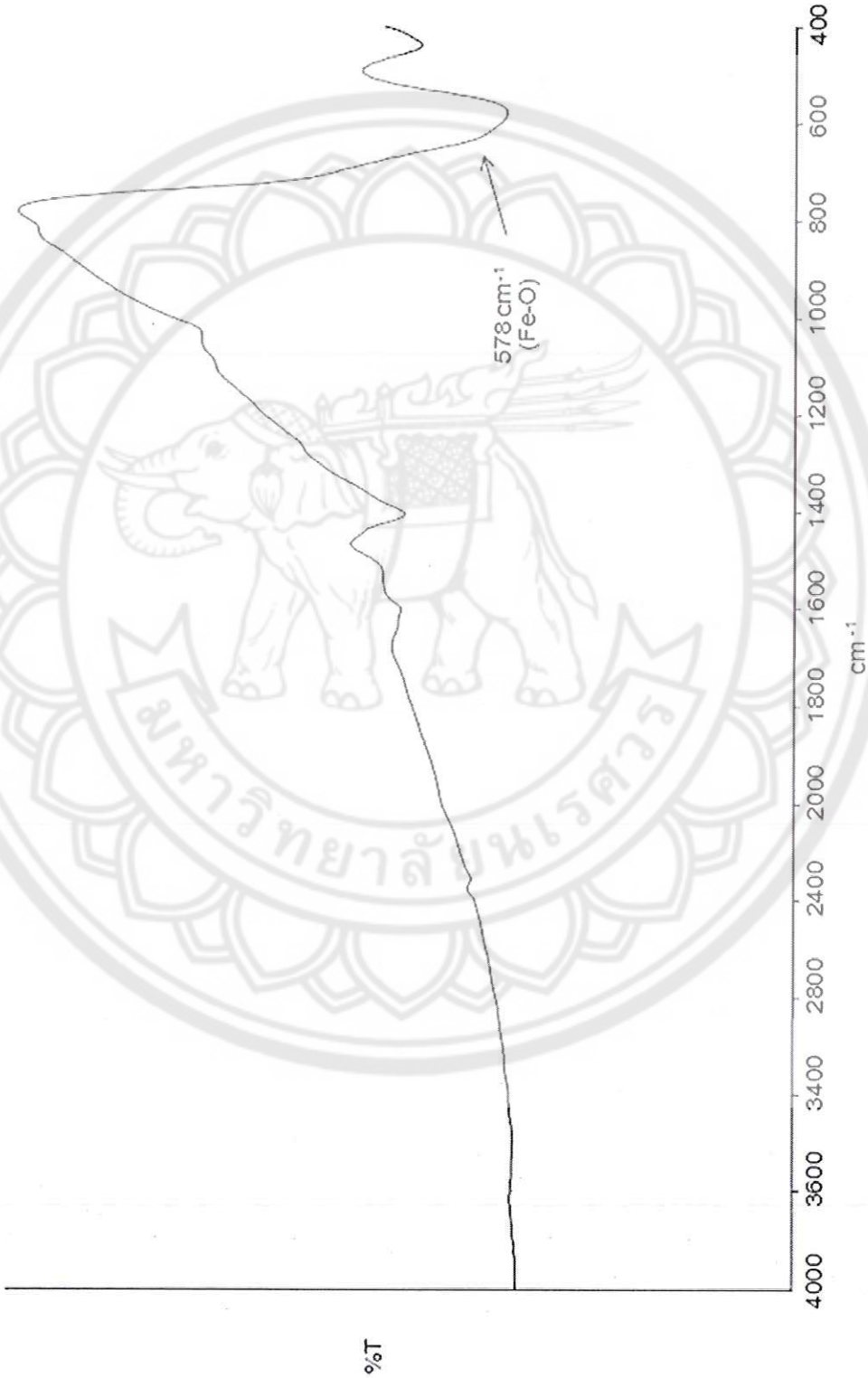

Figure 52 An FT-IR spectrum of bare magnetite nanoparticles (MNPs)

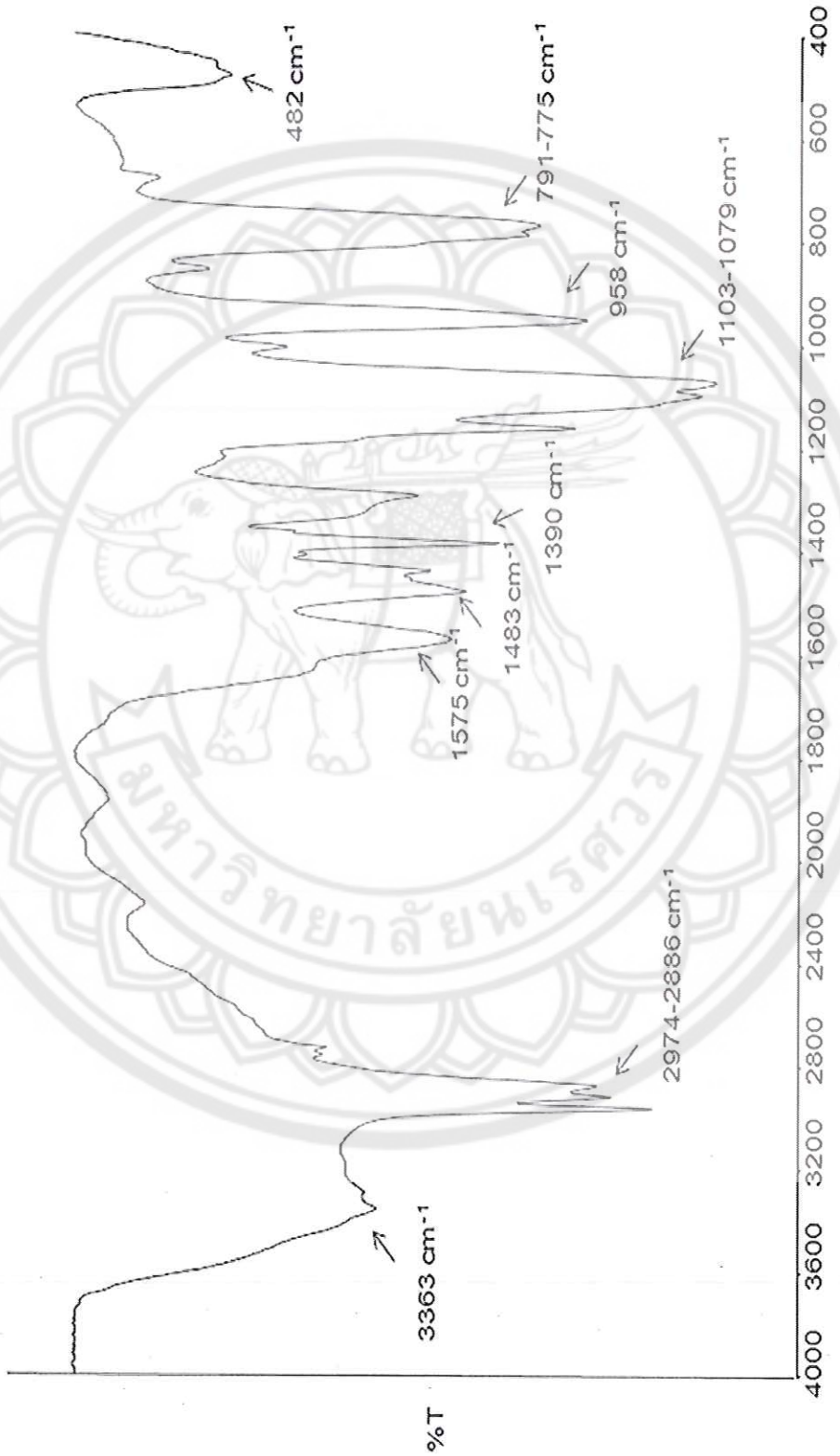

Figure 53 An FT-IR spectrum of 3-aminopropyl triethoxysilane (APS)

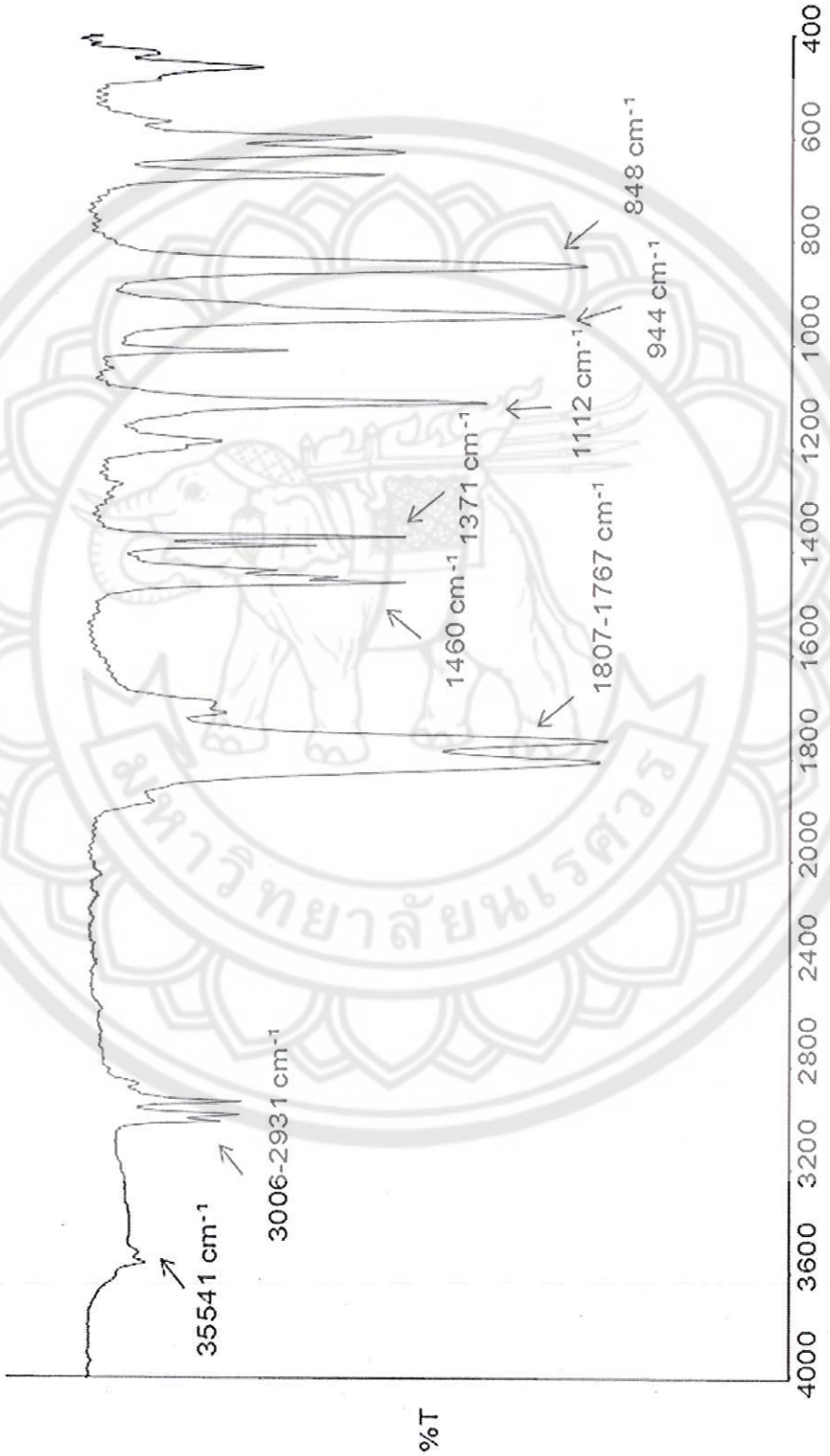

Figure 54 An FT-IR spectrum of 2-bromoisobutyryl bromide (BIBB)

Figure 55 An FT-IR spectrum of 2-bromo-2-methyl-N-(3-triethoxysilyl) propanamide (BTPAm)

Figure 56 An FT-IR spectrum of BTPAm-coated MNPs

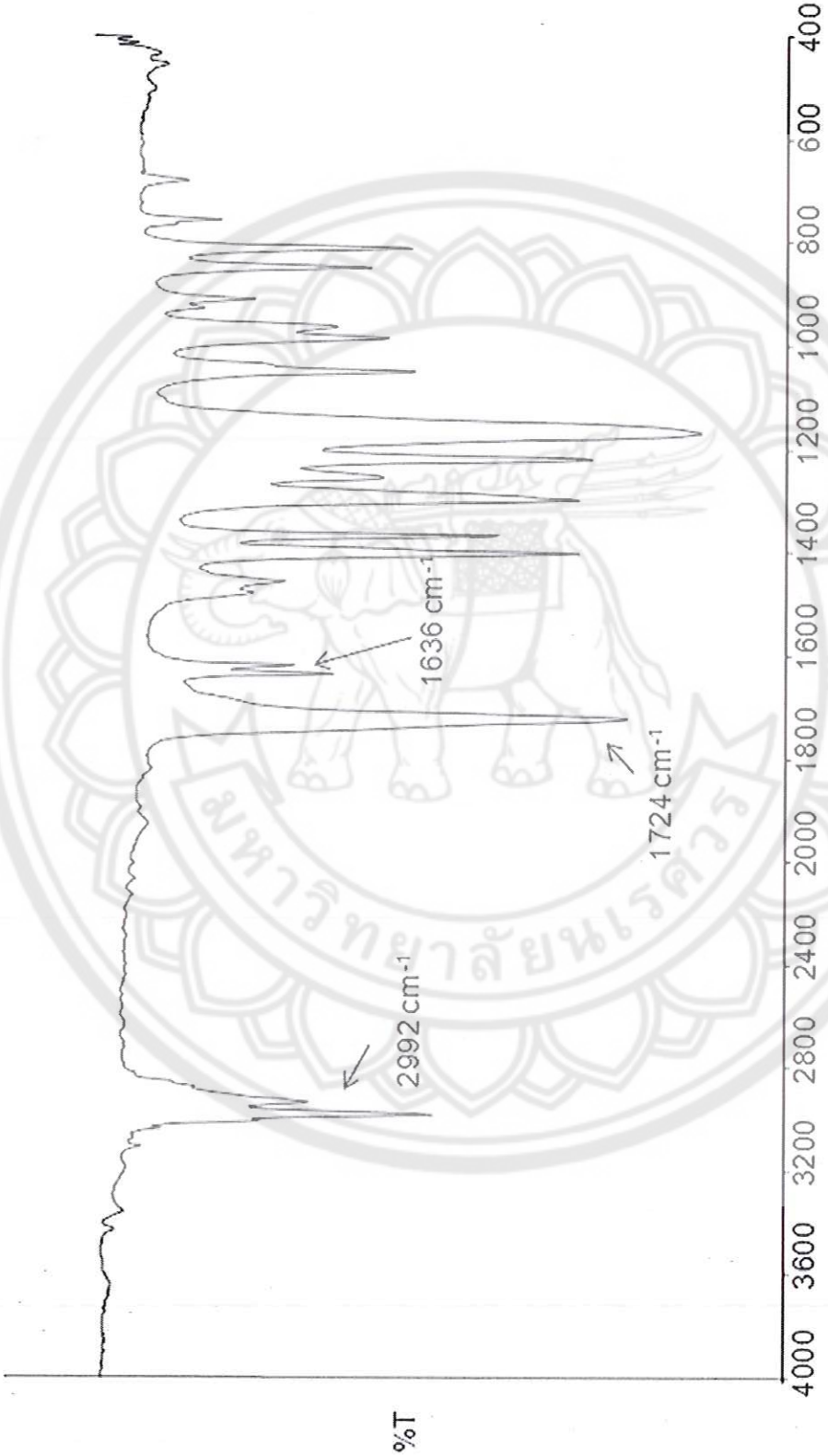

Figure 57 An FT-IR spectrum of *tert*-butyl acrylate (*t*-BA) monomer

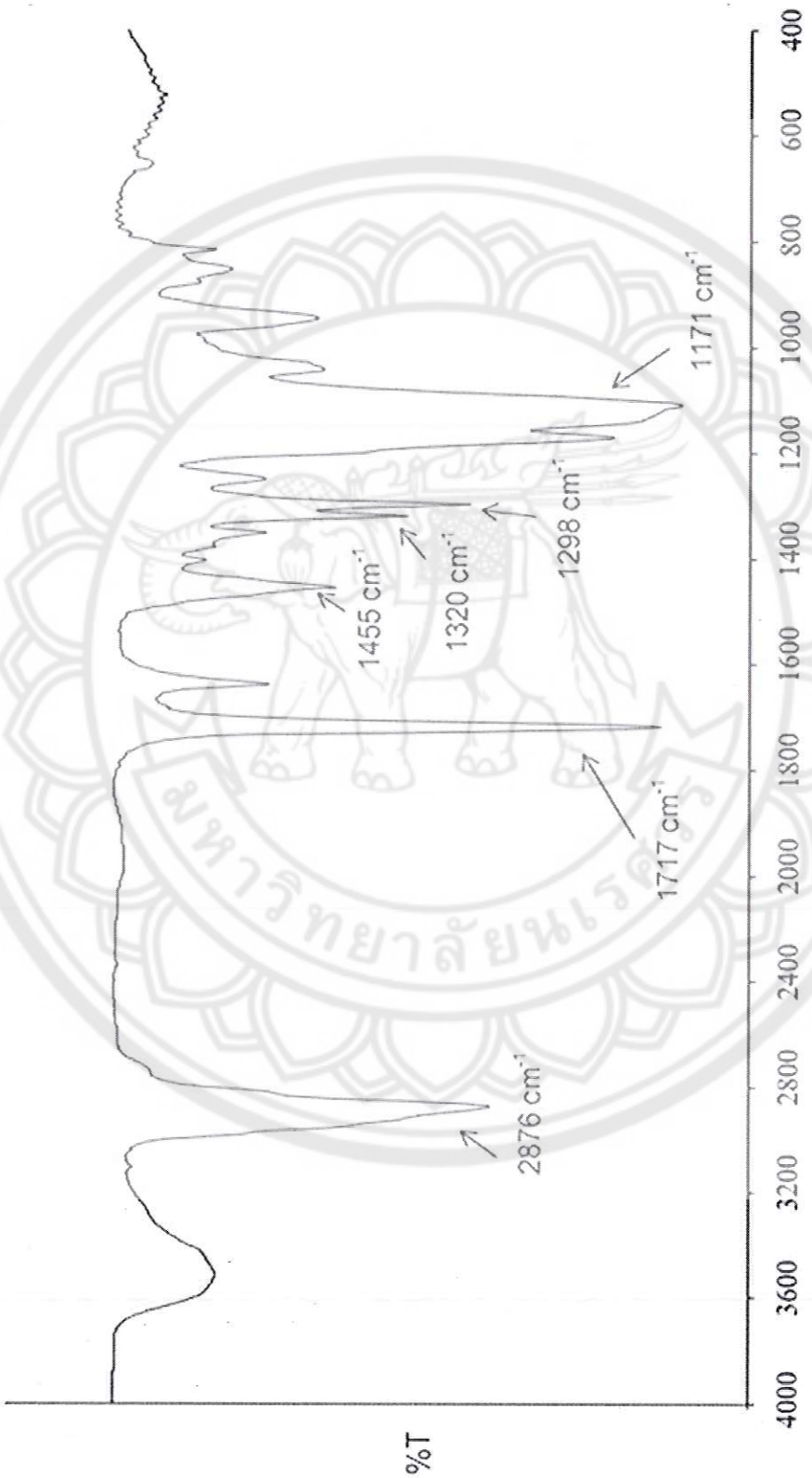

Figure 58 An FT-IR spectrum of PEGMA

Figure 59 An FT-IR spectrum of P(*t*-BA)-coated MNPs

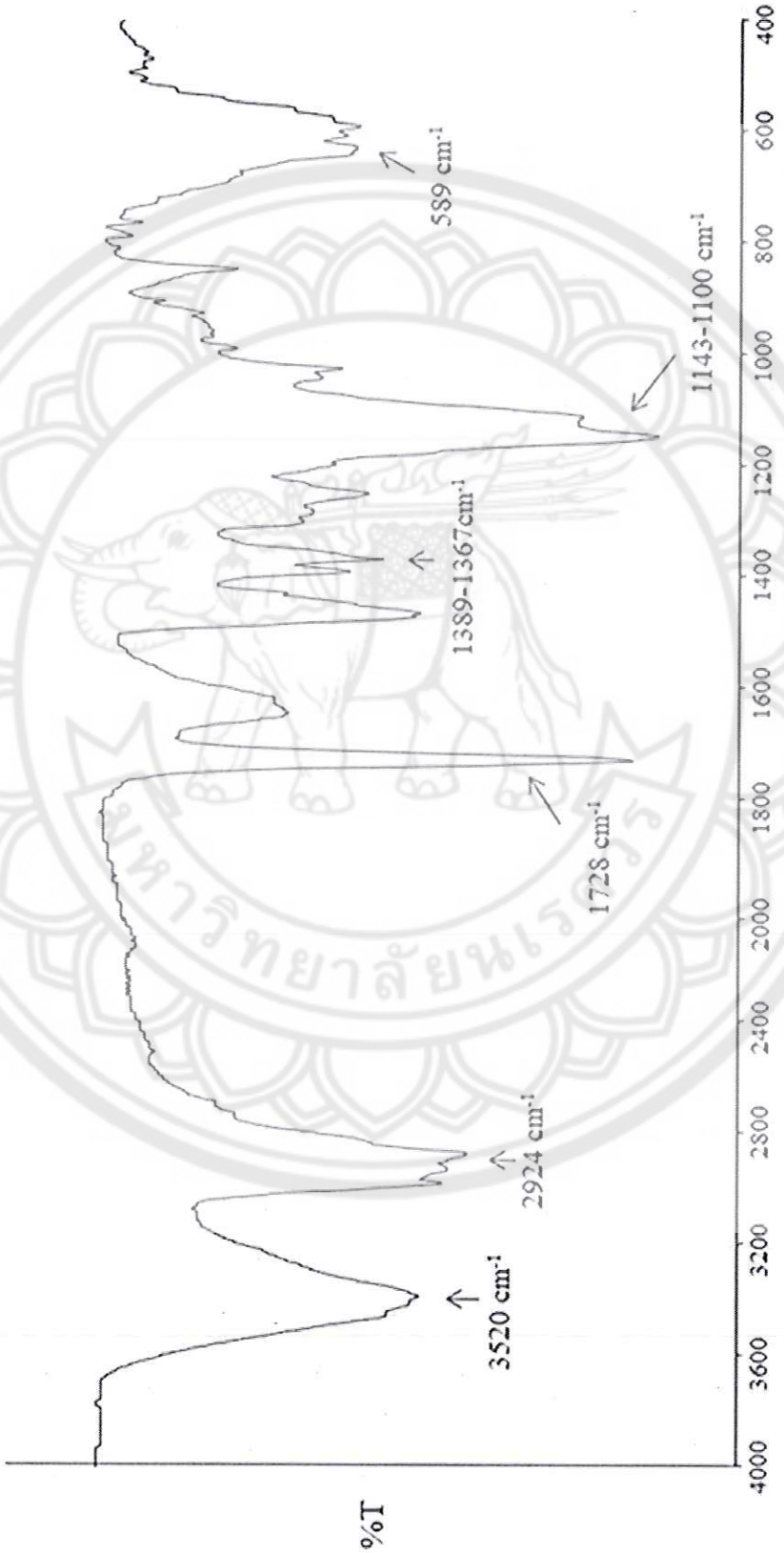

Figure 61 An FT-IR spectrum of P(*t*-BA)/PEGMA(50/50)-coated MNPs

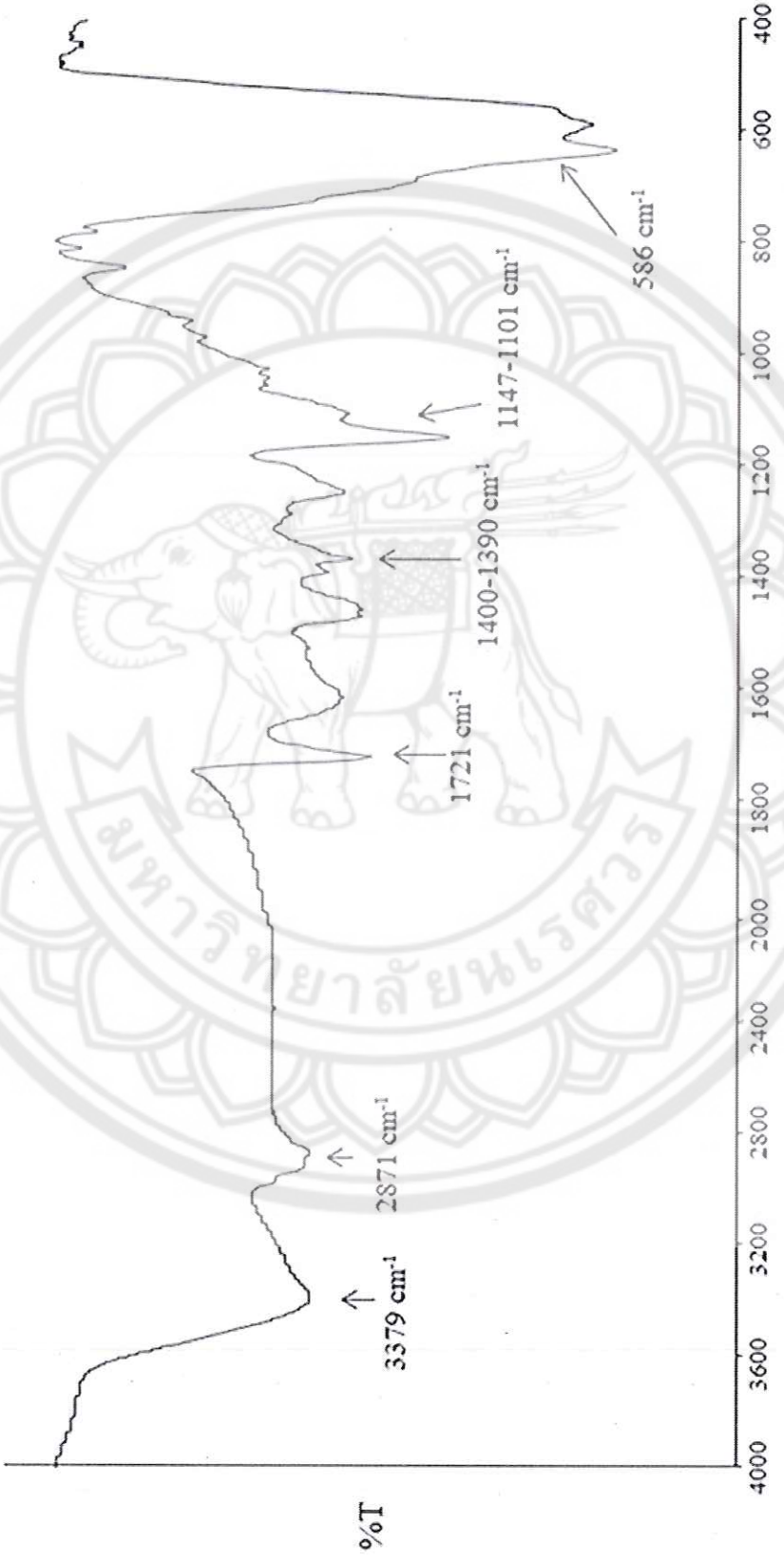

Figure 62 An FT-IR spectrum of P(*t*-BA)/PEGMA (25/75)-coated MNPs

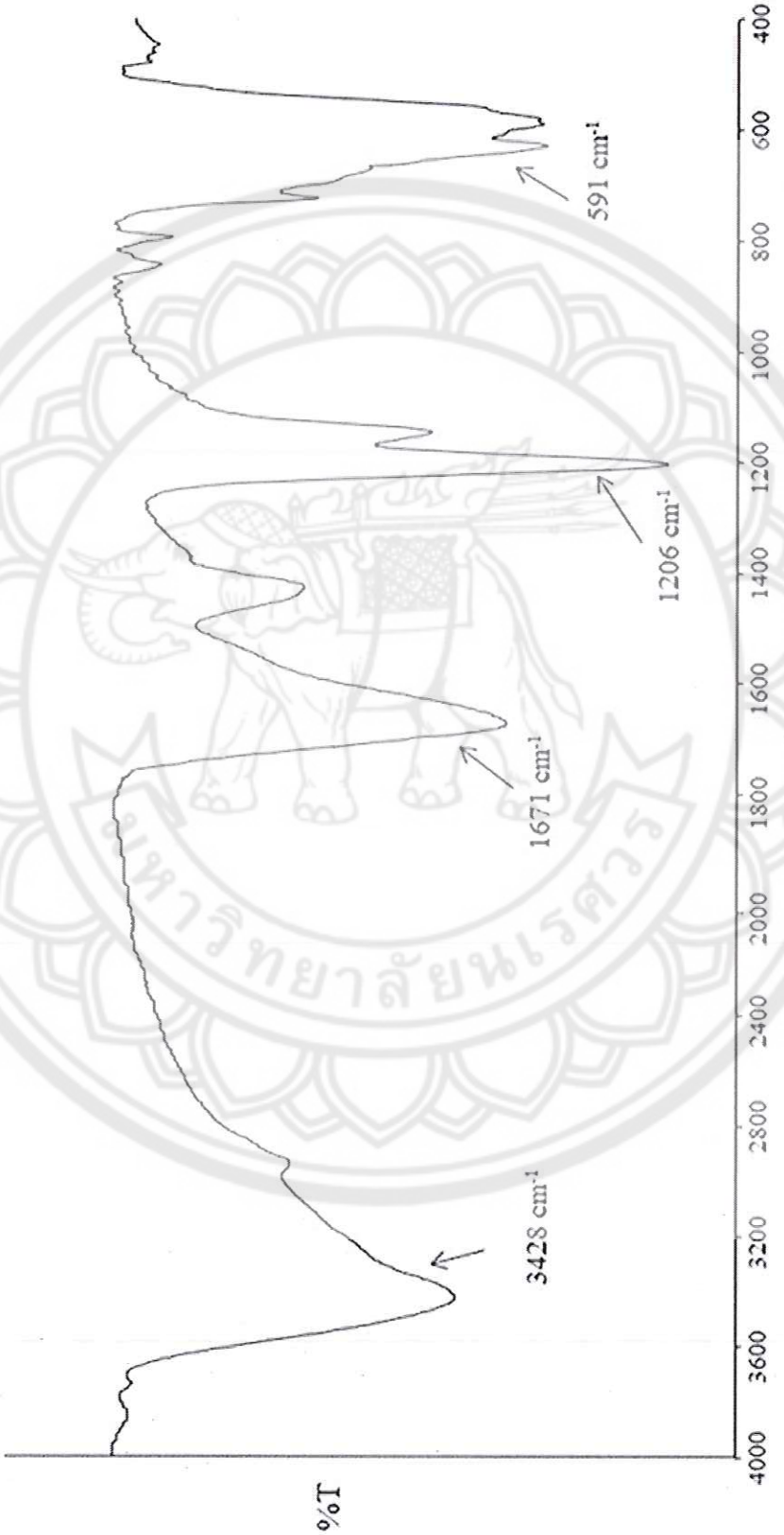

Figure 63 An FT-IR spectrum of PAA-coated MNPs

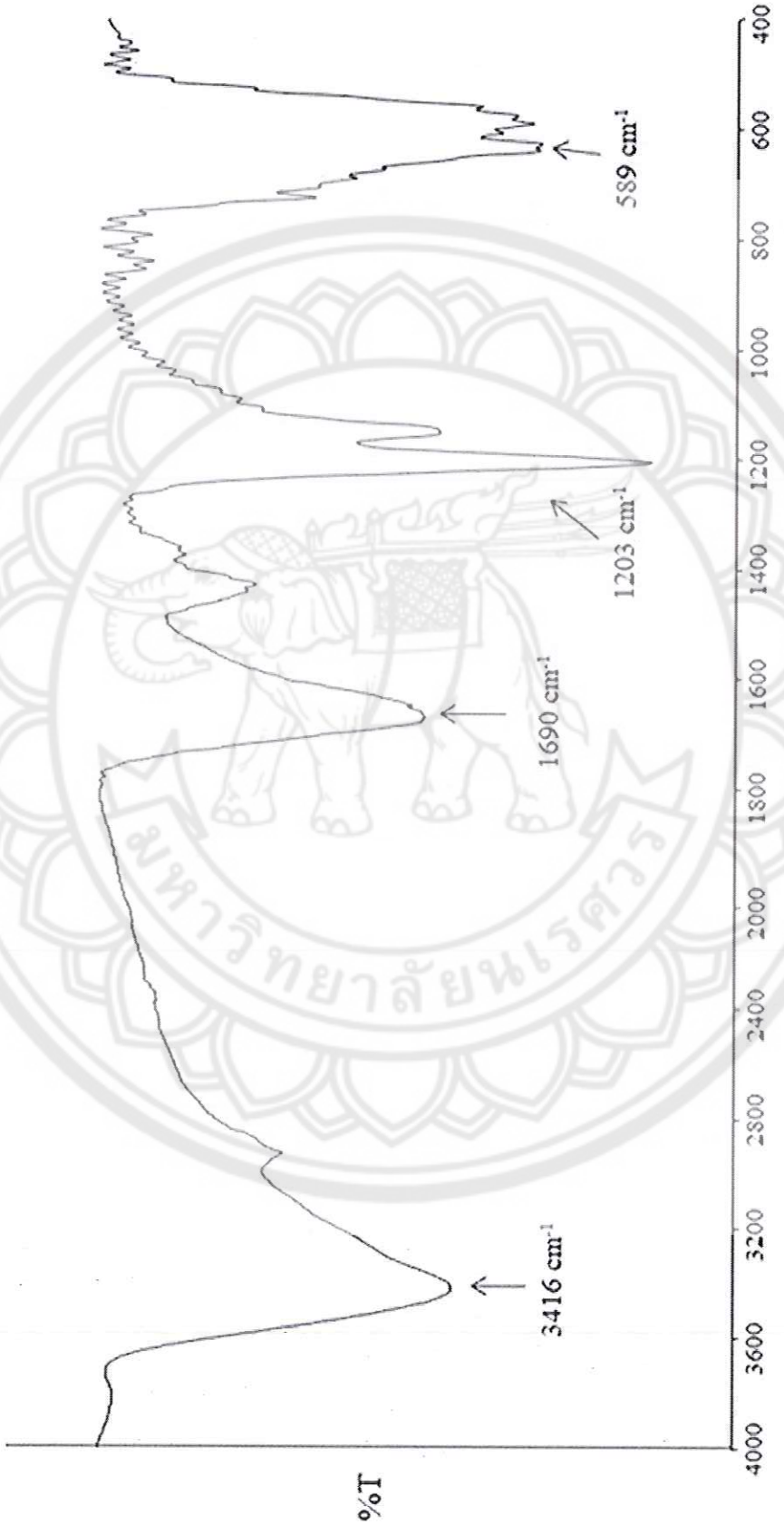

Figure 64 An FT-IR spectrum of PAA/PEGMA (75/25)-coated MNPs

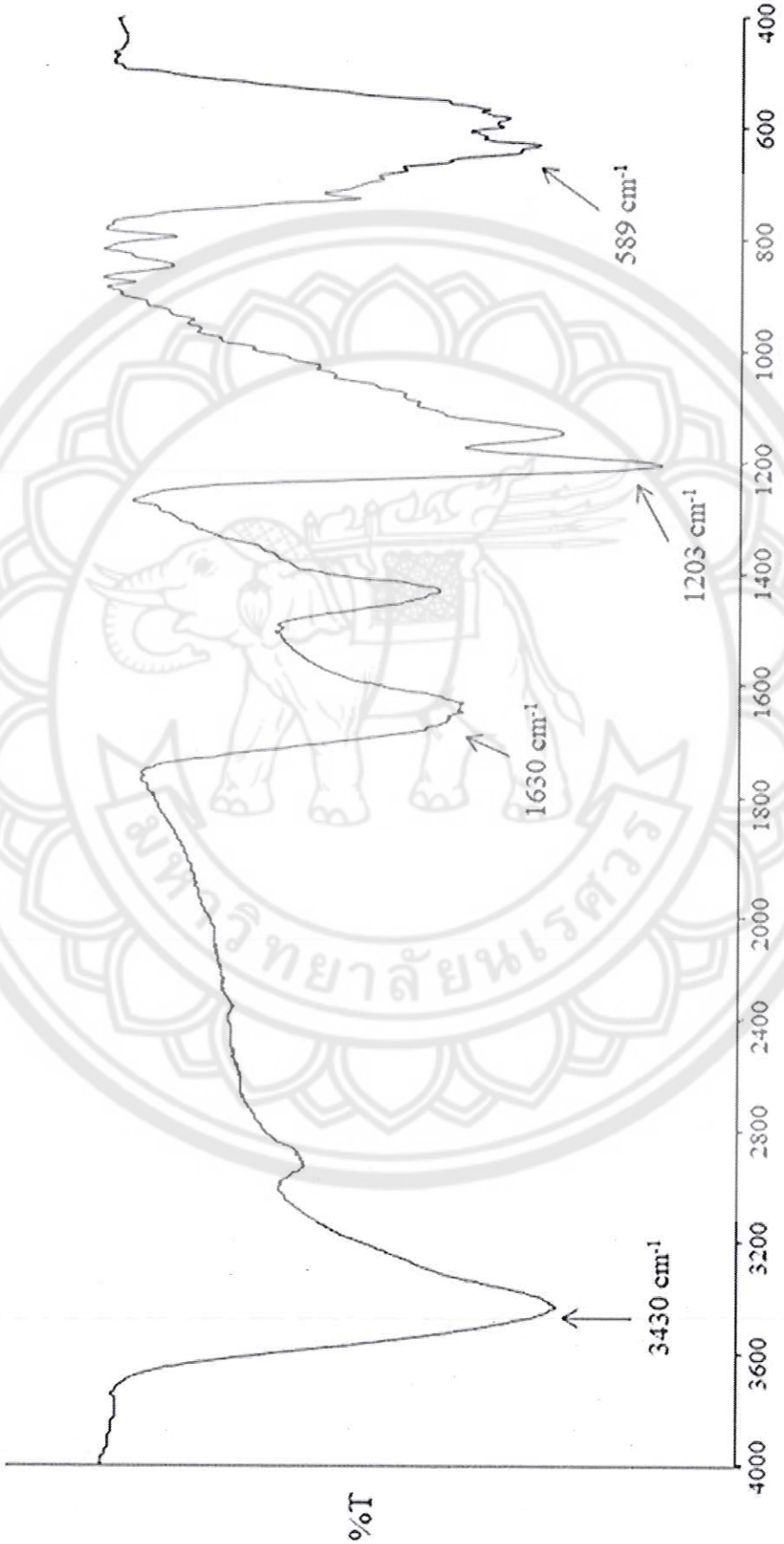

Figure 65 An FT-IR spectrum of PAA/PEGMA (50/50)-coated MNPs

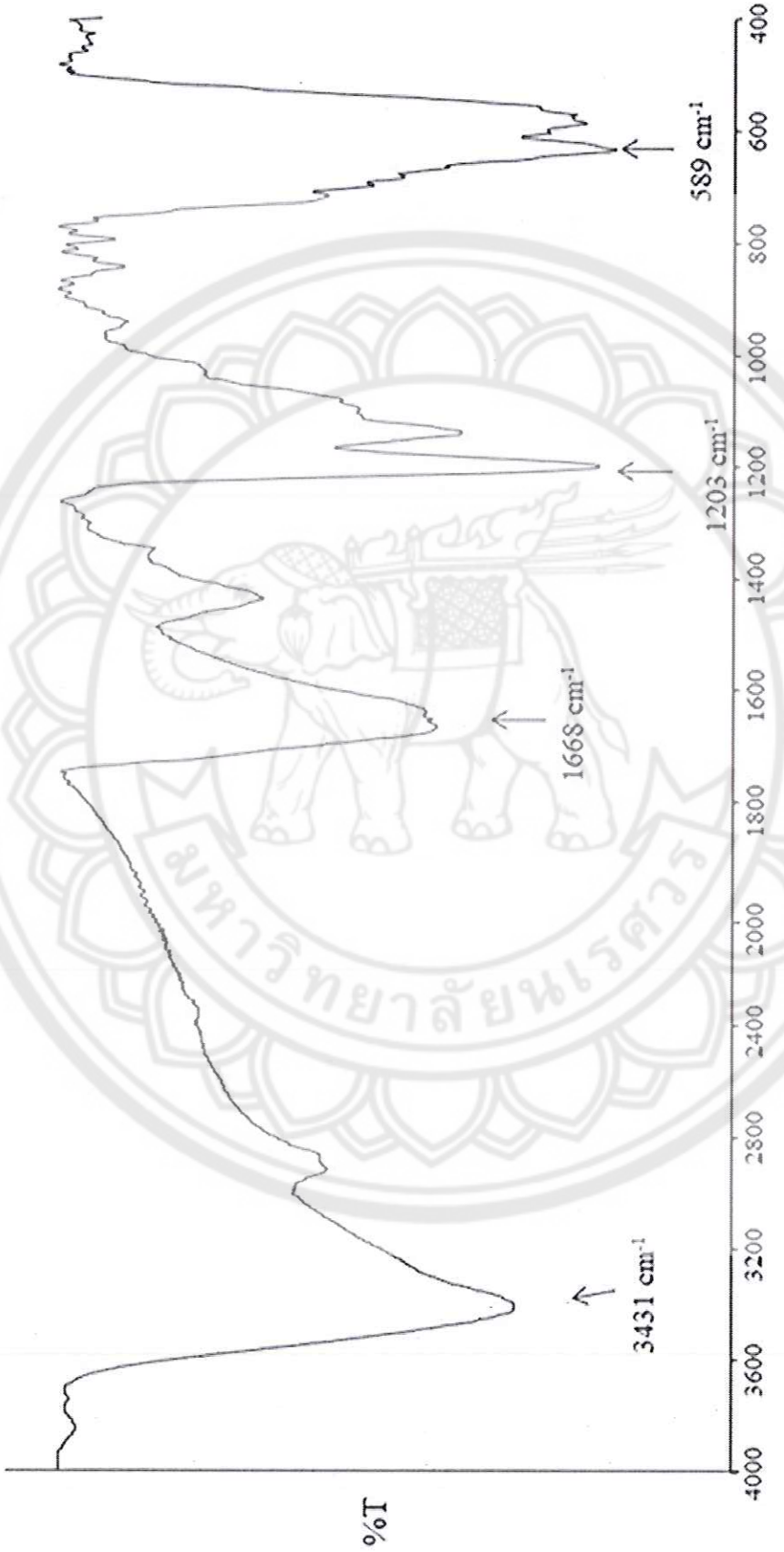

Figure 66 An FT-IR spectrum of PAA/PEGMA (25/75)-coated MNPs

APPENDIX C ^{1}H NMR spectra

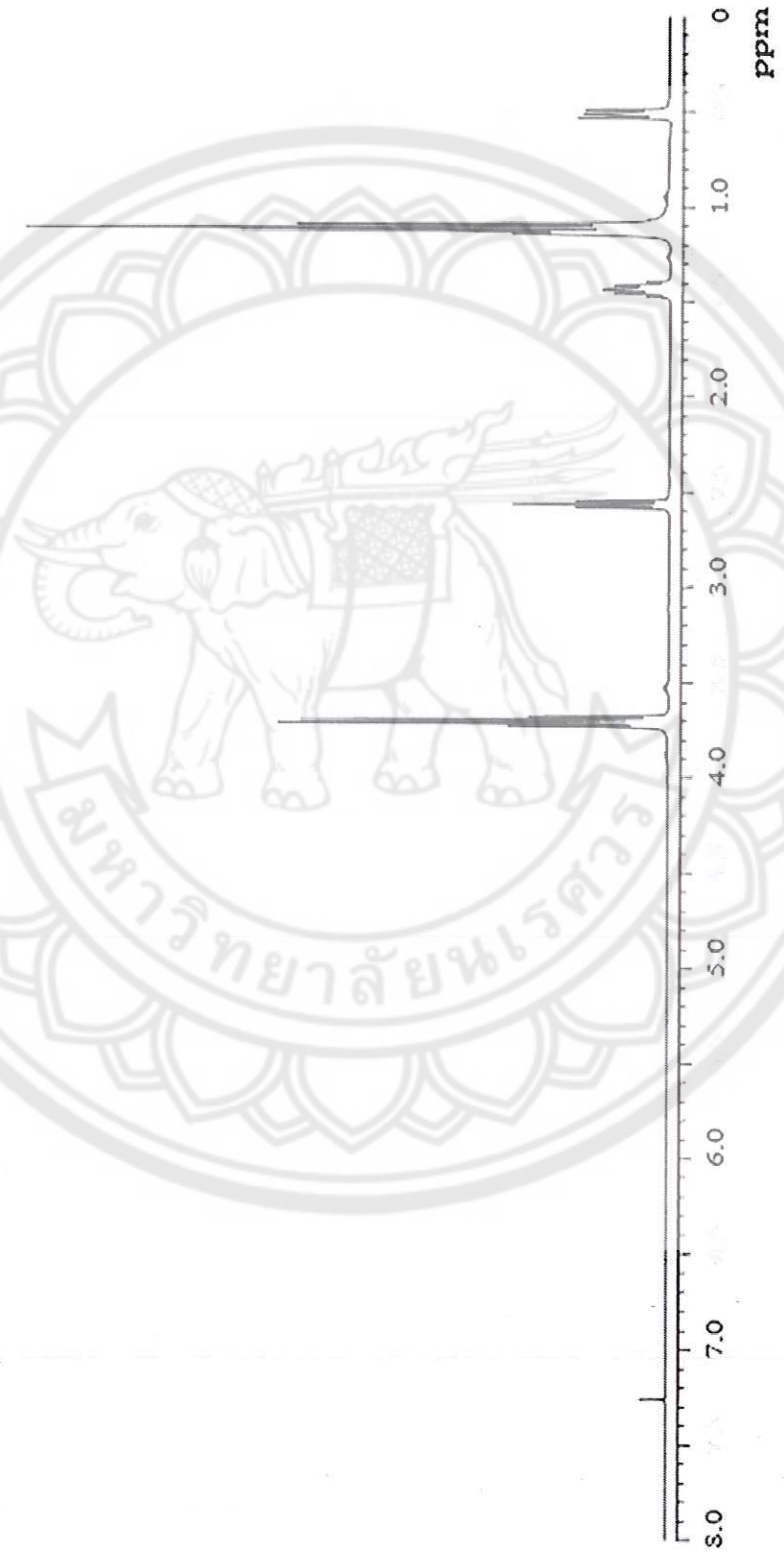

Figure 67 A ^{1}H NMR spectrum of 3-aminopropyl triethoxysilane (APS)

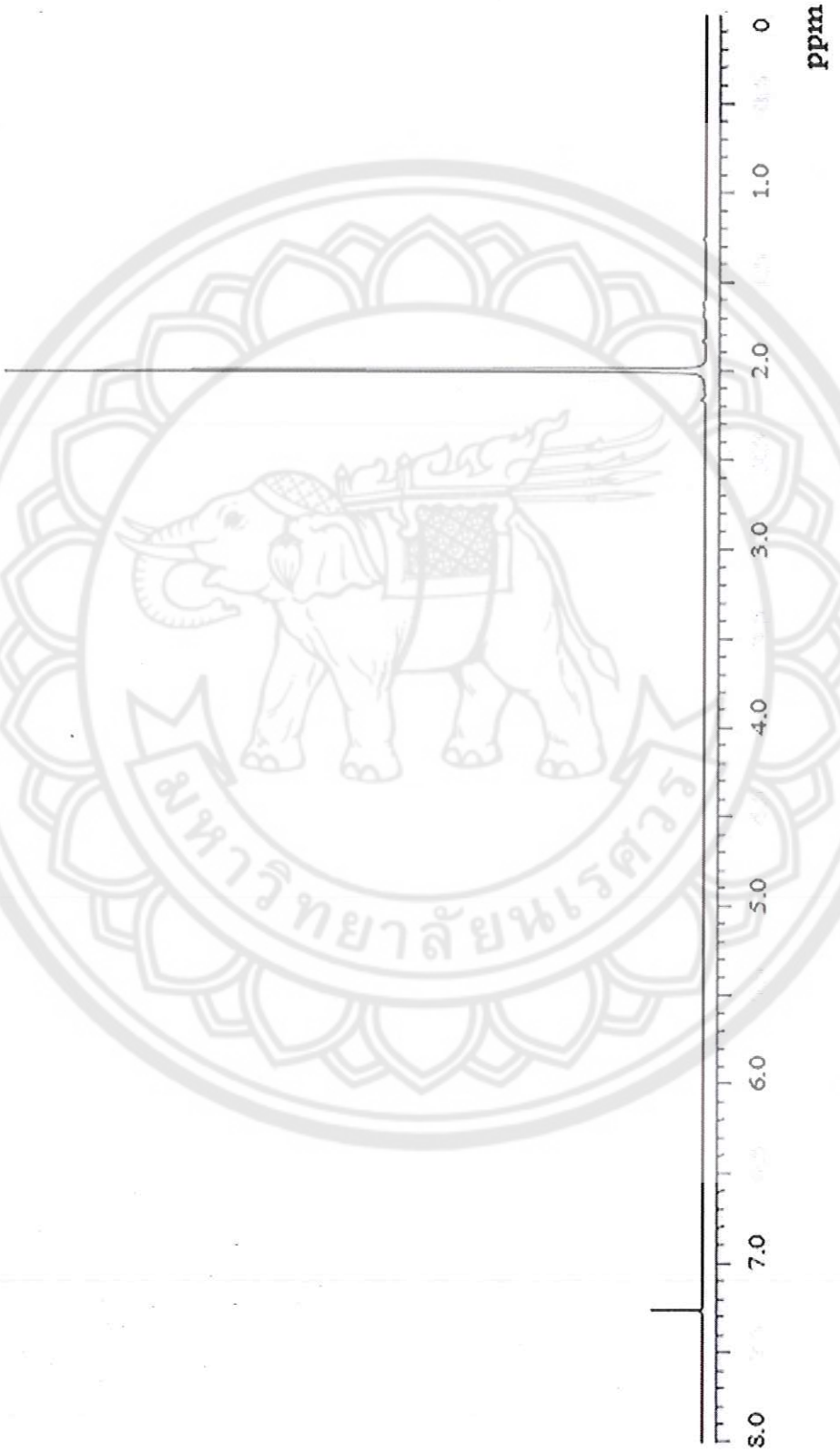

Figure 68 A ^{1}H NMR spectrum of 2-bromoisobutyryl bromide (BIBB)

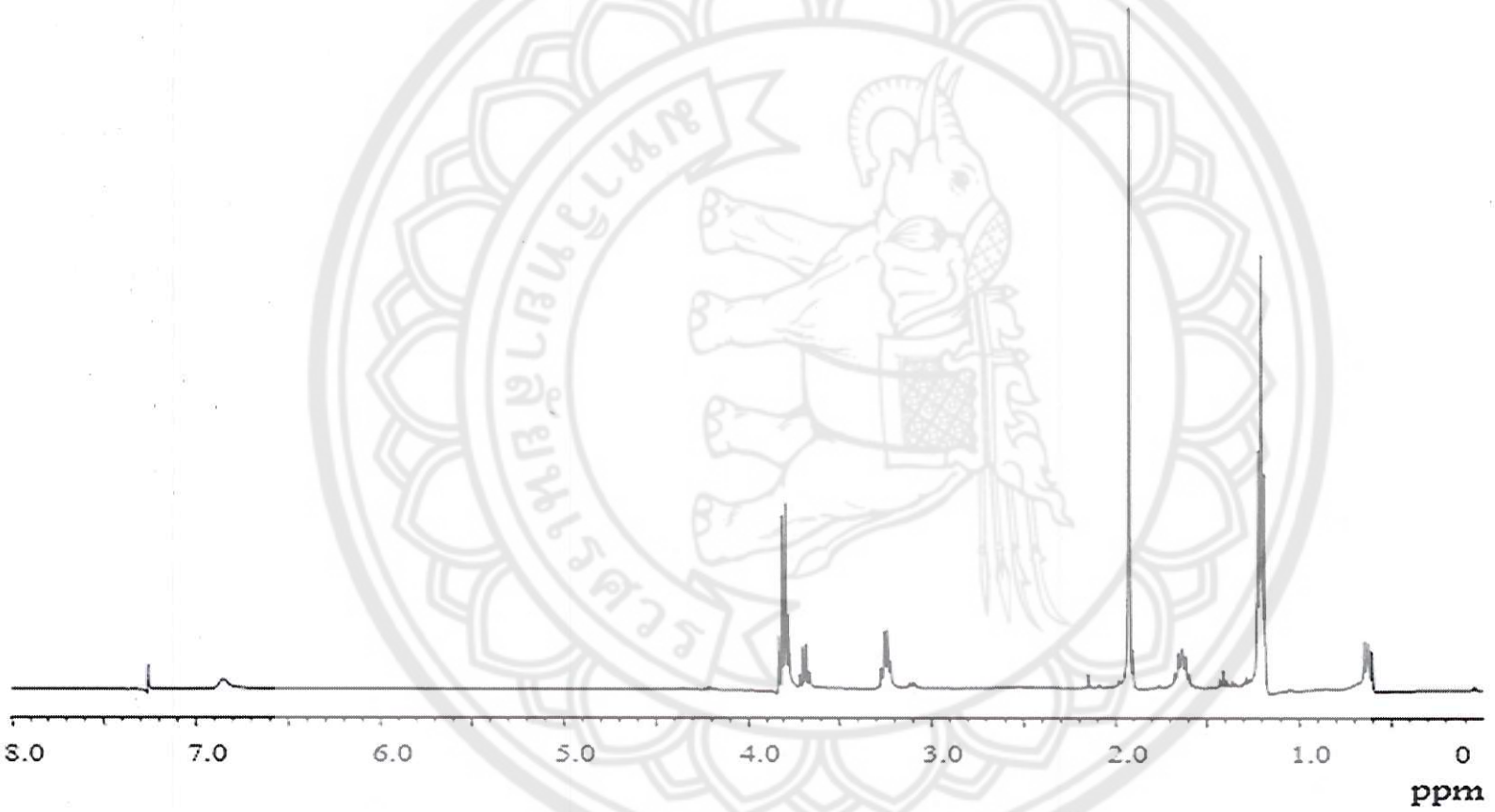

Figure 69 A ^{1}H NMR spectrum of 2-bromo-2-methyl-N-(3-triethoxysilyl) propanamide (BTPAm)

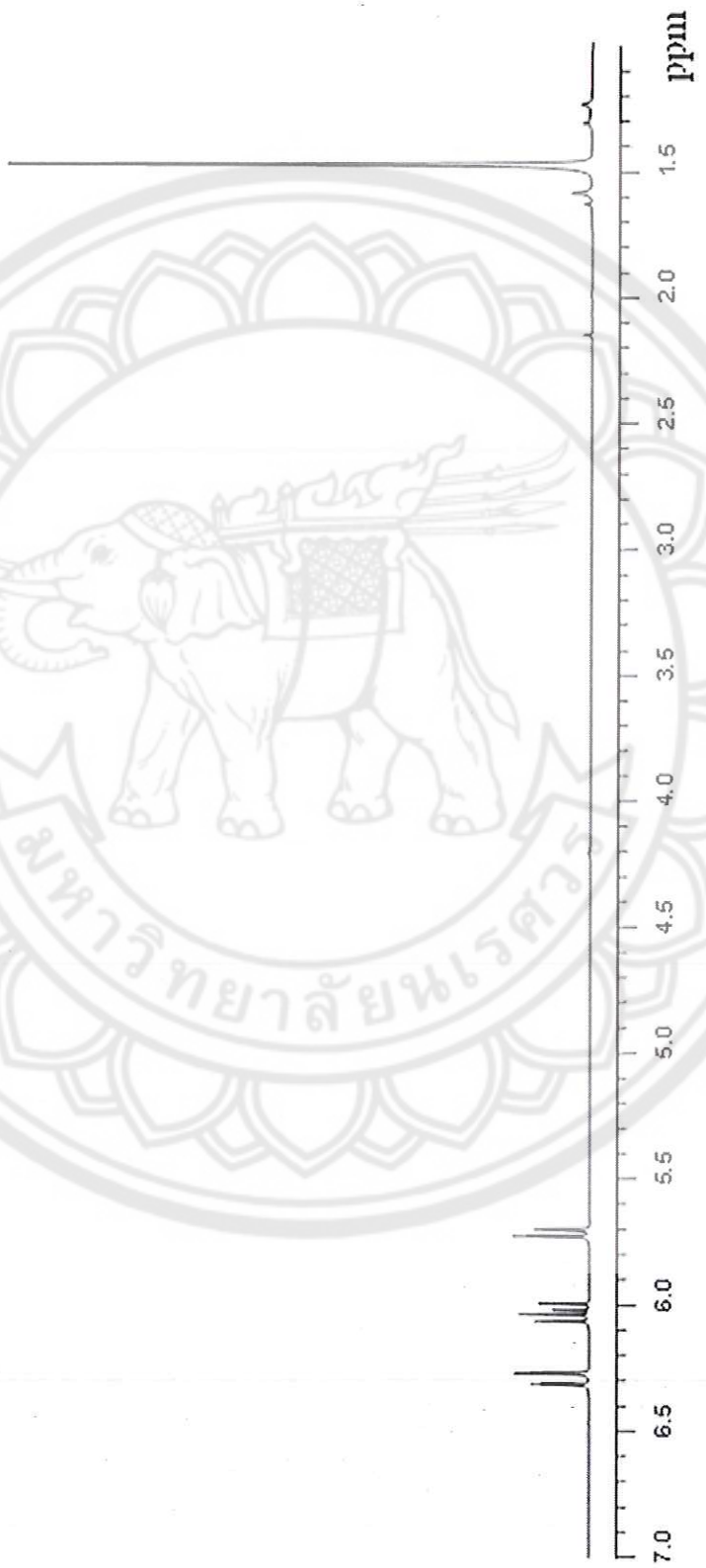

Figure 70 A ^{1}H NMR spectrum of *t*-BA monomer

Figure 71 A ^{1}H NMR spectrum of PEGMA

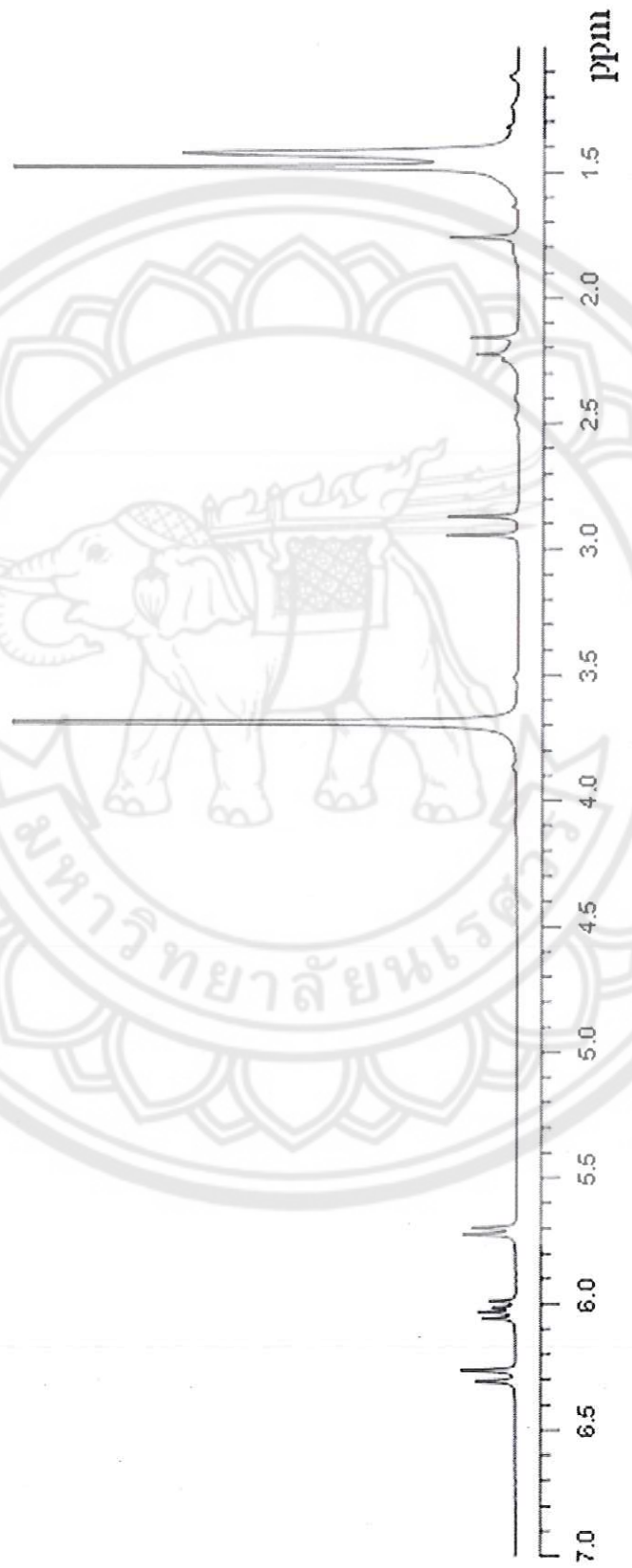

Figure 72 A ^{1}H NMR spectrum of P(*t*-BA)

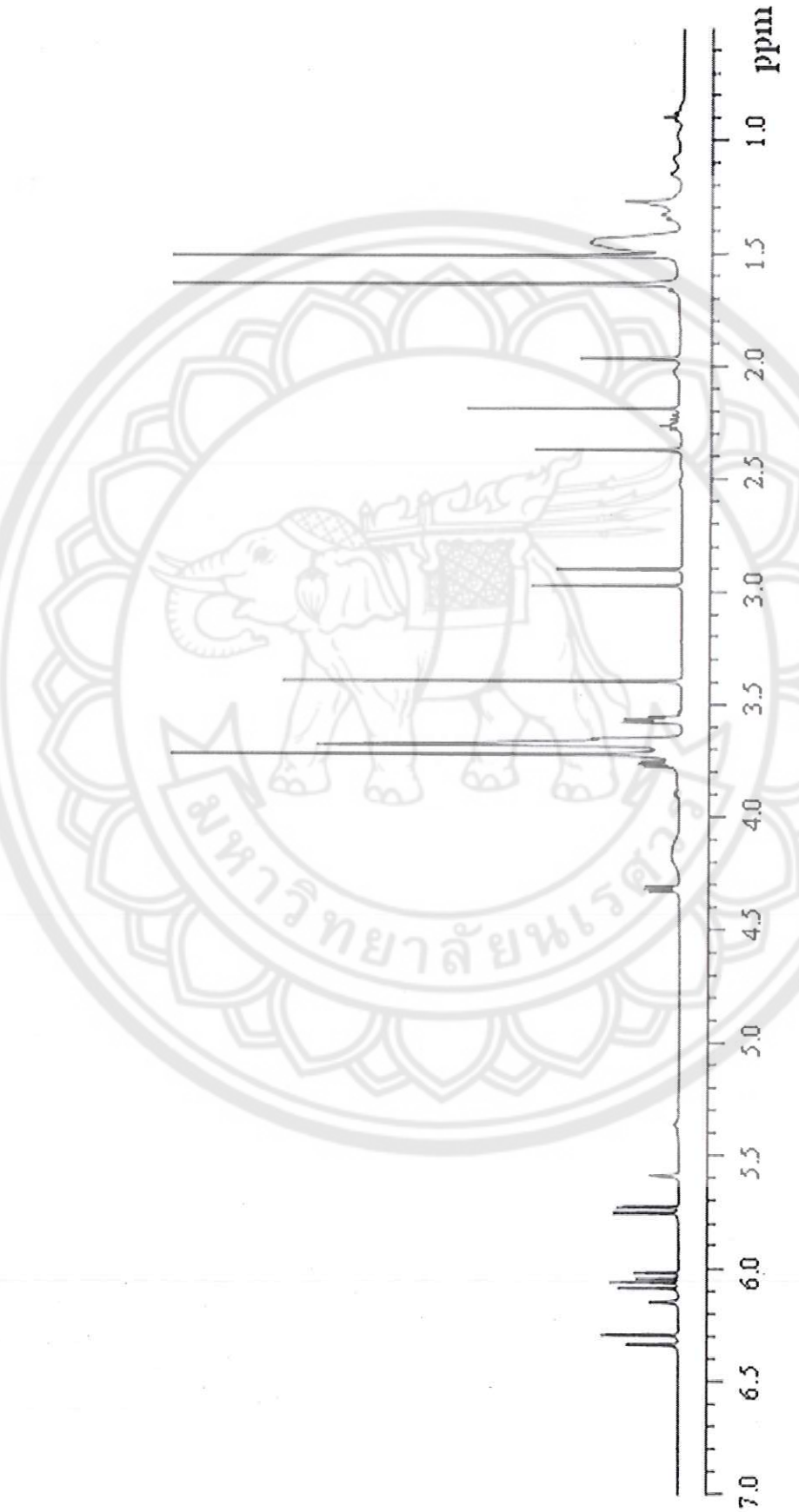

Figure 73 A ^{1}H NMR spectrum of p(*t*-BA)/PEGMA (75/25)

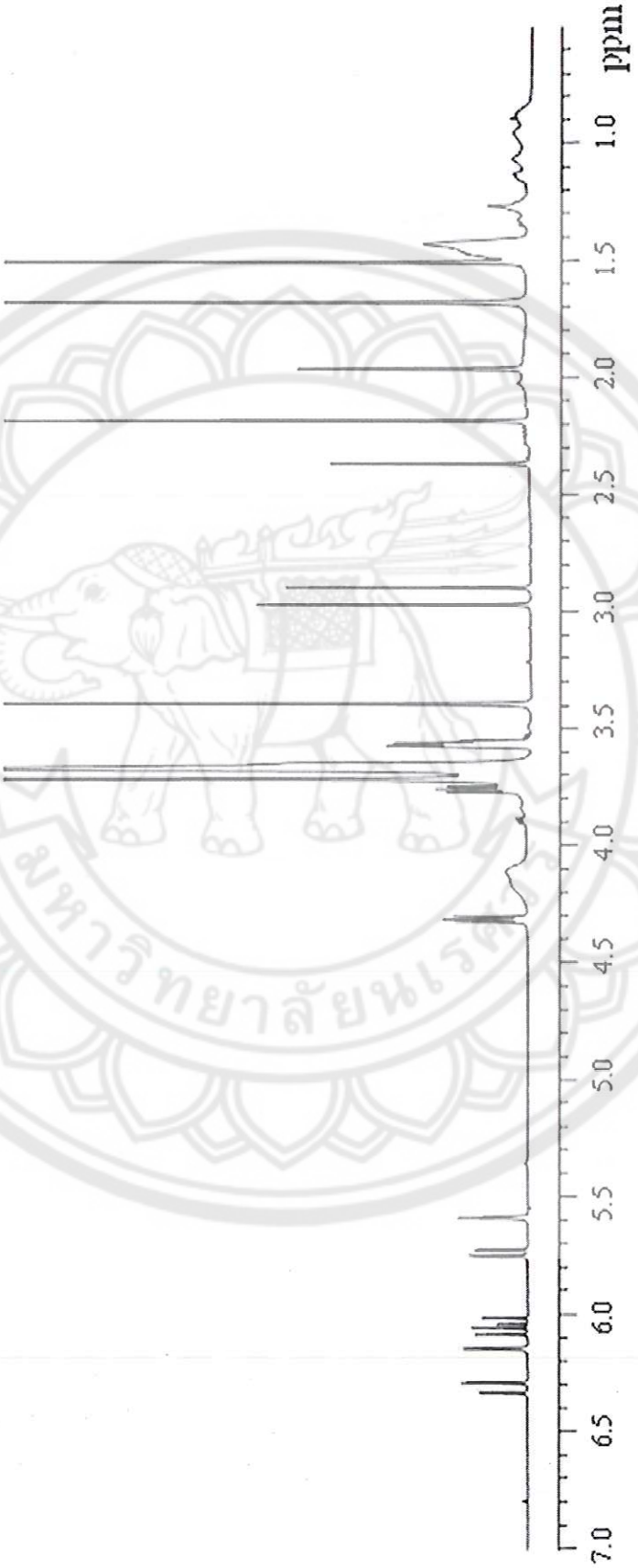

Figure 74 A ^{1}H NMR spectrum of p(*t*-BA)/PEGMA (50/50)

by controlled/living radical polymerizations (CRPs), including nitroxide-mediated radical polymerization (NMRP) [28], reversible addition fragmentation chain transfer (RAFT) polymerizations [29], and atom transfer radical polymerization (ATRP) [30, 31]. Among these methods, ATRP has become one of the most successful methods for polymerization and block copolymerization of a wide range of monomers in a controlled manner. Therefore, ATRP was widely employed to modify MNP surface with well-controlled polymer because of the facile functionalization of MNP with ATRP initiating species (alkyl halides) for a surface-initiated controlled polymerization [32–34].

In the current work, we focused on the surface modification of MNP with poly[(*t*-butyl acrylate)-*stat*-(poly(ethylene glycol) methyl ether methacrylate)] copolymers (P[(*t*-BA)-*stat*-PEGMA]) with varied monomer loading ratios (100 : 0, 75 : 25, 50 : 50, and 25 : 75, resp.) *via* ATRP using a "grafting from" technique (Figure 1). It was hypothesized that the hydrophilic PEGMA in the P[(*t*-BA)-*stat*-PEGMA] copolymers allowed the particles to well disperse in aqueous media, which is a minimum requirement for biomedical applications, while the *t*-BA groups can be cleaved in acidic dispersion to obtain the carboxylate groups on the particle surface. These negatively charged carboxylate groups serve as additional electrostatic stabilization to the particles and also allow for further functionalization with various bioentities, such as peptide, protein, DNA, or drugs. The analysis of the MNPs with carboxylate-enriched surface and their use as nanosupports for coupling with bioentities are underway and will be discussed in the future report. In the present report, the initiator for ATRP was first covalently bound onto the surface of the particles through the combination of a ligand exchange reaction and condensation of triethoxysilane to obtain ATRP initiating sites on their surface. Then, the surface-initiated ATRP of P(*t*-BA) homopolymer and P[(*t*-BA)-*stat*-PEGMA] copolymer mediated by a copper complex was carried out. Kinetic studies were performed to reveal the reactivities of *t*-BA and PEGMA in the copolymerization. Gel permeation chromatography (GPC) was also conducted to investigate the change of the molecular weights of the copolymers as a function of time. The particle size and size distribution of the copolymer-MNP composites were evidenced using transmission electron microscopy (TEM). The magnetic properties of the composites were also investigated via vibrating sample magnetometry (VSM).

2. Materials and Methods

2.1. Materials. Unless otherwise stated, all reagents were used without further purification: iron(III) acetylacetonate ($Fe(acac)_3$), 99% (Acros), benzyl alcohol, 98% (UNILAB), oleic acid (Fluka), ethyl-2-bromoisobutyrate (EBIB), 98% (Aldrich), 2-bromoisobutyryl bromide (BIBB), 98% (Acros), 3-aminopropyl triethoxysilane (APS), 99% (Acros), triethylamine (TEA), 97% (Carlo Erba), copper(I) bromide (CuBr), 99.99% (Aldrich), and *N*,*N*,*N*′,*N*″,*N*″-pentamethyldiethylenetriamine (PMDETA), 99+% (Acros). Poly(ethylene glycol)methyl methacrylate (PEGMA, $\overline{M_n}$ = 300 g/mol) (Aldrich) was used after removing inhibitors by a column filtration through basic and then neutral alumina and stored at −4°C until used. *Tert*-butyl acrylate (*t*-BA, 99% stabilized) (Acros) was stirred overnight over CaH_2 and distilled under reduced pressure prior to use. 2-Bromo-2-methyl-*N*-(3-(triethoxysilyl) propyl)propanamide (BTPAm) was prepared according to the previously reported procedure and the details of the syntheses are provided in the supporting information [35] in the Supplementary Material available online at http://dx.doi.org/10.1155/2015/121369. Toluene, 1,4-dioxane, and *N*,*N*-dimethylformamide (DMF) (UNILAB) were used after distillation over CaH_2.

2.2. Characterization. Proton nuclear magnetic resonance spectroscopy (^{1}H NMR) spectra were obtained from a Bruker AC 200-MHz spectrometer using $CDCl_3$ as a solvent. Fourier transformed infrared spectroscopy (FTIR) experiments were performed on a Perkin-Elmer Model 1600 Series FTIR Spectrophotometer. The samples were prepared by mixing dried solid samples with KBr. The molecular weights and molecular weight distributions were measured by GPC (Spectra System AS1000 autosampler) using tetrahydrofuran (THF) as a solvent and polystyrene standard. Magnetic properties of the particles were determined using a Standard 7403 Series at Lakeshore VSM. Samples for TEM analysis were prepared by drop casting the samples onto a carbon-coated copper grid and the images were taken using a Philips Tecnai 12 operated at 120 kV equipped with a Gatan model 782 CCD camera. Thermogravimetric analysis (TGA) was performed on SDTA 851 Mettler-Toledo at the temperature ranging between 25 and 600°C at a heating rate of 20°C/min under oxygen atmosphere.

2.3. Syntheses

2.3.1. Synthesis of MNP Immobilized with ATRP Initiators (BTPAm-Immobilized MNP). BTPAm-immobilized MNP was synthesized *via* a three-step reaction: (1) synthesis of MNP core, (2) immobilizing the MNP with oleic acid, and (3) immobilizing BTPAm onto the oleic acid-immobilized MNP. MNP was prepared *via* a thermal decomposition reaction of $Fe(acac)_3$ (5 g, 14.05 mmol) in benzyl alcohol (90 mL) [36]. The mixture was set at 180°C for 48 h with nitrogen flow. After the reaction, the precipitant was removed from the dispersion using an external magnet and washed with ethanol and CH_2Cl_2 repeatedly to remove benzyl alcohol and then dried under reduced pressure. To prepare oleic acid-immobilized MNP, MNP dispersion (0.8 g of dried MNP in 30 mL of toluene) was sonicated for 1 h followed by dropwise additions of oleic acid (4 mL) into the dispersion and sonicated for 3 h under nitrogen atmosphere. To immobilize BTPAm onto the MNP surface, the oleic acid-immobilized MNP dispersed in toluene was mixed with BTPAm using TEA and the reaction was carried out at room temperature for 24 h under nitrogen atmosphere. The dispersion was precipitated in methanol and washed with toluene to remove oleic acid and ungrafted BTPAm from the dispersion.

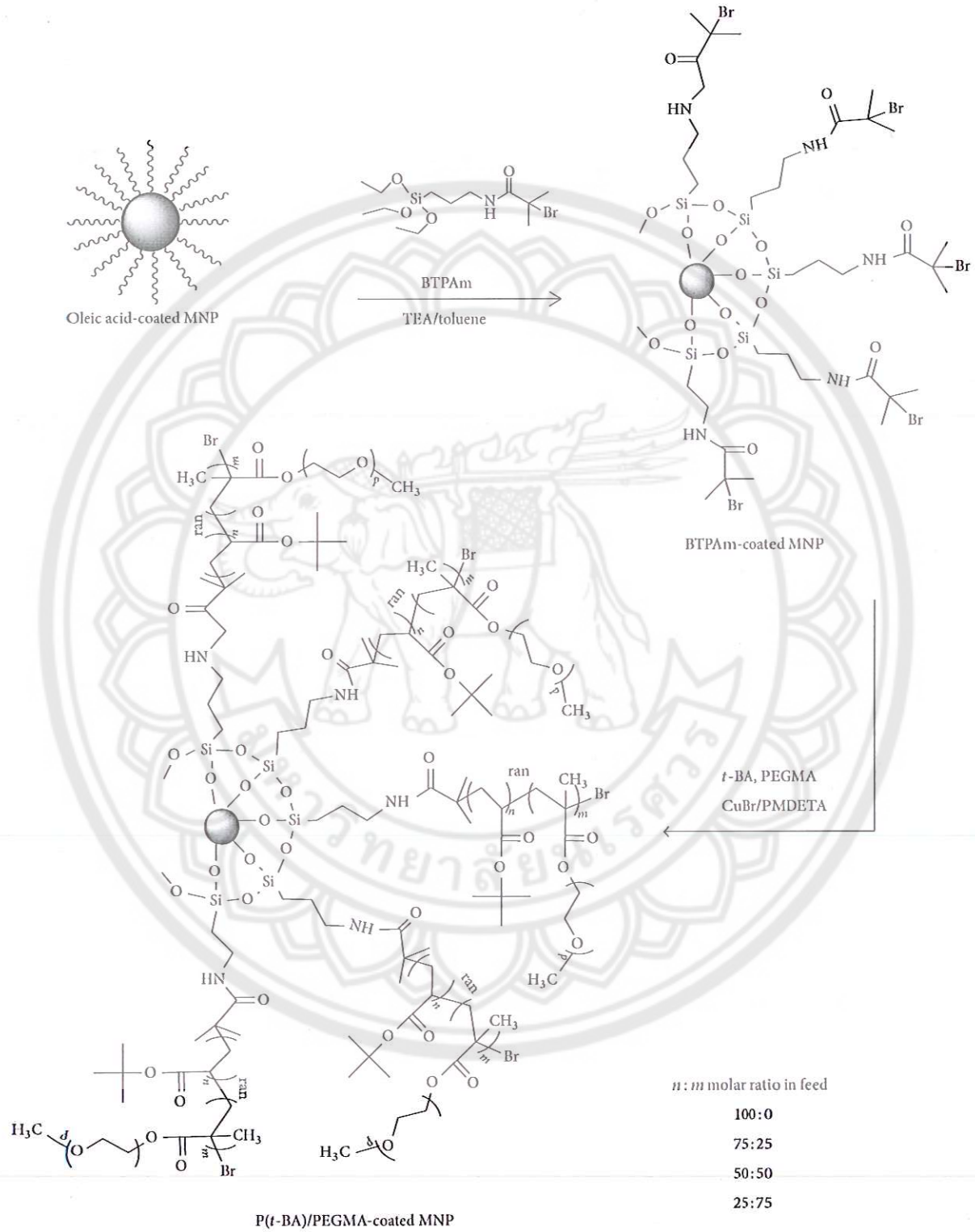

FIGURE 1: Surface modification of MNP with P[(*t*-BA)-*stat*-PEGMA] copolymer *via* a surface-initiated "grafting from" ATRP reaction.

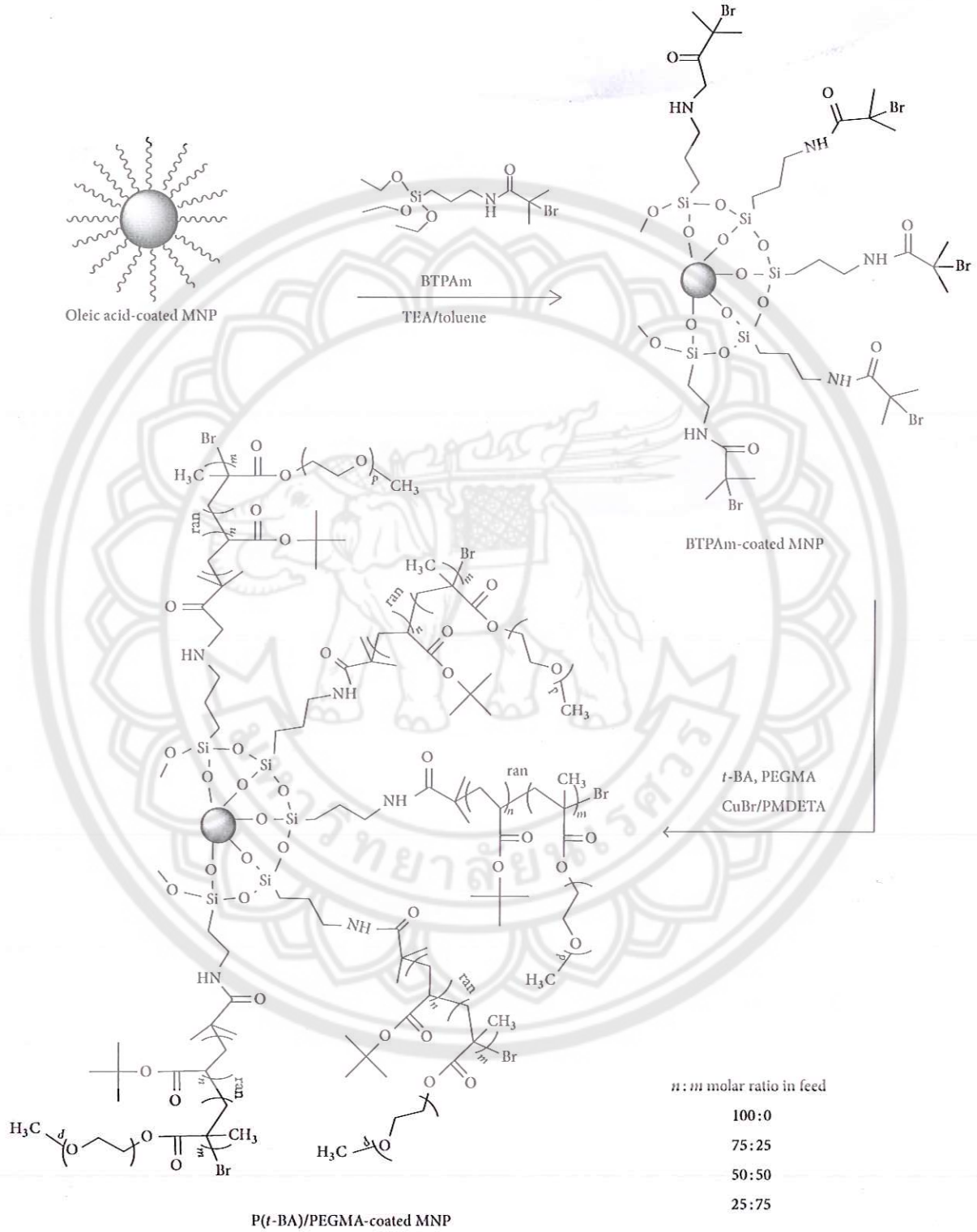

FIGURE 1: Surface modification of MNP with P[(*t*-BA)-*stat*-PEGMA] copolymer *via* a surface-initiated "grafting from" ATRP reaction.

2.3.2. Surface-Initiated ATRP of P[(t-BA)-stat-PEGMA] Copolymers on MNP. In the present work, MNP coated with P[(*t*-BA)-*stat*-PEGMA] copolymers with various molar ratios of each composition (100 : 0, 75 : 25, 50 : 50, and 25 : 75 molar ratios of *t*-BA/PEGMA, resp.) was prepared. An example for the reaction loaded with 50 : 50 molar ratio of *t*-BA/PEGMA was explained. Other copolymer-MNP composites were prepared in a similar fashion with appropriate amounts of reagents used. In the typical procedure, BTPAm-immobilized MNP (0.1 g), *t*-BA (1.45 mL, 0.01 mol), PEGMA (2.86 mL, 0.01 mol), and EBiB (0.03 mL, 0.0002 mol), used as an sacrificial initiator, were mixed in 1,4-dioxane (2.5 mL, 60% w/v) by ultrasonication for 15 min. Then, the mixture was degassed by ultrasonication for 10 min, followed by three freeze-pump-thaw cycles. PMDETA (0.04 mL, 0.0002 mol), CuBr (0.03 g, 0.01 mol), and DMF (0.22 mL, 5% v/v), used as an internal standard, were added into the solution under nitrogen atmosphere, and it was then stirred at 90°C at a given time to initiate the ATRP reactions. The (co)polymer-MNP composite was removed from the dispersion by precipitation in diethyl ether, centrifugation (35,000 rpm for 10 min), and magnetic separation and finally it was dried under reduced pressure.

3. Results and Discussion

3.1. Synthesis of MNP Immobilized with the ATRP Initiator (BTPAm-Immobilized MNP). To prepare MNP, $Fe(acac)_3$ was used as iron precursor and benzyl alcohol as both reducing agent and reaction solvent. Fe^{3+} of $Fe(acac)_3$ was partially reduced to Fe^{2+} by hydroxyl groups of benzyl alcohol to obtain the crystal structure of magnetite (Fe_3O_4 or Fe_2O_3·FeO) [36]. During this process, the initial red-brown complex of $Fe(acac)_3$ changed to black upon heating to 180°C for 48 h, indicating the formation of MNP. After the purification process, FTIR showed a characteristic absorption peak of the Fe-O bond at 578 cm^{-1} (in the supporting information). According to TEM, the particle size was in the range of 5–11 nm with the average of 7.78 ± 1.58 nm in diameter.

Bare MNP was then immobilized with oleic acid to form well dispersible MNP in toluene. BTPAm, an ATRP initiator, was immobilized onto the oleic acid-immobilized MNP through the combination of a ligand exchange reaction and condensation of triethoxysilane to obtain the particles with ATRP initiators on their surface. Figure 2(A) exhibits FTIR characteristic absorption peaks of BTPAm-immobilized MNP: 1648 cm^{-1} (-NH-CO- carbonyl stretching), 1111–1019 cm^{-1} (Si-O stretching), 1529 cm^{-1} (N-H bending), and 3341 cm^{-1} (N-H stretching). In combination with a strong and broad signal of Fe-O bonds (578 cm^{-1}), this showed that BTPAm was immobilized to the MNP surface.

3.2. Surface-Initiated ATRP of P[(t-BA)-stat-PEGMA] Copolymers on MNP. BTPAm immobilized on the particle surface was thought to be able to trigger ATRP reaction. Because the polymers grafted on the particle surface were not detectable *via* an NMR technique due to inherent magnetic properties of MNP, utilization of EBiB as a "sacrificial initiator" was employed to monitor the reaction progress. The conversion *versus* time plots and $\ln([M_0]/[M])$ *versus* time plots of ATRP of P[(*t*-BA)-*stat*-PEGMA] copolymer were determined from the free polymers *via* ^{1}H NMR.

Figure 2 shows FTIR spectra of the copolymer-coated MNP having the molar ratio of 100 : 0, 75 : 25, 50 : 50, and 25 : 75 of *t*-BA/PEGMA, respectively (Figures 2(D)–2(G)). FTIR spectra of BTPAm-immobilized MNP, *t*-BA monomer, and PEGMA oligomer were also provided for comparison in Figures 2(A)–2(C). The success of the grafting reaction of the copolymers onto the particle surface was signified by the presence of the sharp and strong signals of ester groups of PEGMA and *t*-BA repeating units: ~1726 cm^{-1} (-CO-O-) and 1147–1100 cm^{-1} (C-O stretching) (Figures 2(D)–2(G)). In addition, the symmetric vibration of *t*-butyl groups (C-H bending) in P(*t*-BA) as indicated by a doublet ranging between 1390 and 1365 cm^{-1} was clearly observed in the spectra. In all cases, a broad and strong characteristic signal of Fe-O bonds from the MNP cores was obviously apparent (~587 cm^{-1}).

Kinetic studies of ATRP of P(*t*-BA) homopolymer (100 : 0 of *t*-BA/PEGMA) were plotted as a function of the reaction time to show that the reaction was initially fast and its propagation rate decreased after 8 h of the reaction (480 min) (Figure 3(a)). The polymerization was the first-order kinetics during the first 8 h of the reaction (76% conversion after 8 h reaction), indicating a constant concentration of active radical species. The rate of monomer conversion started to deviate from linearity at higher monomer conversion (after 8 h reaction), indicating the presence of irreversible terminations.

In the cased of the copolymerizations, the percent monomer conversions of the reactions having different molar ratios of *t*-BA/PEGMA were determined from ^{1}H NMR spectra using the similar procedure to those of the P(t-BA) homopolymer. Figures 3(b)–3(d) show the individual monomer conversion and the first-order kinetics plots of the copolymerization having various monomer molar ratios in feed. From these three copolymerizations, it can be seen that *t*-BA and PEGMA were consumed rapidly at the beginning period and slow down at the ending period. It was apparent that PEGMA was consumed more quickly than *t*-BA as indicated by the higher monomer conversion of PEGMA than that of *t*-BA at the same reaction time. For example, in the copolymerization with 50 : 50 molar ratio of *t*-BA/PEGMA, the conversion of PEGMA was 88%, while that of *t*-BA was only 64% at 180 min of the reaction (Figure 3(c)). When the reaction was prolonged, the monomer consumption deviated from linearity, indicating that the rate of the ATRP was not directly proportional to the monomer concentration. This was again probably due to the premature termination of active radicals during the copolymerization due to the decrease of the monomer concentration. This phenomenon was confirmed by the rather broad PDI for a controlled radical polymerization when the reaction time was extended (Table 1).

In addition, it was also observed that increasing PEGMA molar ratio in the dispersions seemed to promote the rate

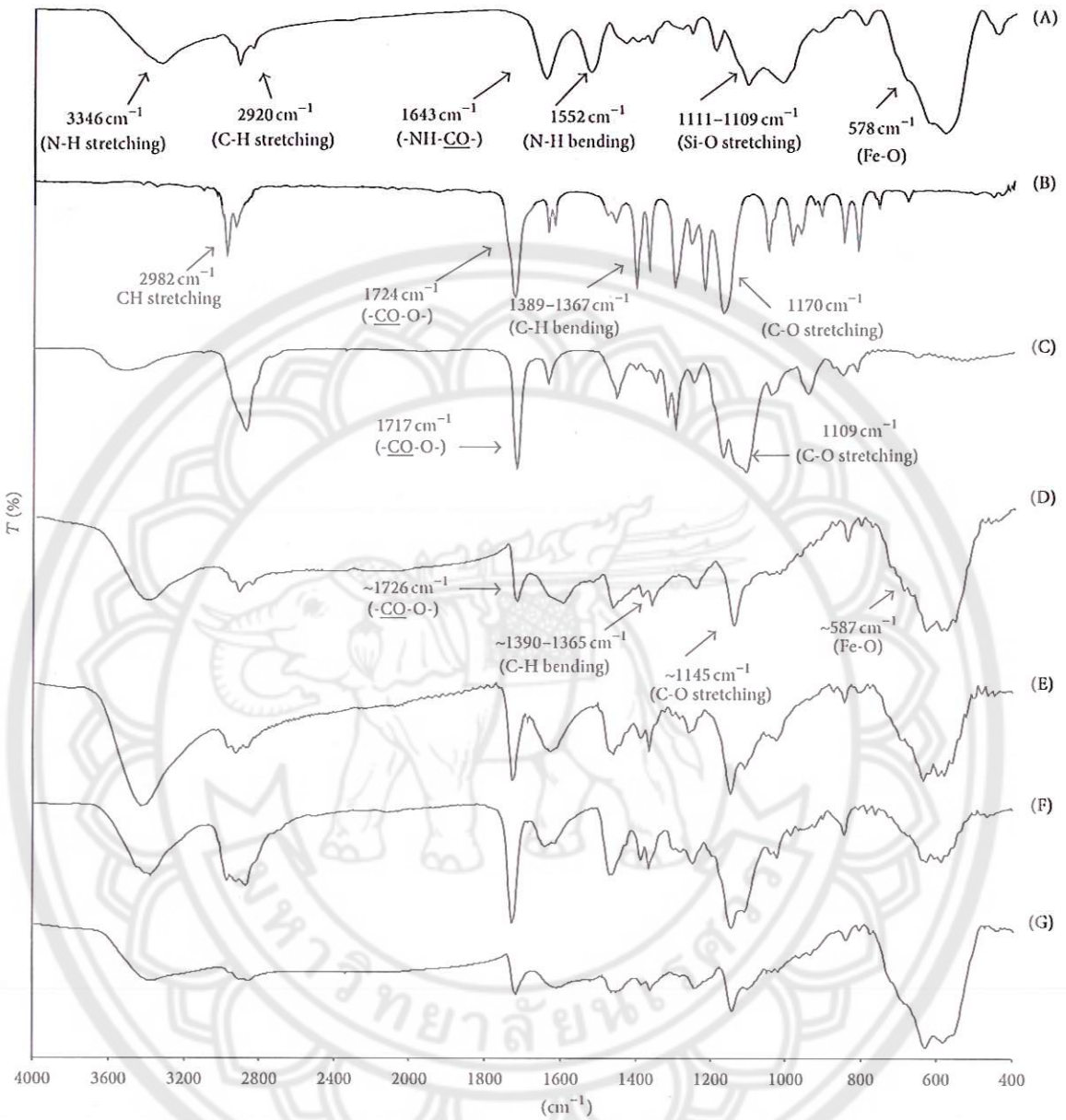

FIGURE 2: FTIR spectra of (A) BTPAm-immobilized MNP, (B) *t*-BA monomer, (C) PEGMA oligomer, and the copolymer-coated MNPs having (D) 100 : 0, (E) 75 : 25, (F) 50 : 50, and (G) 25 : 75 molar ratios of *t*-BA/PEGMA.

TABLE 1: The monomer conversion, $\overline{M}_n$, and PDI of P[(*t*-BA)-*stat*-PEGMA] copolymer (50/50 molar ratio) using 50/50/1/1/1 molar ratio of $[t\text{-BA}]_0/[\text{PEGMA}]_0/[\text{EBiB}]_0/[\text{CuBr}]_0/[\text{PMDETA}]_0$ in 1,4-dioxane at 90°C.

Entry	Reaction time	% conversion[a]		$\overline{M}_n$[b] (exp) (g/mol)	$\overline{M}_n$[c] (theo) (g/mol)	PDI[b]
		t-BA	PEGMA			
1	15 min	11	33	5,898	5,655	1.3
2	45 min	24	55	13,604	9,788	1.5
3	2 h	51	78	18,300	14,968	1.6
4	4 h	72	93	21,419	18,564	1.8

[a]It is determined *via* ^{1}H NMR (monomer depletion monitored relative to DMF signal, which was used as an internal standard).

[b]It is measured *via* GPC (calibrated with polystyrene standard).

[c]$\overline{M}_{n,\text{th}} = ([t\text{-BA}]_0/[\text{EBiB}]_0 \times \text{conv.}_{t\text{-BA}} \times M_{t\text{-BA}}) + ([\text{PEGMA}]_0/[\text{EBiB}]_0 \times \text{conv.}_{\text{PEGMA}} \times M_{\text{PEGMA}})$.

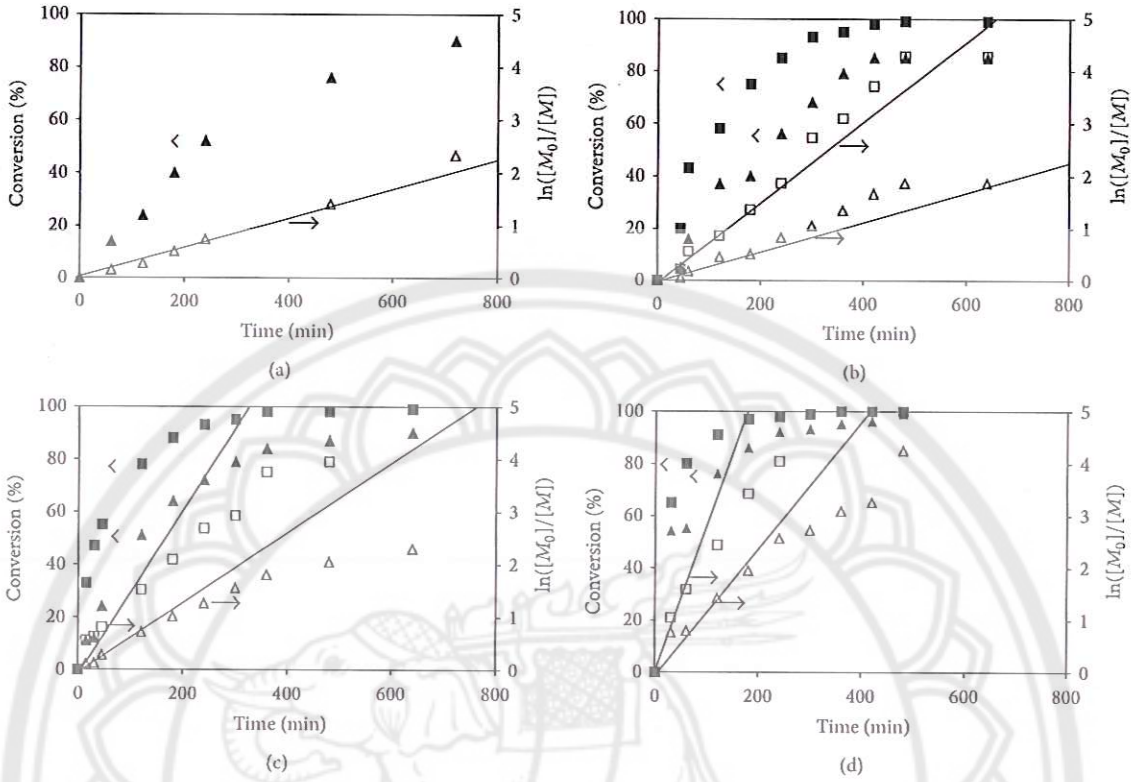

FIGURE 3: The percent conversion *versus* time plots and $\ln([M_0]/[M])$ *versus* time plots of ATRP of the copolymers having (a) 100/0, (b) 75/25, (c) 50/50, and (d) 25/75 molar ratio of *t*-BA/PEGMA, respectively; *t*-BA (▲, △) and PEGMA (■, □).

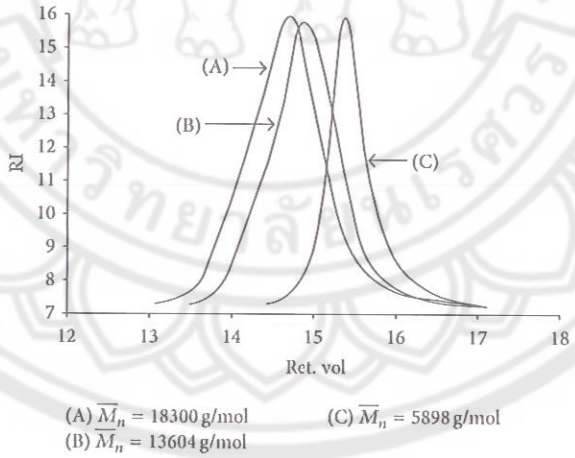

FIGURE 4: GPC chromatograms showing molecular weight distributions of P[(*t*-BA)-*stat*-PEGMA] copolymers with 50 : 50 molar ratio after (A) 2 h, (B) 45 min, and (C) 15 min of the ATRP reactions.

of the ATRP reactions. For example, the copolymer with 25% PEGMA loaded (75 : 25 ratio of *t*-BA/PEGMA) reached 58% PEGMA conversions after 2 h of the reaction. When PEGMA content in the copolymerization increased to 50% (50 : 50 ratio of *t*-BA/PEGMA) and 75% (25 : 75 ratio of *t*-BA/PEGMA), the PEGMA conversions were 78% and 91%, respectively, at the same reaction time (2 h). The accelerated rate of the monomer conversion was also observed in P(*t*-BA) when increasing the PEGMA percentage in the copolymerization reaction. This was attributed to the increase in the solution polarity due to the increment of the PEGMA concentration in the mixture, resulting in the improvement in the copolymer solubility in 1,4-dioxane, the reaction solvent, and thus facilitating the reaction progress.

Table 2: Reaction time, conversions, and the compositions of P[(*t*-BA)-*stat*-PEGMA] copolymers.

Type of copolymer	Reaction time (min)	% conversion[a]		% in the copolymer[b]	
		t-BA	PEGMA	*t*-BA	PEGMA
100 : 0 of *t*-BA/PEGMA	240	52	0	100	0
75 : 25 of *t*-BA/PEGMA	120	37	58	66	34
50 : 50 of *t*-BA/PEGMA	120	42	64	40	60
25 : 75 of *t*-BA/PEGMA	60	54	65	22	78

[a]Reaction conversions were calculated from ^{1}H NMR spectroscopy.

[b]%P(*t*-BA) in the copolymer = $[\%Conv_{t\text{-BA}} \times \%feed_{t\text{-BA}}]/[\%Conv_{t\text{-BA}} \times \%feed_{t\text{-BA}} + \%Conv_{PEGMA} \times \%feed_{PEGMA}]$. % PPEGMA in the copolymer was calculated in a similar fashion.

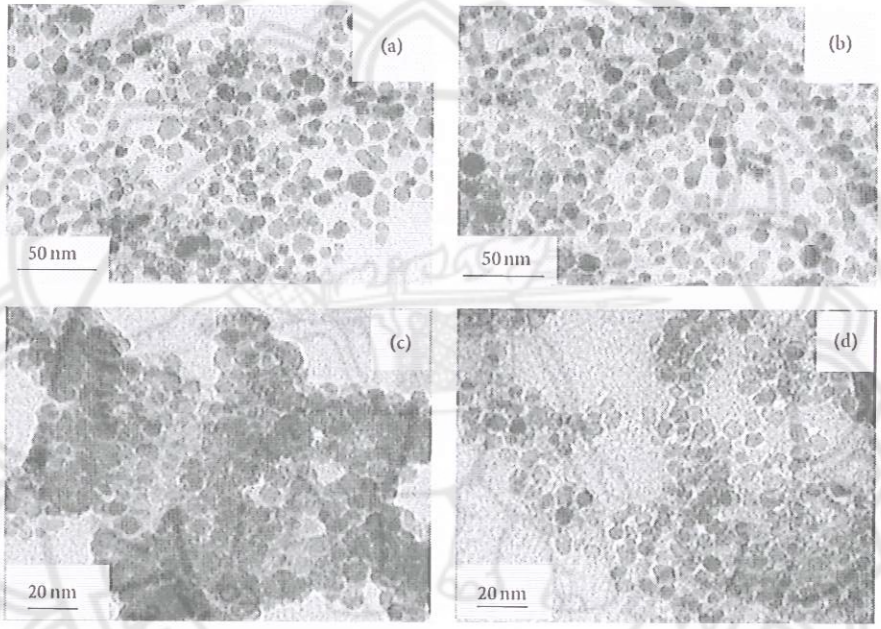

Figure 5: TEM images of (a) BTPAm-immobilized MNP and (b) P(*t*-BA)-coated MNP prepared from toluene dispersions and TEM images of (c) P(*t*-BA)-coated MNP and (d) P[(*t*-BA)-*stat*-PEGMA]-coated MNP (50 : 50 molar ratio) prepared from aqueous dispersions.

Table 1 reports $\overline{M}_n$ and PDI of P[(*t*-BA)-*stat*-PEGMA] copolymer (50 : 50 molar ratio) at four different time intervals during the ATRP copolymerization. It was found that $\overline{M}_n$ gradually increased as the monomer conversions increased, indicating the growth of the copolymer chains. $\overline{M}_n$ calculated from ^{1}H NMR spectroscopy agreed well with those obtained from GPC, indicating the shift of $\overline{M}_n$ toward higher values when increasing reaction time (Figure 4). These ^{1}H NMR spectra are provided in the supporting information. The experimental $\overline{M}_n$ obtained from GPC experiments at different time intervals was comparable to the theoretical $\overline{M}_n$ calculated using the equation shown in the footnote of Table 1.

Table 2 summarizes the reaction time, percent conversion, and the estimated composition of each copolymer. The ATRP reactions were ceased at a given time corresponding to the selected percent conversion (Figure 3). These selected conversions were based on the fact that their conversions were less than 65% in order to lessen feasible reaction termination due to the depletion of the monomer concentration in the mixture. The copolymer compositions were calculated from the feed composition of the monomers, taking its percent conversion into account. Percent PEGMA in the copolymers was calculated in a similar fashion and the results were shown in Table 2. It was found that *t*-BA/PEGMA molar ratios in the copolymers were comparable to the feed compositions. Interestingly, the percentage of PEGMA in the copolymers was found to be slightly higher than its percent feeding in every composition. This result agrees well with the conversion *versus* time plots (Figure 3) indicating the higher reaction reactivity of PEGMA than that of *t*-BA. These copolymers would be then used for TEM, TGA, and VSM studies.

3.3. Properties of the MNP and the Polymer-MNP Composites. TEM images of BTPAm-immobilized MNP (from toluene), P(*t*-BA)-coated MNP (from toluene and water), and P[(*t*-BA)-*stat*-PEGMA]-coated MNP (50 : 50 molar ratio) (from water) are shown in Figure 5. The particle size was in the range of 5–11 nm with the average of 8.1 nm in diameter,

Table 3: Percentages of MNP and the copolymers in each composite.

Type of composite	% char yield[a]	% in the composite		
		MNP	BTPAm	The copolymer
Bare MNP	88	100	—	—
BTPAm-immobilized MNP	81	93	7	—
P[(*t*-BA)-*stat*-PEGMA]-coated MNP				
(100 : 0)	63	71	6	23
(75 : 25)	55	63	5	32
(50 : 50)	52	59	5	36
(25 : 75)	53	60	5	35

[a]It is determined *via* TGA technique.

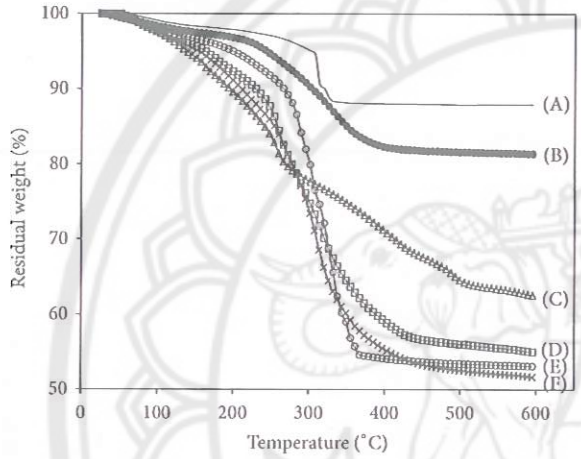

Figure 6: TGA thermograms of (A) bare MNP, (B) BTPAm-immobilized MNP, and the copolymer-coated MNP having molar ratio of *t*-BA/PEGMA of (C) 100 : 0, (D) 75 : 25, (E) 50 : 50, and (F) 25 : 75, respectively.

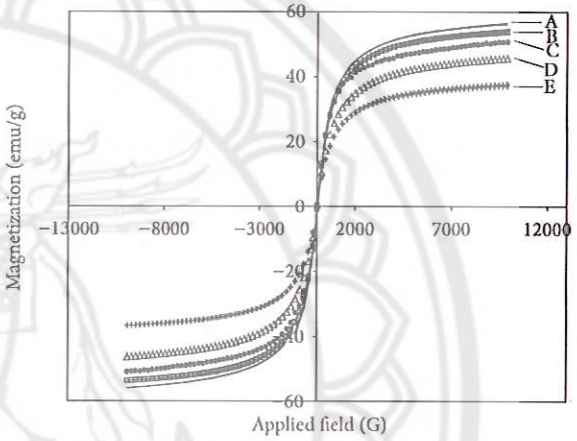

Figure 7: Magnetic properties of (A) bare MNP, (B) BTPAm-immobilized MNP, and P[(*t*-BA)-*stat*-PEGMA] copolymer-coated MNP (50 : 50 molar ratio) after (C) 15 min, (D) 45 min, and (E) 120 min of the ATRP reactions.

regardless of the dispersing media. BTPAm-immobilized MNP and P(*t*-BA)-coated MNP were well dispersed in toluene due to the presence of hydrophobic BTPAm and P(*t*-BA) coating on the particle surface (Figures 5(a) and 5(b)). Interestingly, P(*t*-BA)-coated MNP apparently aggregated when dispersed from aqueous media due to the hydrophobic P(*t*-BA) coating (Figure 5(c)). Dispersibility of the particles in water seemed to be much improved when P[(*t*-BA)-*stat*-PEGMA] copolymers were used for the coating due to the increase in polarity of the coated polymer as compared to P(*t*-BA) homopolymer (Figure 5(d)).

TGA studies were carried out to investigate the mass loss of the organic components in the polymer-MNP composites. The MNP in each step of the reaction showed the distinctive TGA curves, giving rise to the information of the amounts of BTPAm, the copolymers in the coated MNP (Figure 6). The slight loss in mass of bare MNP was probably due to the remaining benzyl alcohol used as the reaction solvent in the MNP preparation step. Using an assumption that % char yield was the weight of iron oxide in the form of magnetite remaining at 600°C, the weight loss of the surface-modified MNPs was thus attributed to the decomposition of organic components including BTPAm and the polymers that were coated to the particle surface. Hence, percent char yield of bare MNP and BTPAm-immobilized MNP were first determined to obtain the percentage of BTPAm in the composites, followed by the polymer-MNP composites. According to the TGA results, the percentage of BTPAm in the composites was about 5–7 wt%, and the percentages of the copolymers in the composites ranged between 23% and 36%, and those of MNPs were in the range of 59–71%. The percentages of MNPs and the polymers in each composite are shown in Table 3.

Magnetic properties of the MNP composites were investigated *via* VSM technique. *M-H* curves of bare MNP, BTPAm-immobilized MNP, and the MNP coated with P[(*t*-BA)-*stat*-PEGMA] copolymer (50 : 50 molar ratio) were presented in Figure 7. They showed superparamagnetic behavior at room temperature as indicated by the absence of magnetic remanence (M_r) and coercivity (H_c) upon removing an external magnetic field. According to the results in Figure 7, the decrease of saturation magnetization (M_s) from 56 emu/g of bare MNP to 54 of BTPAm-immobilized MNP was attributed to the existence of a thin layer of BTPAm on the

particle surface, resulting in the decrease of the percentage of MNP core in the composite. Similarly, the M_s values of the MNP coated with the copolymer were much lower than those of bare MNP, which was again attributed to the decrease in MNP content in the composites because of the presence of the polymeric surfactant on their surface [35]. Increasing the reaction time from 15 min to 120 min further decreased the M_s values of the particles (35–50 emu/g) due to the increase in polymer percentages in the composites, resulting in the decrease in their MNP compositions and a drop of magnetic sensitivity.

4. Conclusions

This work presented a "grafting from" method to modify MNP surface with P[(*t*-BA)-*stat*-PEGMA] copolymer *via* ATRP reactions. The systematic adjustment of molar ratio of *t*-BA to PEGMA in the loading was carried out in the will of fine tuning of water dispersibility of the copolymer-coated MNP. The reaction reactivity of PEGMA in the ATRP reactions was higher than that of *t*-BA. Increasing PEGMA composition in the copolymerization seemed to promote the rate of the ATRP reaction under the condition used in this work (1 : 1 CuBr : PMDETA mol : mol in 1,4-dioxane at 90°C). $\overline{M}_n$ gradually increased as the monomer conversions increased, indicating the steady growth of the copolymer chains in a controllable fashion. TEM indicated that the particles were well dispersible in water due to the presence of hydrophilic PEGMA in the copolymers as compared to those coating with P(*t*-BA) homopolymer. There were about 23–36% of the polymers and 59–71% of MNP cores in the copolymer-MNP composites. After the surface modification, they retained the superparamagnetic properties with the decrease in magnetic responsiveness due to the presence of the copolymers.

Conflict of Interests

The authors declare that there is no conflict of interests regarding the publication of this paper.

Acknowledgments

The authors acknowledge the Thailand Research Fund (TRF) (DBG5580002) and The National Research Council of Thailand (NRCT) (R2558B050) for financial support. They also thank the Center of Excellence for Innovation in Chemistry (PERCH-CIC), Office of the Higher Education Commission, Ministry of Education, for funding and student scholarship.

References

[1] D.-B. Shieh, F.-Y. Cheng, C.-H. Su et al., "Aqueous dispersions of magnetite nanoparticles with NH_3^+ surfaces for magnetic manipulations of biomolecules and MRI contrast agents," *Biomaterials*, vol. 26, no. 34, pp. 7183–7191, 2005.

[2] M. Kumagai, M. R. Kano, Y. Morishita et al., "Enhanced magnetic resonance imaging of experimental pancreatic tumor in vivo by block copolymer-coated magnetite nanoparticles with TGF-β inhibitor," *Journal of Controlled Release*, vol. 140, no. 3, pp. 306–311, 2009.

[3] Y. M. Wang, X. Cao, G. H. Liu et al., "Synthesis of Fe_3O_4 magnetic fluid used for magnetic resonance imaging and hyperthermia," *Journal of Magnetism and Magnetic Materials*, vol. 323, no. 23, pp. 2953–2959, 2011.

[4] G. Liu, R. Y. Hong, L. Guo, Y. G. Li, and H. Z. Li, "Preparation, characterization and MRI application of carboxymethyl dextran coated magnetic nanoparticles," *Applied Surface Science*, vol. 257, no. 15, pp. 6711–6717, 2011.

[5] Z. Liao, H. Wang, R. Lv et al., "Polymeric liposomes-coated superparamagnetic iron oxide nanoparticles as contrast agent for targeted magnetic resonance imaging of cancer cells," *Langmuir*, vol. 27, no. 6, pp. 3100–3105, 2011.

[6] J.-J. Yuan, S. P. Armes, Y. Takabayashi et al., "Synthesis of biocompatible poly[2-(methacryloyloxy)ethyl phosphorylcholine]-coated magnetite nanoparticles," *Langmuir*, vol. 22, no. 26, pp. 10989–10993, 2006.

[7] M. Rutnakornpituk, S. Meerod, B. Boontha, and U. Wichai, "Magnetic core-bilayer shell nanoparticle: a novel vehicle for entrapmentof poorly water-soluble drugs," *Polymer*, vol. 50, no. 15, pp. 3508–3515, 2009.

[8] S. Dandamudi and R. B. Campbell, "The drug loading, cytotoxicity and tumor vascular targeting characteristics of magnetite in magnetic drug targeting," *Biomaterials*, vol. 28, no. 31, pp. 4673–4683, 2007.

[9] M. Kamat, K. El-Boubbou, D. C. Zhu et al., "Hyaluronic acid immobilized magnetic nanoparticles for active targeting and imaging of macrophages," *Bioconjugate Chemistry*, vol. 21, no. 11, pp. 2128–2135, 2010.

[10] K. Cheng, S. Peng, C. Xu, and S. Sun, "Porous hollow Fe_3O_4 nanoparticles for targeted delivery and controlled release of cisplatin," *Journal of the American Chemical Society*, vol. 131, no. 30, pp. 10637–10644, 2009.

[11] Z. Li, M. Kawashita, N. Araki, M. Mitsumori, M. Hiraoka, and M. Doi, "Magnetite nanoparticles with high heating efficiencies for application in the hyperthermia of cancer," *Materials Science and Engineering C*, vol. 30, no. 7, pp. 990–996, 2010.

[12] A. A. M. Elsherbini, M. Saber, M. Aggag, A. El-Shahawy, and H. A. A. Shokier, "Magnetic nanoparticle-induced hyperthermia treatment under magnetic resonance imaging," *Magnetic Resonance Imaging*, vol. 29, no. 2, pp. 272–280, 2011.

[13] T. Kikuchi, R. Kasuya, S. Endo et al., "Preparation of magnetite aqueous dispersion for magnetic fluid hyperthermia," *Journal of Magnetism and Magnetic Materials*, vol. 323, no. 10, pp. 1216–1222, 2011.

[14] J. Qu, G. Liu, Y. Wang, and R. Hong, "Preparation of Fe_3O_4-chitosan nanoparticles used for hyperthermia," *Advanced Powder Technology*, vol. 21, no. 4, pp. 461–467, 2010.

[15] A. Ito, M. Fujioka, T. Yoshida et al., "4-S-Cysteaminylphenol-loaded magnetite cationic liposomes for combination therapy of hyperthermia with chemotherapy against malignant melanoma," *Cancer Science*, vol. 98, no. 3, pp. 424–430, 2007.

[16] R. Hergt, S. Dutz, R. Müller, and M. Zeisberger, "Magnetic particle hyperthermia: nanoparticle magnetism and materials development for cancer therapy," *Journal of Physics Condensed Matter*, vol. 18, no. 38, pp. S2919–S2934, 2006.

[17] H. Dong, J. Huang, R. R. Koepsel, P. Ye, A. J. Russell, and K. Matyjaszewski, "Recyclable antibacterial magnetic nanoparticles grafted with quaternized poly(2-(dimethylamino)ethyl methacrylate) brushes," *Biomacromolecules*, vol. 12, no. 4, pp. 1305–1311, 2011.

[18] S. M. Kang, I. S. Choi, K. B. Lee, and Y. Kim, "Bioconjugation of poly(poly(ethylene glycol) methacrylate)-coated iron oxide magnetic nanoparticles for magnetic capture of target proteins," *Macromolecular Research*, vol. 17, no. 4, pp. 259–264, 2009.

[19] M. Rudolph and U. A. Peuker, "Coagulation and stabilization of sterically functionalized magnetite nanoparticles in an organic solvent with different technical polymers," *Journal of Colloid and Interface Science*, vol. 357, no. 2, pp. 292–299, 2011.

[20] S. Meerod, G. Tumcharern, U. Wichai, and M. Rutnakornpituk, "Magnetite nanoparticles stabilized with polymeric bilayer of poly(ethylene glycol) methyl ether-poly(ε-caprolactone) copolymers," *Polymer*, vol. 49, no. 18, pp. 3950–3956, 2008.

[21] L. Jiang, W. Sun, and J. Kim, "Preparation and characterization of ω-functionalized polystyrene-magnetite nanocomposites," *Materials Chemistry and Physics*, vol. 101, no. 2-3, pp. 291–296, 2007.

[22] C. Liu, J. Guo, W. Yang, J. Hu, C. Wang, and S. Fu, "Magnetic mesoporous silica microspheres with thermo-sensitive polymer shell for controlled drug release," *Journal of Materials Chemistry*, vol. 19, no. 27, pp. 4764–4770, 2009.

[23] J. Zhou, L. Meng, Q. Lu, J. Fu, and X. Huang, "Superparamagnetic submicro-megranates: Fe_3O_4 nanoparticles coated with highly cross-linked organic/inorganic hybrids," *Chemical Communications*, no. 42, pp. 6370–6372, 2009.

[24] M. Garza-Navarro, A. Torres-Castro, V. González, U. Ortiz, and E. de la Rosa, "Magnetite and magnetite/silver core/shell nanoparticles with diluted magnet-like behavior," *Journal of Solid State Chemistry*, vol. 183, no. 1, pp. 99–104, 2010.

[25] J. Huang, R. R. Koepsel, H. Murata et al., "Nonleaching antibacterial glass surfaces via 'grafting onto': the effect of the number of quaternary ammonium groups on biocidal activity," *Langmuir*, vol. 24, no. 13, pp. 6785–6795, 2008.

[26] N. Pothayee, S. Balasubramaniam, R. M. Davis et al., "Synthesis of 'ready-to-adsorb' polymeric nanoshells for magnetic iron oxide nanoparticles via atom transfer radical polymerization," *Polymer*, vol. 52, no. 6, pp. 1356–1366, 2011.

[27] K. Matyjaszewski, H. Dong, W. Jakubowski, J. Pietrasik, and A. Kusumo, "Grafting from surfaces for 'everyone': ARGET ATRP in the presence of air," *Langmuir*, vol. 23, no. 8, pp. 4528–4531, 2007.

[28] C. J. Hawker, A. W. Bosman, and E. Harth, "New polymer synthesis by nitroxide mediated living radical polymerizations," *Chemical Reviews*, vol. 101, no. 12, pp. 3661–3688, 2001.

[29] C. Boyer, V. Bulmus, T. P. Davis, V. Ladmiral, J. Liu, and S. Perrier, "Bioapplications of RAFT polymerization," *Chemical Reviews*, vol. 109, no. 11, pp. 5402–5436, 2009.

[30] K. Matyjaszewski and J. Xia, "Atom transfer radical polymerization," *Chemical Reviews*, vol. 101, no. 9, pp. 2921–2990, 2001.

[31] W. A. Braunecker and K. Matyjaszewski, "Controlled/living radical polymerization: features, developments, and perspectives," *Progress in Polymer Science*, vol. 32, no. 1, pp. 93–146, 2007.

[32] P. Theamdee, B. Rutnakornpituk, U. Wichai, and M. Rutnakornpituk, "Recyclable magnetic nanoparticle grafted with pH-responsive polymer for adsorption with DNA," *Journal of Nanoparticle Research*, vol. 16, pp. 2494–2506, 2014.

[33] Y. Pray-In, B. Rutnakornpituk, U. Wichai, T. Vilaivan, and M. Rutnakornpituk, "Hydrophilic azlactone-functionalized magnetite nanoparticle for conjugation with folic acid," *Journal of Nanoparticle Research*, vol. 16, no. 4, article 2357, 2014.

[34] T. Theppaleak, M. Rutnakornpituk, U. Wichai, T. Vilaivan, and B. Rutnakornpituk, "Anion-exchanged nanosolid support of magnetic nanoparticle in combination with PNA probes for DNA sequence analysis," *Journal of Nanoparticle Research*, vol. 15, no. 12, pp. 2106–2117, 2013.

[35] M. Rutnakornpituk, N. Puangsin, P. Theamdee, B. Rutnakornpituk, and U. Wichai, "Poly(acrylic acid)-grafted magnetic nanoparticle for conjugation with folic acid," *Polymer*, vol. 52, no. 4, pp. 987–995, 2011.

[36] N. Pinna, S. Grancharov, P. Beato, P. Bonville, M. Antonietti, and M. Niederberger, "Magnetite nanocrystals: nonaqueous synthesis, characterization, and solubility," *Chemistry of Materials*, vol. 17, no. 11, pp. 3044–3049, 2005.